J. HARDEN FILE COPY

29 APRIL 1971

LMSC-A989204
ACS-126

AERODYNAMIC CHARACTERISTICS OF LOCKHEED DELTA-BODY ORBITER AND STAGE-AND-ONE-HALF LAUNCH VEHICLE

CONTRACT NAS 8-26362

MANNED SPACE PROGRAMS, SPACE SYSTEMS DIVISION

LOCKHEED MISSILES & SPACE COMPANY

A GROUP DIVISION OF LOCKHEED AIRCRAFT CORPORATION

SUNNYVALE, CALIFORNIA

MSFC-DRL No. 216
Line Item No. 5

LMSC-A989204
ACS-126
29 April 1971

AERODYNAMIC CHARACTERISTICS OF LOCKHEED DELTA-BODY ORBITER AND STAGE-AND-ONE-HALF LAUNCH VEHICLE

Contract NAS 8-26362

Prepared by

F. A. Velligan
Aerodynamics

H. O. Svendsen
Aerodynamics

Approved by

G. L. Alexander
Flight Technology

J. T. Lloyd, Study Manager
Space Shuttle Phase A
Alternate Concepts Study

Prepared for George C. Marshall Space Flight Center
by Manned Space Programs, Space Systems Division

LOCKHEED MISSILES & SPACE COMPANY

FOREWORD

This report is being submitted as partial fulfillment of Data Requirement Item SE-006M, Aerothermal Wind Tunnel Data, as identified in the Phase A Alternate Concepts Study (Contract NAS 8-26362). It is the intent of this document to present pertinent results and analyses of aerodynamic data from the two NASA-sponsored Phase A wind tunnel test programs. In addition, selected data from a Lockheed low-speed parametric wind tunnel test program are presented. Consistent with the Data Requirement Item, the NASA tunnel results have been input into the SADSAC Space Shuttle Aerothermodynamic Data Management System and published in the following reports: DMS-DR-1085 (SSPD-41) and DMS-DR-1103. The Lockheed low-speed testing is documented in LMSC-A990514.

SUMMARY

An experimental wind tunnel test program was conducted to investigate the subsonic through high supersonic aerodynamic characteristics of the Lockheed delta lifting body orbiter and stage-and-one-half launch vehicle. Analyses and results of these data are presented in the following report.

A 0.01-scale model of the LS 200-5 system was designed and fabricated under NASA Contract NAS 8-26362 for testing in the Ames 6 ft x 6 ft and the Langley Unitary Plan Wind tunnels. Orbiter and launch configurations were tested in the Ames facility (80 hr occupancy) over a speed range of Mach 0.6 to 2.0, whereas only the orbiter was tested in the Langley facility over a speed range of Mach 2.3 to 4.6. Six-component force and moment data, base pressures, and Schlieren photos were obtained at various angles-of-attack and sideslip.

A 0.03-scale model of the orbiter was also designed, fabricated, and tested in the Lockheed 8 ft x 12 ft Low-Speed Wind Tunnel (40 hr occupancy). Six-component force and moment data, base pressure, and a limited amount of tuft flow visualization data were obtained on a variety of configuration combinations.

Analyses of these experimental data indicate that the delta lifting body orbiter meets or exceeds all aerodynamic requirements of the space shuttle orbiter regardless of launch arrangement (e.g., two-stage or stage-and-one-half). The orbiter has neutral or better static stability throughout the entry attitude-velocity operating regime. The trim and control authority is adequate for all cargo-airbreather combinations and can accommodate a center-of-gravity range in excess of 5-1/2 percent of the vehicle reference length. A sizable operating corridor exists throughout the entry-to-landing Mach number range in which the vehicle is statically stable and trimmable. There are NO OPERATING AREAS OF AERODYNAMIC INSTABILITY. Flow visualization studies at a high Mach number

($M_\infty = 4.6$) have shown that there are NO AREAS OF SHOCK IMPINGEMENT – an item of significance in Thermal Protection System (TPS) development and reusability. The entry configuration does not require excessive windward trim and control surface deflections ($\delta_E \leq 5$ deg). Consequently, these surfaces do not require exotic thermal protection system materials.

Maximum subsonic trimmed lift-to-drag ratios (L/D's) approaching 6 are inherent in a properly tuned configuration, and this is entirely adequate for low-speed performance. Sufficient hypersonic L/D is available to generate crossranges in excess of the 1100 nm requirement. Low-speed lift characteristics indicate that the lifting body configuration has acceptable landing speeds and attitudes.

Analyses of the launch configuration characteristics have indicated that reasonable estimates had been used in preliminary trajectory and control system studies. In comparison with pretest estimates, the wind tunnel data showed less drag, more C_{N_α}, approximately the same pitch plane aerodynamic center locations, further aft yaw plane aerodynamic center locations, and more negative C_{ℓ_β}.

CONTENTS

SYMBOLS AND NOMENCLATURE

A_{REF}	Orbiter reference area, 1.02 L_{REF}^2 (tan 90 - Λ)
C_A	Axial force coefficient, axial force/q_∞ A_{REF}, positive downstream (includes base axial force)
C_D	Drag coefficient, $C_A \cos \alpha + C_N \sin \alpha$
C_{D_0}	Drag coefficient at zero lift coefficient
CG	Center-of-gravity location
C_L	Lift coefficient, $C_N \cos \alpha - C_A \sin \alpha$
C_ℓ	Rolling moment coefficient, rolling moment/q_∞ A_{REF} L_{REF}, positive right side down
C_{ℓ_β}	Rolling moment coefficient derivative in the stability axis, $C_{\ell_{\beta_{B.A.}}} \cos \alpha + C_{n_{\beta_{B.A.}}} \sin \alpha$, 1/deg
$C_{\ell_{\beta_{B.A.}}}$	Rolling moment coefficient derivative in the body axis, $\partial C_\ell / \partial \beta$, 1/deg
$C_{\ell_{\delta_A}}$	Rolling moment control derivative, $\partial C_\ell / \partial \delta_A$, 1/deg
C_m	Pitching moment coefficient, pitching moment/q_∞ A_{REF} L_{REF}, positive nose up
C_N	Normal force coefficient, normal force/q_∞ A_{REF}, positive upward
C_{N_α}	Normal force coefficient slope, $\partial C_N / \partial \alpha$, 1/deg
C_n	Yawing moment coefficient, yawing moment/q_∞ A_{REF} L_{REF}, positive nose right
C_{n_β}	Yawing moment coefficient derivative in the stability axis, $C_{n_{\beta_{B.A.}}} \cos \alpha - C_{\ell_{\beta_{B.A.}}} \sin \alpha$, 1/deg
$C_{n_{\beta_{B.A.}}}$	Yawing moment coefficient derivative in the body axis, $\partial C_n / \partial \beta$, 1/deg

$C_{n_{\beta_{DYN}}}$	Dynamic yawing moment coefficient derivative, $C_{n_{\beta_{B.A.}}} \cos \alpha - C_{\ell_{\beta_{B.A.}}} \frac{I_{zz}}{I_{xx}} \sin \alpha$, 1/deg
$C_{n_{\delta_A}}$	Yawing moment control derivative, $\partial C_n / \partial \delta_A$, 1/deg
C_Y	Side force coefficient, side force/$q_{\infty} A_{REF}$, positive to the right
C_{Y_β}	Side force coefficient derivative, $\partial C_Y / \partial \beta$, 1/deg
I_{xx}	Roll moment of inertia about the X-X axis
I_{zz}	Yaw moment of inertia about the Z-Z axis
L_{REF}	Orbiter reference length, distance from orbiter theoretical sharp nose (in plan view) to Station 1752
	Launch vehicle reference length, distance from tank nose to orbiter Station 1752
L/D	Lift-to-drag ratio
L/D_{Max}	Maximum lift-to-drag ratio
MRP	Moment reference point
M_{∞}	Freestream Mach number
q_{∞}	Freestream dynamic pressure
$Re_{\infty L_{REF}}$	Freestream Reynolds number based on reference length
S_{REF}	Launch vehicle reference area, tank planform area plus orbiter reference area
V_{∞}	Freestream velocity
$\bar{V}_{\infty}$	Viscous correlation parameter, $M_{\infty} / \sqrt{Re_{\infty L_{REF}}}$
α	Angle-of-attack of horizontal reference line (body axis parallel to flat lower surface), degrees, positive nose up
$\alpha_{L/D_{Max}}$	Angle-of-attack for maximum lift-to-drag ratio, degrees
α_{TRIM}	Trimmed angle-of-attack, degrees

β	Angle of sideslip of horizontal reference line, degrees, positive nose to the left
Δh	Vertical distance of lower flap hinge line above the ground
δ_A	Elevon deflection for roll, $\frac{\delta_{F_L} + \delta_{F_R}}{2}$, degrees, positive deflection produces positive rolling moment
δ_C	Lower elevon deflection, degrees, positive trailing edge down, subscript L for left elevon, subscript R for right elevon
δ_E	Lower trim flap deflection, degrees, positive trailing edge down
δ_F	Upper elevon deflection, degrees, negative trailing edge up, subscript L for left, subscript R for right
δ_R	Rudder deflection, degrees, positive trailing edge to the left, subscript L for left rudder, subscript R for right rudder
δ_S	Speed brake deflection, degrees, positive trailing edge to the left, subscript L for left brake, subscript R for right brake
$\partial C_m / \partial C_N$	Pitch stability margin, decimal fraction of L_{REF}
Λ	Sweep of body leading edge, 78 degrees
ω_D	Undamped natural frequency of the dutch roll mode, $\left[q_\infty A_{REF} L_{REF} / I_{zz} C_{n_{\beta_{DYN}}} \right]^{1/2}$

PRECEDING PAGE BLANK NOT FILMED

LIST OF ILLUSTRATIONS

Section 1
INTRODUCTION

The delta lifting body orbiter has been actively and continuously studied by Lockheed for the past 12 years. Considerable experimental and analytical background has led to the development of the current configurations (see Fig. 1). Detailed analyses of the latest configurations have been performed under the Alternate Concepts Study. An experimental wind tunnel program (Task III) was funded under this study to investigate the aerodynamic characteristics of the Lockheed (LS 200-5) delta lifting body orbiter (see Fig. 2) and the stage-and-one-half launch vehicle. A 0.01-scale model was designed and fabricated for testing in the Ames 6 ft by 6 ft and the Langley Unitary Plan Wind Tunnels. Six-component force and moment data, base pressures, and Schlieren photos were obtained at various angles-of-attack and sideslip.

Concurrent with this Phase A effort, a 0.03-scale model of the LS 200-5 delta-body orbiter with parametric variations was designed, fabricated, and tested in the Lockheed 8 ft by 12 ft Low-Speed Wind Tunnel. Six-component force and moment data, base pressures, and a limited amount of tuft flow visualization data were obtained on a variety of configuration combinations.

The objectives of both programs respectively were: (1) to provide an experimental data verification of the Lockheed aerodynamic estimates, and (2) to define a credible baseline of data for future engineering studies. The tests were directed specifically at the LS 200-5 stage-and-one-half system which consists of a reusable delta-body orbiter with expendable propellant droptanks. Under the Alternate Concepts Study, a design effort also was conducted on a delta-body orbiter for use on a two-stage system. The external geometry of both configurations is nearly identical regardless of concept, thus allowing the use of the measured LS 200-5 aerodynamic data interchangeably.

Depending upon mission requirements, the stage-and-one-half orbiter can have C.G. locations between 75.1 and 78 percent of the reference length (146 ft) – fuselage stations 1316 and 1367, respectively. The two-stage orbiter for identical missions has C.G. locations between 72.5 and 78 percent – fuselage Stations 1270 and 1367, respectively. Since the two-stage system is the present NASA baseline and since the presently configured two-stage delta-body orbiter requires a greater C.G. operating range than the stage-and-one-half configuration, the material presented herein emphasizes the two-stage centers-of-gravity and the flexibility of the delta-body orbiter to accommodate these extremes.

It should also be mentioned that the LS 200-5 results have been applied to the current orbiter baseline configurations (LS 400-7A, Two-Stage and LS 200-10, Stage-and-One-Half). Despite minor geometry differences, the LS 200-5 aerodynamic characteristics are considered to be representative of these current designs unless noted otherwise.

Section 2
ORBITER

Results and analyses of experimental data are presented for the two-stage application of the delta lifting body orbiter. Throughout the discussion, the following center-of-gravity extremes will be addressed: 78 percent L_{REF} (0 lb cargo, airbreather system in) and 72.5 percent L_{REF} (40 klb cargo, airbreather system out). Worthy of note is the fact that the 78 percent C.G. location occurs only at landing, whereas above Mach 0.6 the furthest aft C.G. is located at 76.8 percent of the reference length.

2.1 AERODYNAMIC REQUIREMENTS

Several basic aerodynamic requirements have been imposed on the orbiter configuration – either from NASA or from Lockheed. Since most entry flight time is in the subsonic and hypersonic speed regimes, the aerodynamic design emphasis has been largely influenced by the requirements associated with these particular regimes. The basic aerodynamic performance philosophy is to attain most of the required 1100-nm crossrange through the use of the hypersonic lift-to-drag ratio (L/D) and to achieve adequate subsonic L/D for an acceptable landing approach; also, subsonic L/D significantly impacts the orbiter ferry-range capability. Therefore, the transonic/supersonic performance has been purposely desensitized, the prime requirements in this regime being stability and control. Neutral or better longitudinal, lateral, and directional static stability have been emphasized throughout the operating attitudes and Mach numbers. Sufficient trim authority must be available to accommodate the center-of-gravity extremes afforded by the various payload combinations both with and without airbreather engines. When aerodynamic heating is severe, an additional requirement has been imposed to limit the windward trim and control surfaces deflection to 5 deg or less, thus assuring TPS material compatibility with anticipated thermal environment.

2.2 CONFIGURATION DESCRIPTION

The orbiter (see Fig. 3) is a delta planform lifting body with appropriate aerodynamic surfaces, configured for adequate performance, stability, and control. Leading edge sweep and radii have been parametrically studied to assure aerodynamic and aerothermodynamic compatibility. A triangular, flat-bottom body surface is required to assure a successful compromise between subsonic trim and hypersonic longitudinal stability and trim. The aft body is shaped to eliminate flow separation and to minimize the large base area associated with the delta-body orbiter. Aft-body compression-sharing surfaces have been utilized in an attempt to optimize the basic body shape for hypersonic yaw-stability considerations. Ideally, the body sides are rolled in to prevent excessive heating, drag, and loss of directional stability at the hypersonic design angle-of-attack. To facilitate improved packaging capability – specifically where it enhances a forward C.G. location – the forebody side roll-in requirement has been relaxed to some extent.

To accommodate the aft C.G. locations inherent in the delta-body orbiter, the addition of aerodynamic surfaces is necessary to provide acceptable longitudinal and directional static stability margins. Two aft-mounted side fins have been sized and positioned (toe-in and rollout) – based on directional stability requirements throughout the operating speed regime. The fins also contribute significantly to the low-speed lift-to-drag performance and longitudinal stability.

An aft trim flap hinged at the body-bottom base has been sized to allow acceptable hypersonic stability and subsonic trim authority. Pitch control is accomplished by deflection of two elevon surfaces which comprise the aft portion of the trim flap. These same surfaces can be differentially deflected for roll control and roll damping.

Roll coordination, dutch roll mode damping, crosswind landing and sideslip control capability, pitch trim authority, and hypersonic yaw stability are provided by two rudders (one on each fin). Also, a speed brake-control surface is located beneath each rudder to provide glide path control; it can also be used to increase hypersonic yaw stability.

Two elevons are mounted on the orbiter upper surface between the vertical fins. The functions of these surfaces are roll control and damping, takeoff rotation, landing trim and derotation, transonic/supersonic pitch stability, and trim authority.

2.3 FLIGHT CHARACTERISTICS

The orbiter data will be discussed by speed regime — subsonic, transonic-supersonic, and hypersonic — followed by summary charts of general aerodynamic characteristics and specific cases relating the reference entry trajectory. Figure 4 identifies the axis system and nomenclature used throughout the report.

2.3.1 Subsonic

A low-speed wind tunnel test (Fig. 5) was conducted at the Lockheed 8 ft by 12 ft Low-Speed Wind Tunnel on a 0.03-scale model of the delta lifting body orbiter. A wide variety of configuration combinations were run in an effort to define the low-speed aerodynamic configuration. High lift-to-drag ratios (L/D's) were emphasized in addition to static stability and trim authority. The detailed results and analyses of this program are presented in Reference 1. Figure 6 indicates acceptable longitudinal stability and trim characteristics for the anticipated C.G. extremes. The aft C.G. condition requires the rudders and speed brakes to be biased inward 15 and 20 deg, respectively, providing a positive C_{m_o} increment in addition to increased longitudinal stability. To trim at meaningful lift coefficients and angles-of-attack,

the lower trim flap (δ_E) is deflected upward, effectively reducing the large base areas associated with the delta lifting body arrangement. Deflection of the upper elevon is not required for the aft C.G. trim arrangement.

Because of the increased stability afforded by the forward C.G. condition, additional rudder biasing (25 deg in) is required to ensure a trimmed longitudinal configuration. The trim philosophy for the forward C.G. condition is to utilize the full lower trim flap authority (δ_E = -25 deg) before going to the upper elevons. When deflected together, the upper elevons provide substantial pitch trim authority; however, this is accomplished at the expense of reduced L/D. The results presented in Fig. 6 are based entirely on wind tunnel data – either exact data or increments obtained on other combinations of the baseline configuration (see Ref. 1).

The corresponding trim lift and lift-to-drag ratios are presented in Fig. 7. Maximum full-scale trimmed L/D's of 5.10 and 5.85 are predicted for the fore and aft C.G.'s, respectively. These values reflect a +0.20 increment in maximum L/D above the measured test results and can be expected because of the decreased friction coefficient associated with the full-scale vehicle. All L/D data include the total drag of the orbiter (including realistic base drag).

Landing speeds have been computed at various angles-of-attack using the aforementioned trimmed lift coefficients. Again, the mission extremes have been presented to illustrate the range of anticipated landing speeds and attitudes (see Fig. 8).

Condition	Landing Speed at $\alpha_{L/D_{Max}}$	Landing Speed at $\alpha_{Tailscrape}$*
40 klb Cargo In/Airbreather Engines Out (Most Forward C.G.)	180 knots	152 knots
Cargo Out/Airbreather Engines In (Most Aft C.G.)	154 knots	122 knots

*$\alpha_{Tailscrape}$ = 22 deg

Ground proximity effects have not been included in the preceding table; however, data are available and indicate reduced landing speed and/or attitudes. Figure 9 is a photo illustrating the 0.03-scale model being tested with a ground plane installation. Significant increases in lift coefficient were measured in the ground plane proximity. These increments have been added to the previously discussed trimmed lift coefficients and are presented in Fig. 10. The physical clearance limits caused by the landing gear geometry will establish a maximum lift value actually attainable on the vehicle (see Fig. 10). The increased lift in the ground effect will contribute to lower landing speeds, and if prolonged float times are allowed, these effects could result in as much as 15 knots reduction in landing speed (see Fig. 11).

Directional stability criteria for the Space Shuttle orbiter have been the subject of considerable discussion (see Fig. 12). Throughout this report both C_{n_β} (stability axis) and $C_{n_{\beta DYNAMIC}}$ are presented. At subsonic speeds, both criteria indicate a directionally stable $(+C_{n_\beta})$ configuration (see Figs. 13 and 14) at all operational angles-of-attack. Side force and rolling moment derivatives are presented in Fig. 15.

Because earlier lifting body vehicles encountered adverse roll-yaw coupling with differential upper elevon deflections (δ_A), a wind tunnel study was conducted to specifically investigate and solve this problem (see Fig. 16). The problem can best be described as follows: When the upper elevon is differentially deflected for roll control, the positive pressure field created by the deflected surface reacts against the adjacent fin surface, causing an adverse yawing moment. Earlier lifting body vehicles remedied the problem by installing a centerline vertical fin, thereby negating this effect. The LS 200-5 as configured showed unfavorable coupling, $C_{\ell_{\delta A}}/C_{n_{\delta A}} \approx -2.5$. The addition of a large centerline vertical fin produced favorable coupling with $C_{\ell_{\delta A}}/C_{n_{\delta A}} \approx 2.7$. Smaller center fin geometries could be employed to eliminate any significant yaw due to roll. Modifying the trapezoidal elevon planform of the LS 200-5 to a rectangular shape resulted in a ratio of $C_{\ell_{\delta A}}/C_{n_{\delta A}} \approx -13$. Moving this surface even farther back of the fins appeared to almost completely

eliminate the coupling. An elevon arrangement somewhere between these last two cases would therefore be desirable rather than the centerline fin installation, with its added weight.

Considering the importance of the fins in obtaining subsonic performance (body alone L/D $\approx$ 2.7), tuft flow visualization studies were conducted on the fins and the upper aft body being endplated by these fins. Figures 17 through 21 show the flow pattern at 5, 10, 15, 20, and 25 deg angle-of-attack and the measured force coefficients coincident with these conditions. The configuration shown is identical to that recommended for the subsonic aft C.G. case — e.g., δ_E = -20 deg, δ_F = 0 deg, and δ_R = 15 deg in. Near 25 deg angle-of-attack, total fin separation was evident accompanied by asymetric roll characteristics; however, these conditions occur beyond the expected operational attitudes.

2.3.2 Transonic/Supersonic

A 0.01-scale steel model of the orbiter configuration was tested in NASA/Ames 6 ft by 6 ft Tunnel and the NASA/Langley Unitary Plan Wind Tunnel (Fig. 22). Most of the test program was concentrated on obtaining configuration combinations which would allow acceptable static stability and trim authority for the C.G. range. Results from the NASA Ames and Langley programs are presented in References 2 and 3. Neutral or better longitudinal stability and adequate trim characteristics are typical of the Mach 0.6 to 2.0 regime and are illustrated in Figs. 23 through 27.

Initial testing of the orbiter at Mach 0.6 and 0.9 indicated extensive fin separation at angles-of-attack above approximately 8 deg. Deflection of the upper body elevons (20 deg up) remedied the problem (see Fig. 23) at the expense of L/D. Since Mach 0.6 is considered to be representative of the start of the landing approach, L/D is significant, and extensive use of the upper elevons is not recommended. Refinement of the fin contours is therefore

required to ensure acceptable operating L/D's at Mach 0.6. Above Mach 0.6, the prime requirement is stability, trim, and control; and the flap, elevons, rudders, etc. can be used without concern for L/D. Asymmetric roll characteristics were also observed at low transonic speeds for $\delta_F = 0$ and reinforce the conclusion that additional airfoil refinement is necessary. It should be emphasized that the use of the upper elevons was very effective in providing acceptable vehicle aerodynamic characteristics by preventing fin flow separation. The impact of this separation is diminished as Mach number is increased above Mach 0.9, and the presented data are considered representative providing fin location and planform remain unchanged.

Depending on Mach number, the maximum angle-of-attack where at least neutral stability is maintained ranges between 15 and 20 deg for the 78 percent center-of-gravity location. For the forward C.G. condition, the maximum attainable angle-of-attack is limited by available trim authority (see Figs. 26 and 27) at Mach 1.6 and 2.0 rather than longitudinal stability.

Sideslip characteristics are presented in Figs. 28 through 33 between Mach 0.6 to 2.0 at 7.6 and 15.3 deg angle-of-attack. Yawing moment derivatives (C_{n_β} and $C_{n_{\beta_{DYNAMIC}}}$), side force derivatives (C_{Y_β}), and rolling moment derivatives (C_{ℓ_β}) are presented for rudders biased inward 10 and 20 deg. Using $C_{n_{\beta_{DYNAMIC}}}$ as the directional stability criterion, a stable configuration is indicated for all test conditions (see Figs. 29 and 32).

Similar longitudinal stability and trim characteristics are presented for the Langley data in Figs. 34 through 37 ($2.3 \leq M_\infty \leq 4.6$). Experimental data have been obtained at angles-of-attack as high as 60 deg to investigate the aerodynamic characteristics of the lifting body if a high angle-of-attack entry and subsequent transition were employed for low crossrange NASA missions. The high angle-of-attack entry minimizes entry duration time and results in reduced total heating and TPS weights. The degree of rudder bias, 10 deg out (aft C.G.) and 0 deg (forward C.G.), is recommended after considering both pitch trim and directional stability characteristics.

Accompanying sideslip data are presented in Figs. 38 through 49 for several rudder combinations; 20 deg biased in, 0 deg (undeflected), and 10 deg flared out.

2.3.3 Hypersonic

Hypersonic characteristics are presented in Figs. 50 and 51. These are based on the Hypersonic Arbitrary Body Computer Program (Reference 4) modified to reflect previously obtained increments between experimental and analytical results on a similar configuration. The vehicle is longitudinally stable and trimmable over a wide range of angles-of-attack. Consistent with the anticipated thermal environment and the thermal protection system material, no windward deflections in excess of 2 deg are required for hypersonic trim of the 78 percent C.G. at L/D_{Max}. However, the actual C.G. of 76.8 percent L_{REF} requires no windward deflection ($\delta_E < 0$ deg). The maximum trimmed angle-of-attack will be limited to approximately 43 deg for the forward C.G. condition because of the trim flap deflection limit ($\delta_E = -25$ deg). Maximum trimmed L/D's of 1.60 and 1.65 are estimated for the fore and aft C.G. locations at Mach 20 and 200 kft altitude. Figure 52 compares the LS 200-5 maximum trimmed lift-to-drag ratio variation with altitude and $\bar{V}_\infty$ (viscous correlation parameter) to available test data on a similar configuration. The hypersonic L/D of 1.65 is more than adequate to provide 1100 nm crossrange. The most representative lateral-directional characteristics are those shown for Mach 4.6 with rudders undeflected ($\delta_R = 0$ deg) as seen in Figs. 47 through 49.

2.3.4 Summary

Sideslip characteristics – C_{n_β}, C_{Y_β}, C_{ℓ_β}, and $C_{n_{\beta DYNAMIC}}$ – are presented versus Mach number and angle-of-attack in Figs. 53 through 64. Varying degrees of rudder biasing; 20 deg in, 0 deg (undeflected), and 10 deg flared out; are shown.

The selected mode of rudder biasing is dependent on the Mach number. Emphasizing aerodynamic heating constraints, the rudders are nominally set at 0 deg above Mach 6.0. For the aft C.G. condition, in the speed regime of Mach numbers 2 to 6, the rudders are flared 10 deg out for added directional stability, thus, effectively increasing the angle-of-attack range where stability is maintained. The rudders remained undeflected for the forward C.G. case between Mach 2 and 6 because of the increased directional stability afforded by the forward C.G. location. The rudders are biased inward 20 deg between Mach numbers 0.6 to 2.0 to improve the trim authority required for the far forward center-of-gravity locations. In the landing approach (Mach 0.6 to touchdown), the rudders have been nominally set at 25 deg and 15 deg in for the fore and aft C.G. locations, thus taking advantage of the positive trim pitching moment increment, increased L/D, and slightly increased longitudinal stability offered by the rudder biasing.

Maximum trimmed lift-to-drag ratio is presented versus Mach number for the C.G. extremes. Full-scale subsonic conditions indicate trimmed L/D_{Max} of 5.10 and 5.85, and 1.60 and 1.65 for the hypersonic conditions (see Fig. 65).

The most descriptive summary plots illustrating the delta-body orbiter flight capability are shown in Figs. 66 and 67. These plots clearly illustrate the trimmed angle-of-attack range where neutral or better static stability is achieved by indicating the boundaries where neutral stability occurs. Also, the figures indicate areas where the boundaries are determined by criteria other than stability – e.g., pitch trim authority. As can be observed from both figures, there is a sizable operating corridor throughout the entry Mach numbers where the vehicle is statically stable and trimmable. There are NO OPERATING AREAS OF AERODYNAMIC INSTABILITY.

Figure 68 is a typical reference entry trajectory for the high-crossrange mission illustrating angle-of-attack, Mach number, altitude, and crossrange. Since most crossrange is attained at hypersonic speeds, considerable freedom is

available to tailor the trajectories below Mach 6.0 to conform with the aforementioned aerodynamic operating corridor. Figures 69 and 70 present the pitch stability margin and the directional stability summaries of the delta-body orbiter for this particular reference entry trajectory. As is evident, the configuration is longitudinally and directionally stable and attains at least 1100-nm crossrange for all cases.

Section 3
LAUNCH CONFIGURATION

3.1 AERODYNAMIC REQUIREMENTS

Aerodynamic performance considerations have been minimal in the launch vehicle system arrangement. However, acceptable relationships between the launch system center-of-gravity locations – with available aerodynamic static stability and engine gimbal-control capability – have influenced the tank placement on the orbiter. Also, the tank's forebody shape and arrangement were considered in tradeoff studies on minimizing ascent drag losses.

3.2 CONFIGURATION DESCRIPTION

The launch configuration consists of the previously described orbiter with two external side-mounted propellant (LO_2 and LH_2) droptanks. These are described in considerable detail in Reference 5, Section 2.5. The launch vehicle axis system is referenced to the orbiter system shown in Fig. 4. All moments are referenced about the launch vehicle nose station with the reference length equal to 2,472 in. and the reference area equal to 12,463 ft^2.

3.3 FLIGHT CHARACTERISTICS

The stage-and-one-half launch configuration was tested between Mach number 0.6 and 2.0 in the NASA Ames 6 ft by 6 ft Wind Tunnel (Fig. 71) with the transonic region of maximum dynamic pressure being of most interest. Carpet plots of the vehicle's normal force, axial force, and pitch stability characteristics with Mach number ($0.6 < M_\infty < 2.0$) and angle-of-attack ($-6 \text{ deg} < \alpha_{nom} < 10 \text{ deg}$) are presented in Figs. 72 through 74. A summary of pertinent longitudinal linear characteristics (normal force coefficient slope, pitch-plane aerodynamic center location, and zero lift-drag coefficients) is shown

in Fig. 75. A similar summary of lateral-directional characteristics (side-force derivative, yaw-plane aerodynamic center location, and rolling-moment derivative) is presented in Fig. 76.

The pretest estimates (Ref. 6) have also been included on there summary plots and are indicative of reasonable correlation. Compared with the estimated aerodynamic characteristics, the data show less drag, more C_{N_α}, approximately the same pitch plane aerodynamic center location, further aft yaw plane aerodynamic center location, and more negative C_{ℓ_β}.

Section 4
CONCLUSIONS AND RECOMMENDATIONS

4.1 CONCLUSIONS

The Lockheed delta lifting body orbiter is aerodynamically acceptable as a candidate for the space shuttle orbiter. The design is characterized by neutral or better static stability throughout its operational flight regime. Trim and control authority is available to accommodate a center-of-gravity range in excess of 5-1/2 percent of the reference length. A sizable aerodynamic operating corridor exists throughout the entry Mach number range in which the vehicle is statically stable and trimmable. There are NO OPERATING AREAS OF AERODYNAMIC INSTABILITY. High-speed flow visualization studies have shown that there are NO AREAS OF SHOCK IMPINGEMENT. The entry configuration does not require windward trim and control surface deflections exceeding 5 deg.

Maximum trimmed subsonic L/D's of 5.1 and 5.85 are characteristic of the LS 200-5 fore and aft C.G. conditions. Hypersonic L/D's of 1.60 to 1.65 are sufficient for generating crossranges in excess of 1100 nm. Low-speed lift characteristics indicate acceptable landing speeds and altitudes.

Analyses of the stage-and-one-half launch configuration characteristics have indicated that representative estimates have been used in preliminary trajectory and control system studies. In comparison with pretest estimates, the wind tunnel data show less drag, more C_{N_α}, approximately the same pitch plane aerodynamic center locations, further aft yaw plane aerodynamic center locations, and more negative C_{l_β}.

4.2 RECOMMENDATIONS

Various modifications are recommended for incorporation in the Lockheed delta lifting body aerodynamic design. Figure 77 is a general arrangement drawing of the current LS 400-7A configuration which utilized the findings of the LS 200-5 wind tunnel test series.

The LS 400-7A configuration has a hemispherical nosecap rather than the 2:1 ellipsoid of revolution used on the LS 200-5. It also has reduced fin leading edge radii, which are consistent with the reduced 1100 nm crossrange requirement (the LS 200-5 fin radii and nose cap design used 1500 nm criteria). These differences should result in decreased hypersonic drag with a corresponding increase in hypersonic L/D to 1.87 (see Figs. 51 and 65).

A wind tunnel program in a large high Reynolds number facility is recommended to systematically investigate potential fin refinements to allow improved subsonic and low transonic aerodynamic performance. Subsonic L/D's approaching 6.0 are inherent in a properly tuned fin configuration. Improved stall characteristics must also be considered in the fin airfoil redesign.

The revised upper body surfaces of LS 400-7A are consistent with improved stability and trim characteristics. Considerable attention has been focused on improving the local aft contouring for providing increased C_{m_o} without increasing the orbiter base drag contribution. The upper body elevon has been reconfigured and relocated to minimize adverse roll-yaw coupling in addition to providing increased longitudinal trim authority.

Rearranging the vehicle's forward components has resulted in minor forebody cross-section modifications, thereby favorably increasing the hypersonic directional stability.

A machine drawing from the Hypersonic Arbitrary Body Aerodynamic Computer Program of the recommended aerodynamic configuration (LS 400-7A) is shown in Fig. 78.

Section 5

REFERENCES

1. H. H. Drosdat: Low-Speed Testing of a Lockheed Delta-Body Space Shuttle Reentry Vehicle, LMSC-A990514, 17 May 1971

2. Jack Brownson, ARC; F. A. Velligan, and H. O. Svendsen, LMSC: Static Aerodynamic Characteristics of the LMSC Stage-and-One-Half Space Shuttle Configuration (M = .60 to 2.0), DMS-DR-1085 (SSPD-41), April 1971

3. DMS-DR-1103, To be published.

4. Arvel F. Gentry: Hypersonic Arbitrary Body Aerodynamic Computer Program (Mark III Version), DAC 61552, April 1968

5. J. T. Lloyd, et al: Final Report – Study of Alternate Space Shuttle Concepts, Volume II, LMSC-A989142, 29 April 1971

6. H. H. Drosdat: LS 200-5 Stage-and-One-Half Launch Vehicle Aerodynamic Characteristics, EM I2-01-M1-4, 17 Nov 1970

Section 6

ILLUSTRATIONS

LOCKHEED

DELTA BODY EVOLUTION

AEROTHERMODYNAMIC TEST HISTORY

1967 - 1970

FDL-5A

AERO TEST: 500 HRS
THERMO TEST: 140 HRS

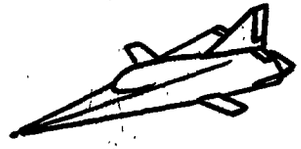

FDL-5B

AERO TEST: 336 HRS
THERMO TEST: 42 HRS

1964 - 1967

AF-5 F-3 F-4 F-5

AERO TEST: ~700 HRS
THERMO TEST: 495 HRS

F-1 V-4 V-5 FV-5

FIG. 1

SPACE SHUTTLE ORBITERS

1968 - 1970

LSC-8AX

AERO TEST: 20 HRS
THERMO TEST: 40 HRS

LSC-8MX

AERO TEST: 641 HRS
THERMO TEST: 83 HRS

FDL-5LC FDL-8H FDL-5LD

AERO TEST: 365 HRS

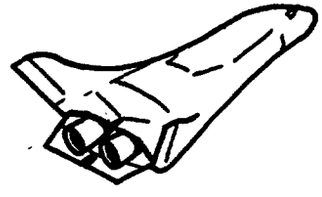

2-STAGE ORBITER
L2S - 112
THERMO TEST: 56 HRS

TEST TIME

AERO:	2,800 HRS
THERMO:	912 HRS
TOTAL	3,712 HRS

1971 LS200-5
SPACE SHUTTLE

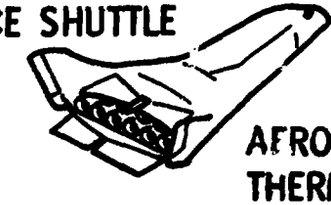

AERO TEST: 260 HRS
THERMO TEST: 56 HRS

D02887(2)

GENERAL ARRANGEMENT – ORBITER

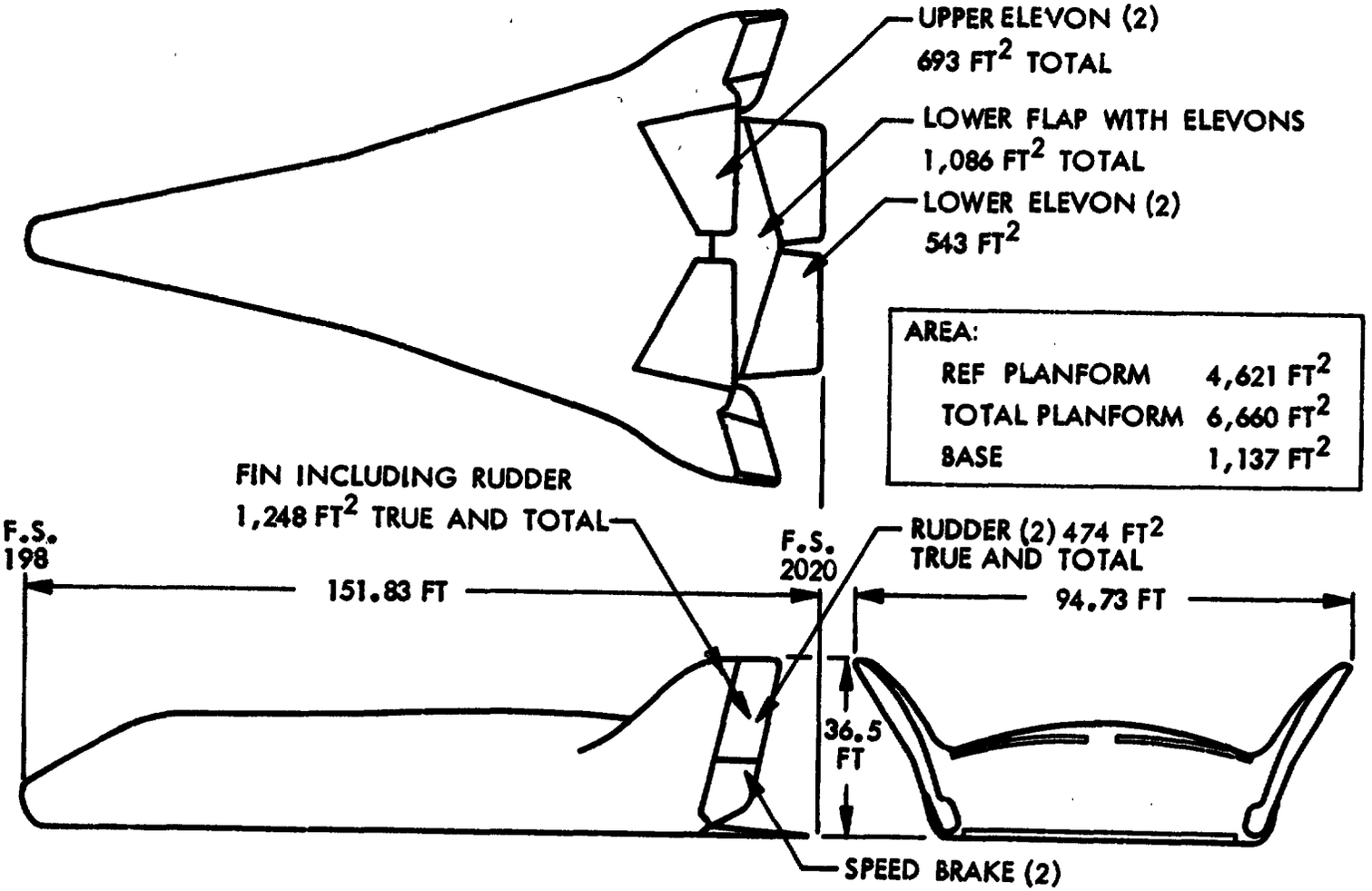

FIG. 2

D03350

DELTA-BODY ORBITER

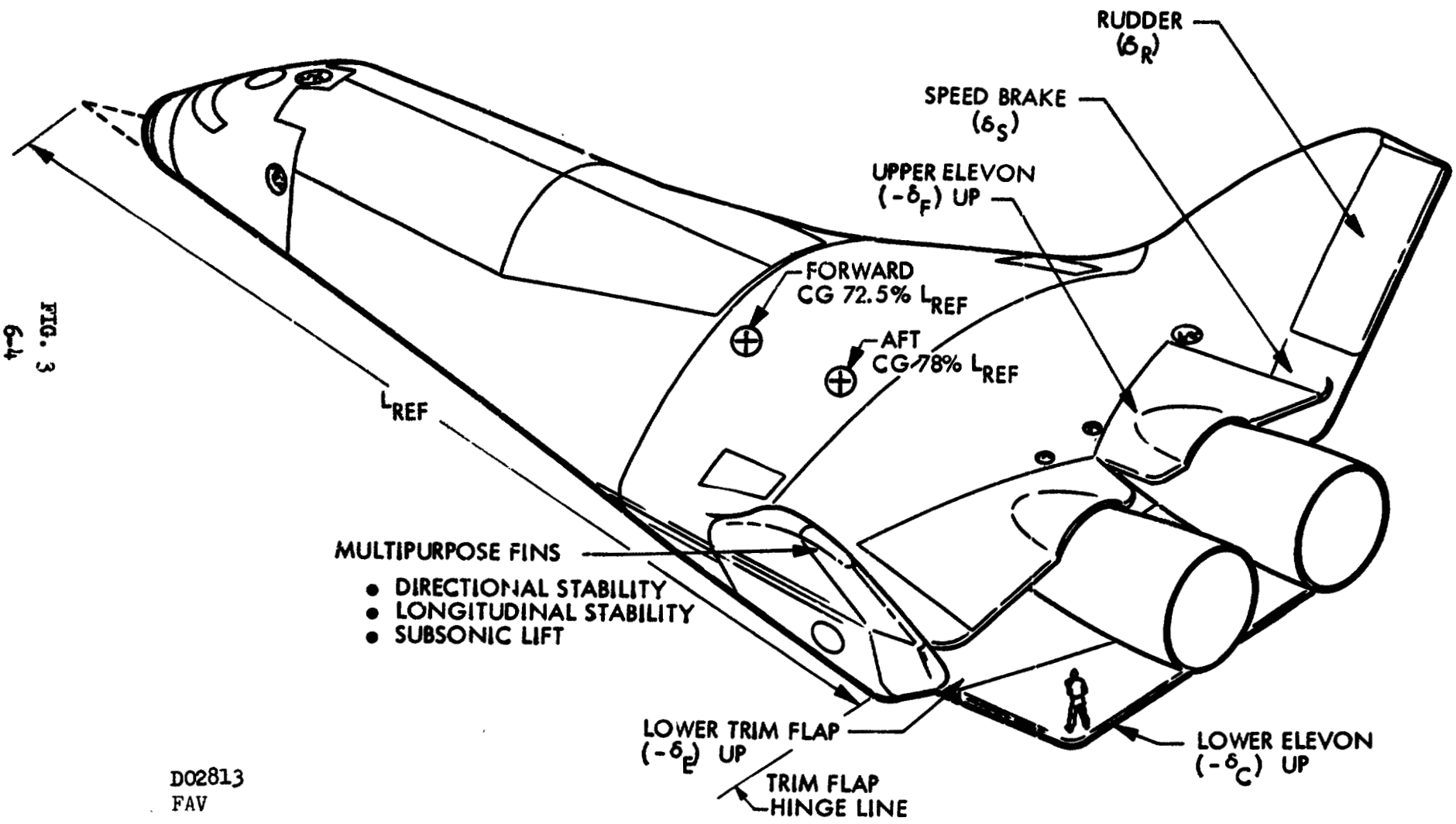

FIG. 3
6-4

D02813
FAV

ORBITER—BODY AXIS SYSTEM

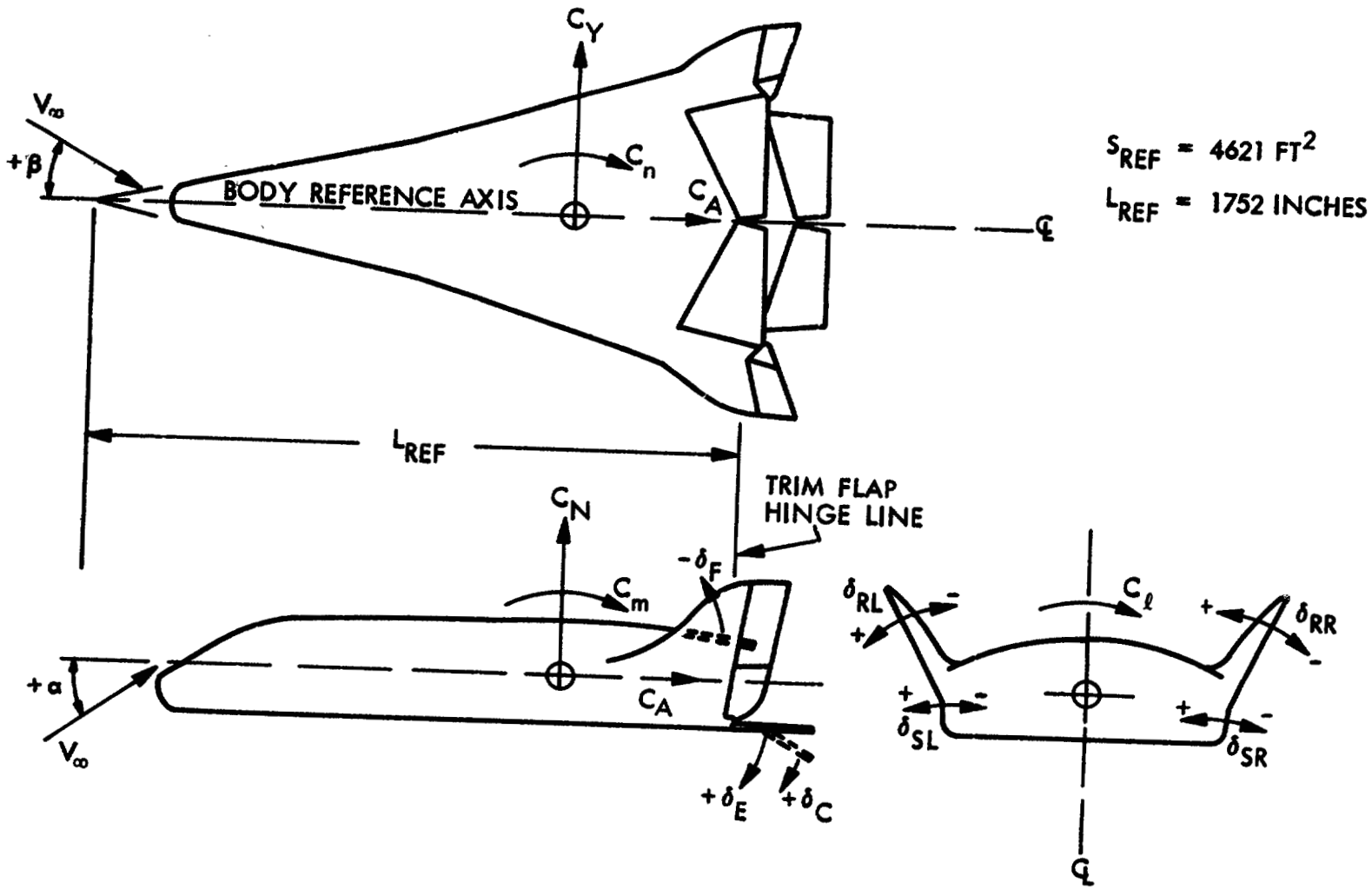

D03249

FIG. 4

LOW-SPEED WIND TUNNEL TEST

- LOCKHEED 8 FT x 12 FT LOW-SPEED WIND TUNNEL
- TEST CONDITIONS
  - MACH NUMBER = 0.23
  - ANGLE-OF-ATTACK = $-4 \longrightarrow 26^{0}$
  - SIDESLIP ANGLE = $-4 \longrightarrow 10^{0}$
  - REYNOLDS NUMBER = 1.7×10^{6} PER FT
- TEST DURATION = 40 HR – 60 RUNS
- CONFIGURATION PARAMETERS
  - TRIM FLAP DEFLECTION
  - LOWER ELEVONS DEFLECTION
  - UPPER ELEVONS DEFLECTION
  - RUDDER DEFLECTION
  - DRAG BRAKE DEFLECTION
  - TRIM FLAP
  - BOAT-TAILING
  - CENTER FIN
  - UPPER ELEVON LOCATION
  - GROUND PLANE

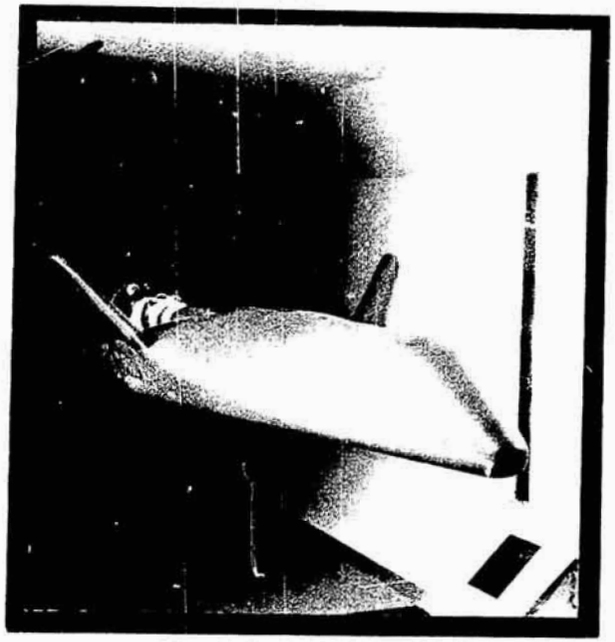

FIG. 5

fav
3-2-71

D02552(1)

$M_\infty = 0.23$*

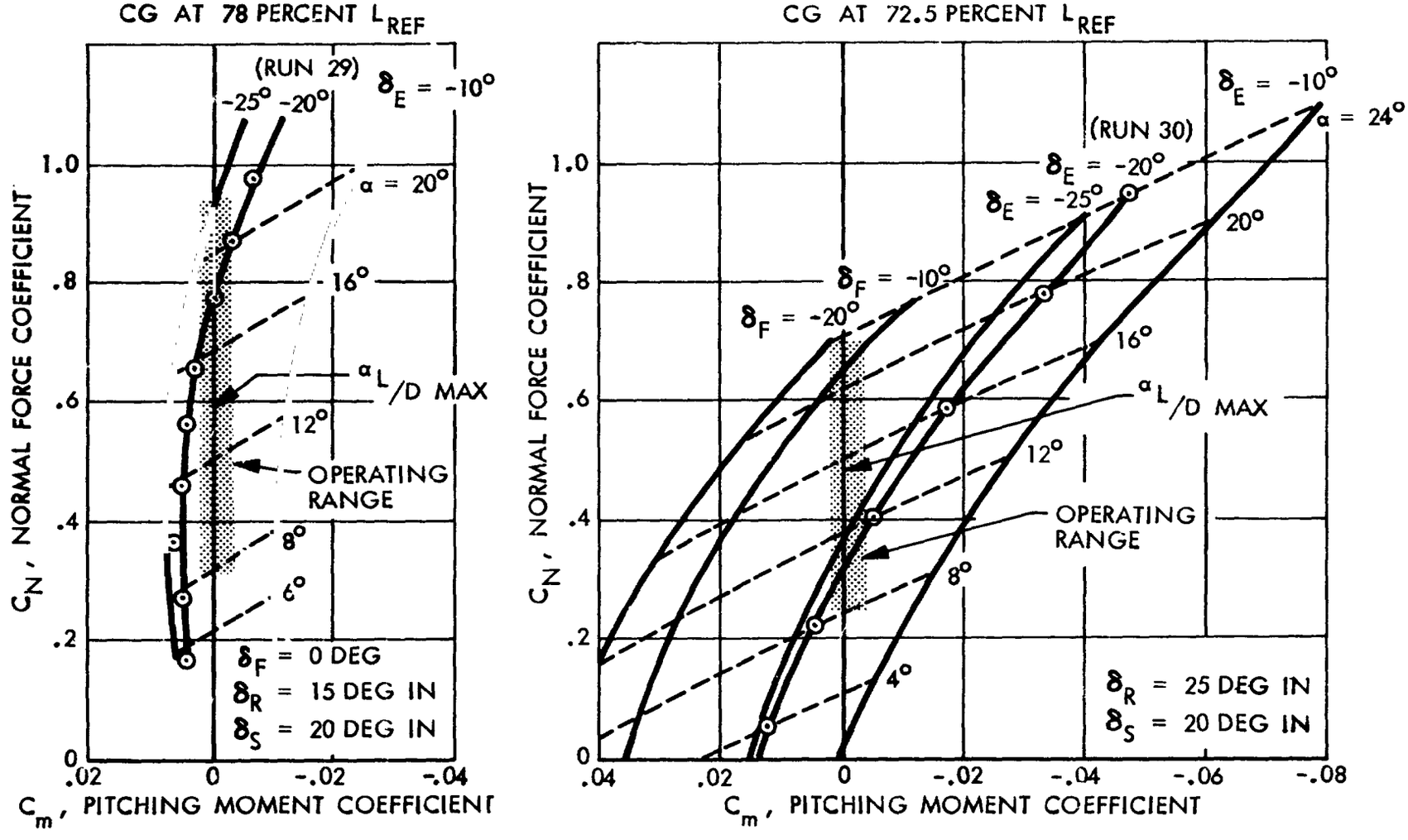

FIG. 6

6-7

*LOCKHEED 8 FT X 12 FT WIND TUNNEL TEST L-324

D03266

LIFT AND DRAG CHARACTERISTICS

$M_\infty = 0.23$*

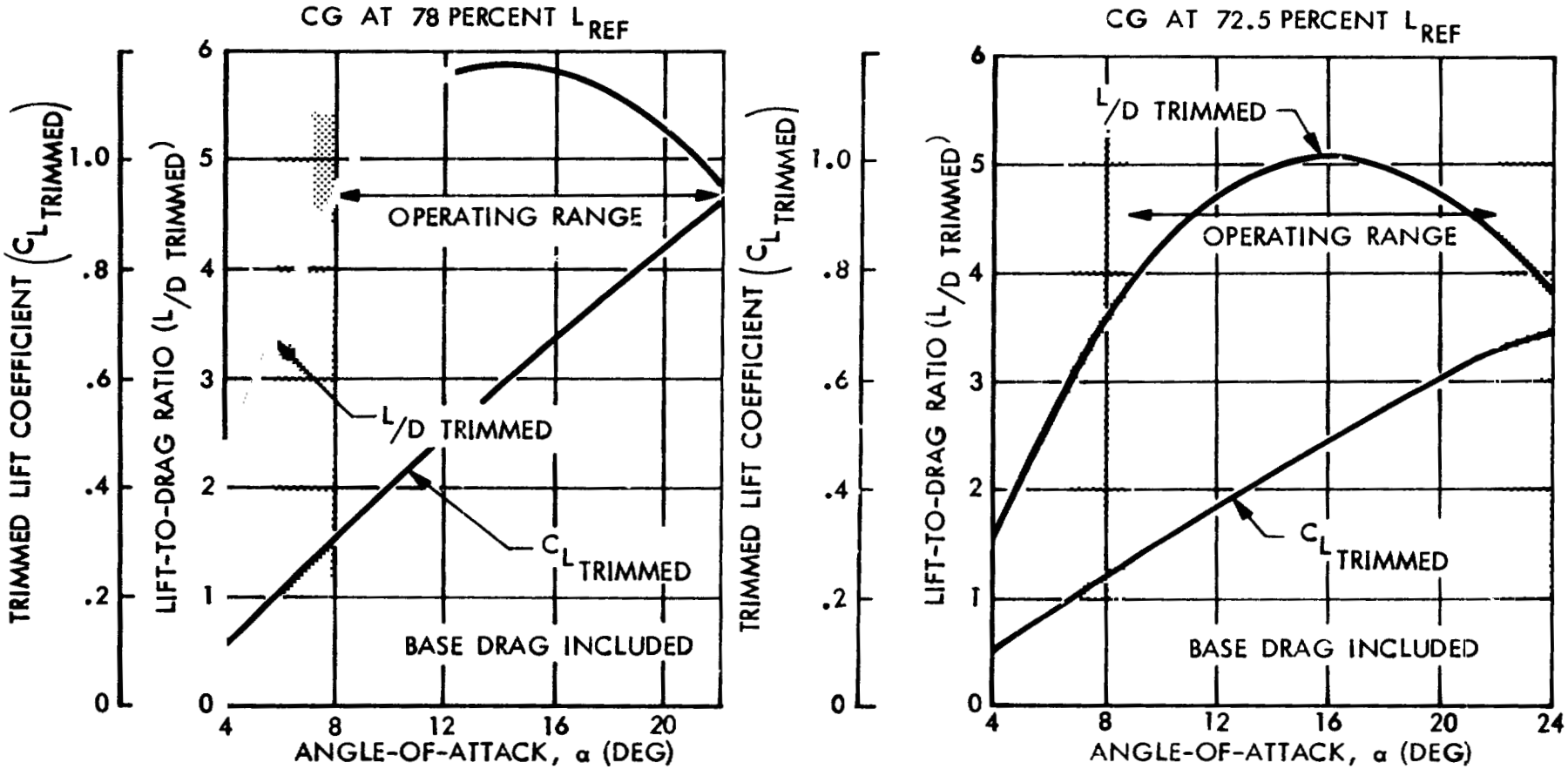

*LOCKHEED 8 FT X 12 FT WIND TUNNEL TEST NO. L-324

FIG. 7
6-8

D03267

LANDING SPEED AND ATTITUDE

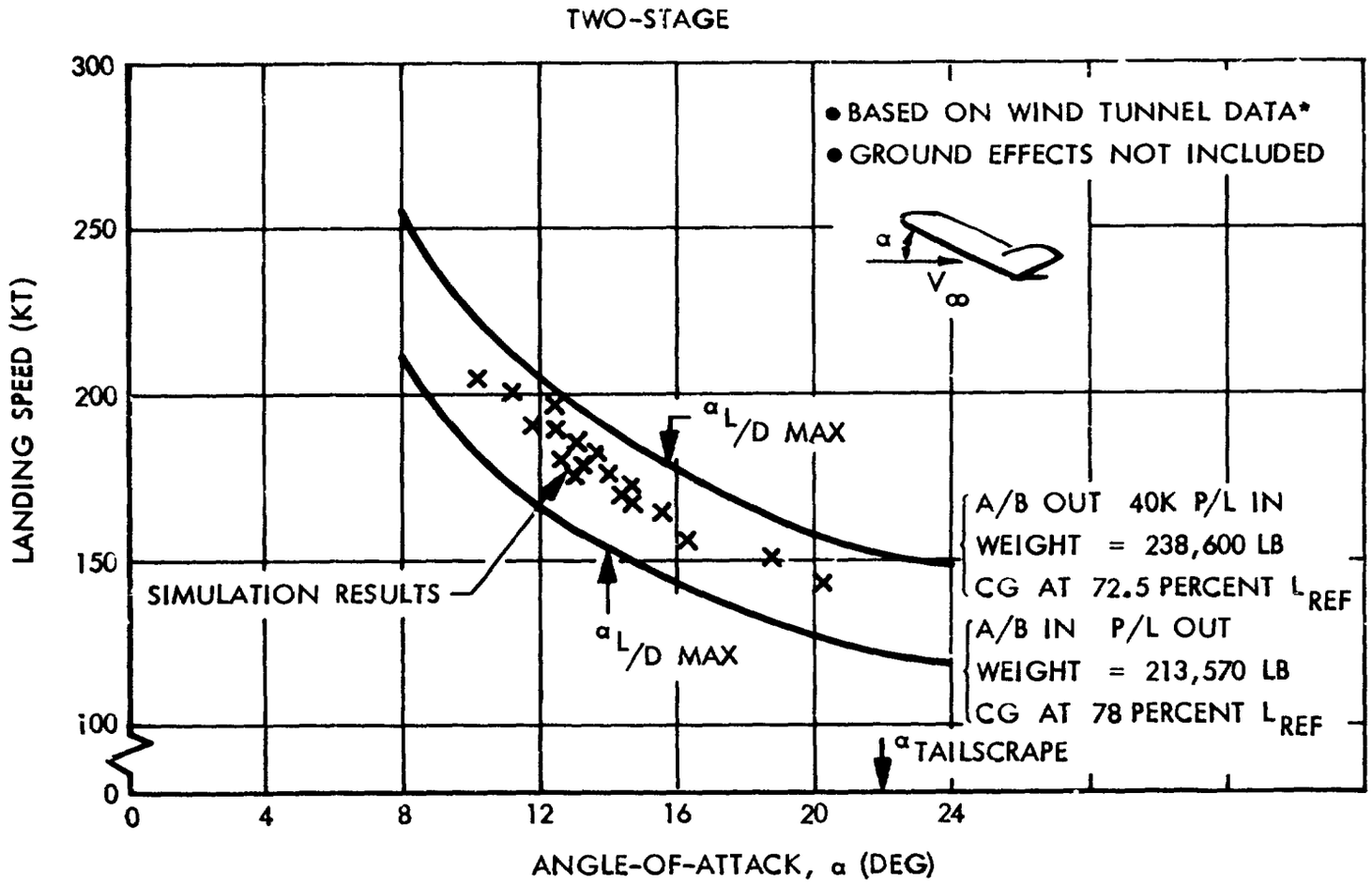

FIG. 8

6-9

*LOCKHEED 8 FT X 12 FT WIND TUNNEL TEST NO. L-324

D03068

GROUND PLANE INSTALLATION

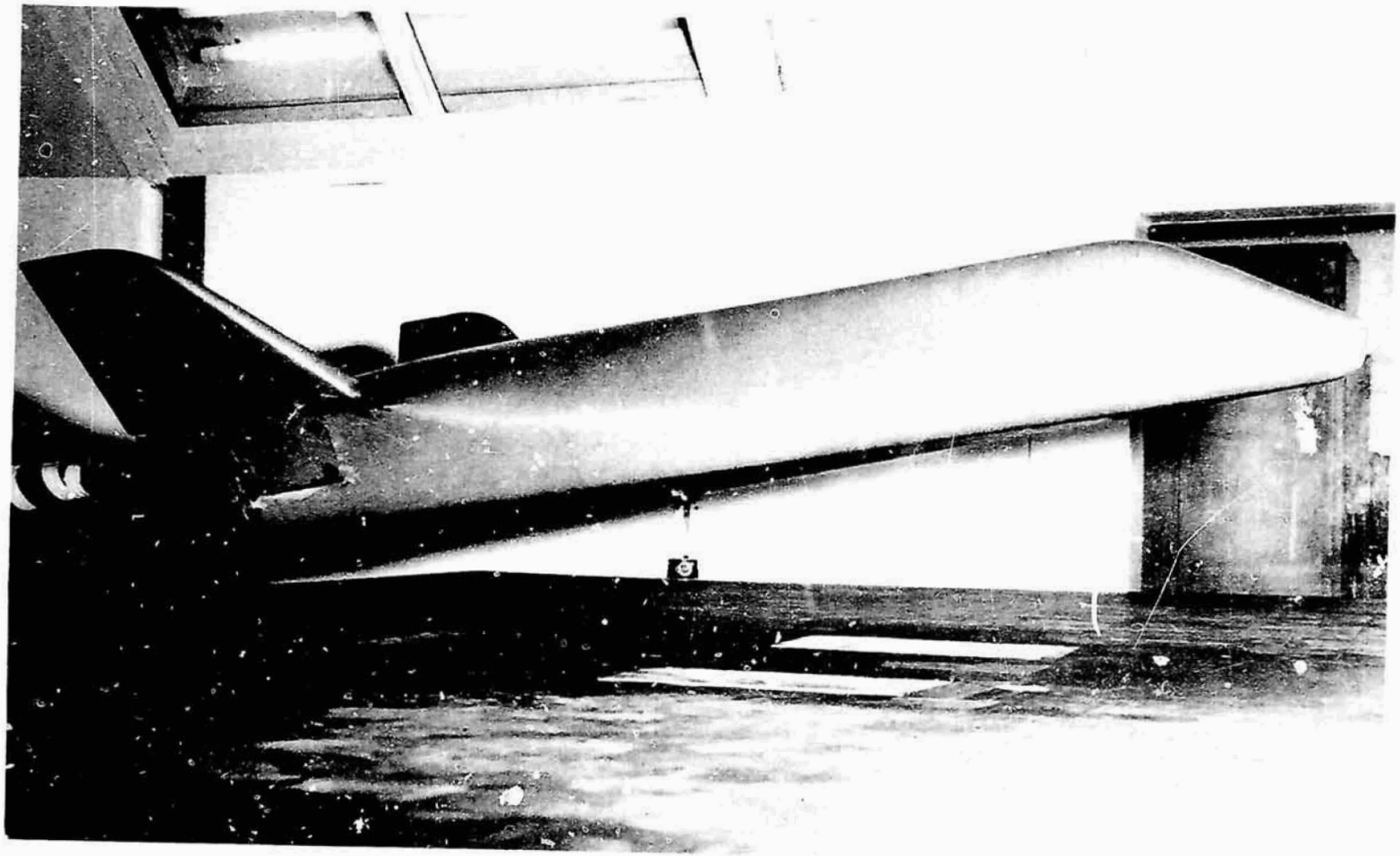

FIG. 9

D02777

F4V

α = 10 DEG

GROUND EFFECTS

$M_\infty = 0.23$*

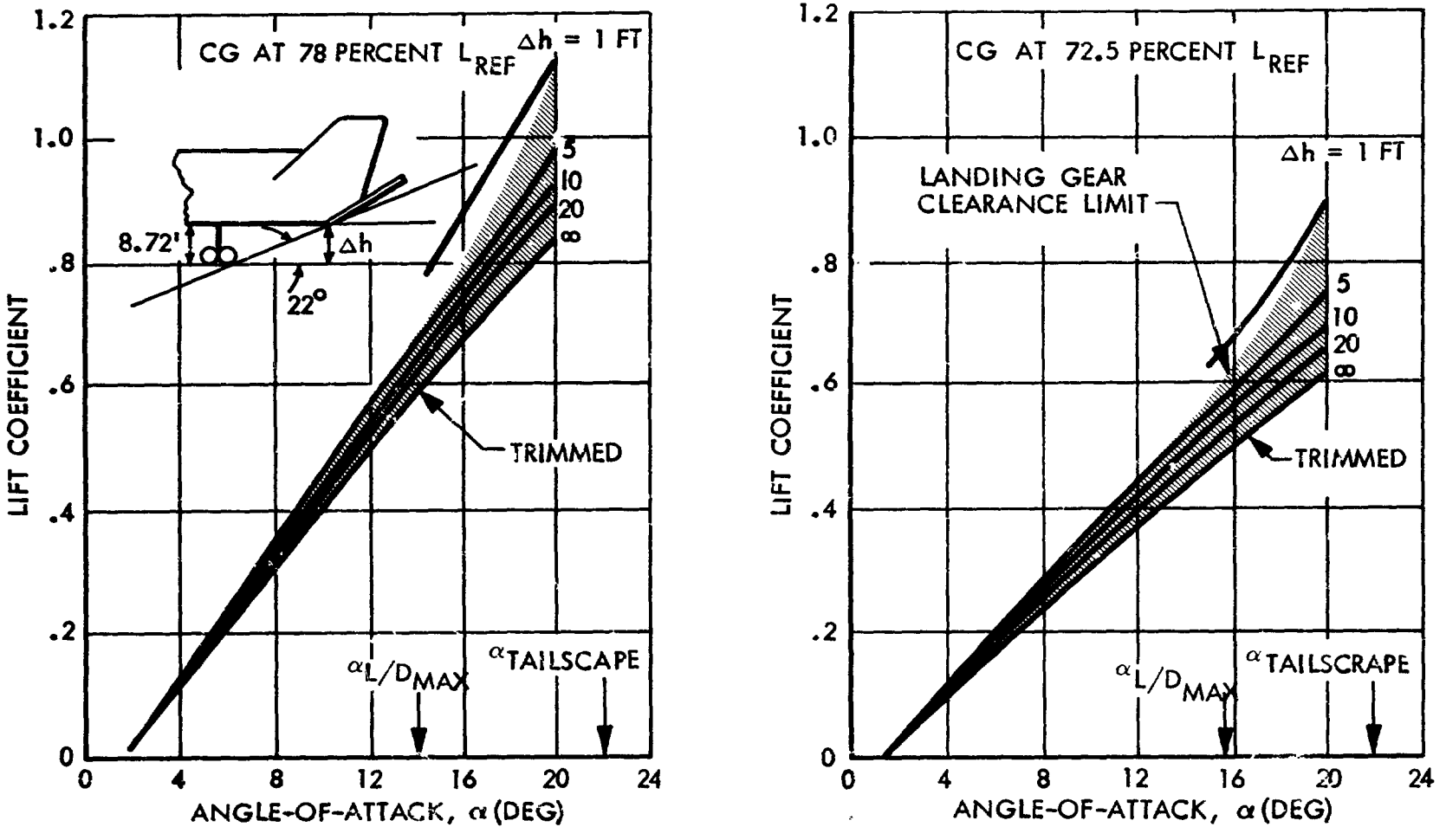

FIG. 10

*LOCKHEED 8 FT X 12 FT WIND TUNNEL TEST NO. L-324

DC3351

LANDING SPEED AND ATTITUDE IN GROUND EFFECT

2-STAGE

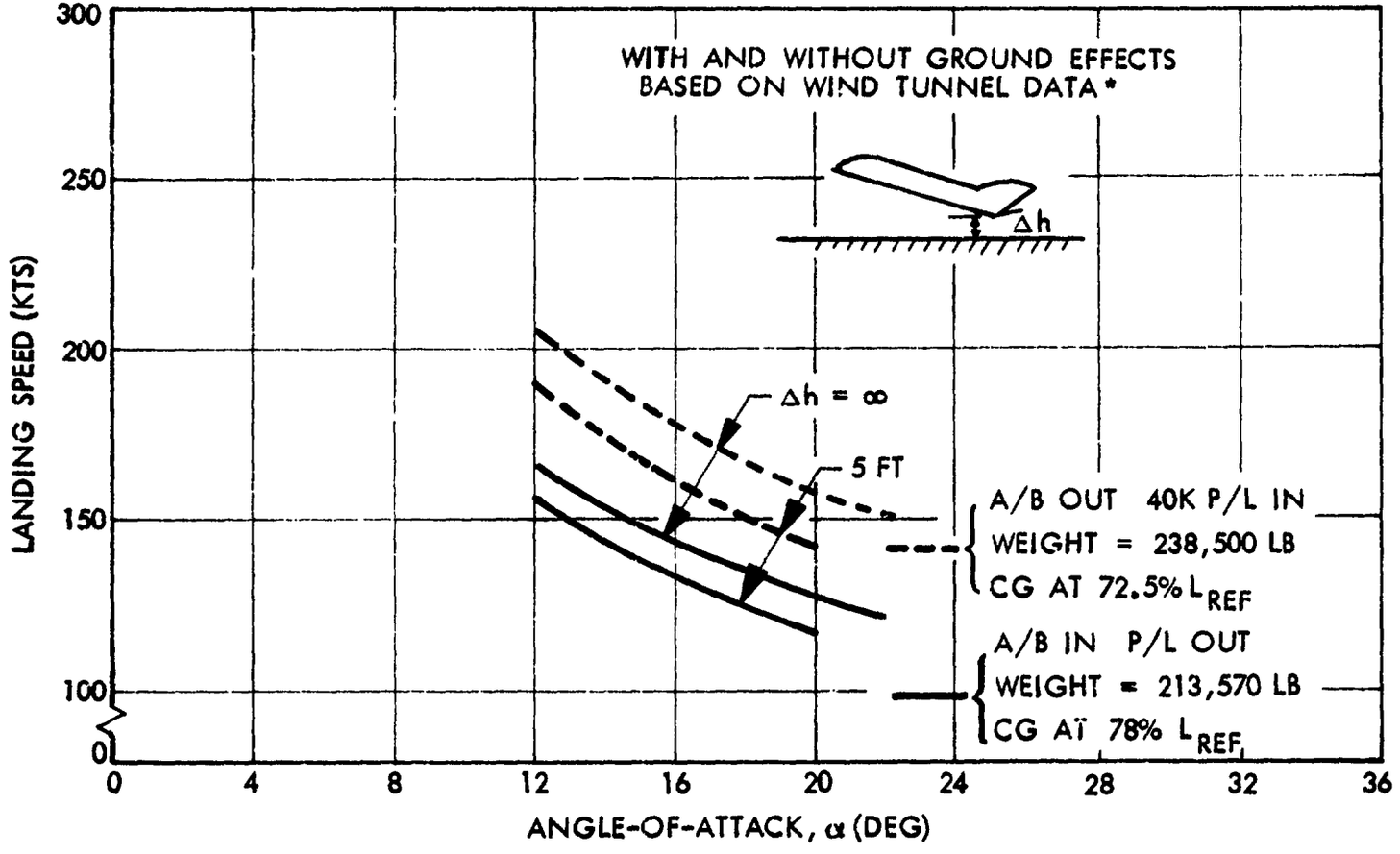

*LOCKHEED 8 FT X 12 FT WIND TUNNEL TEST NO. L-324

FIG. 11
6-12

D03352

DIRECTIONAL STABILITY CRITERIA

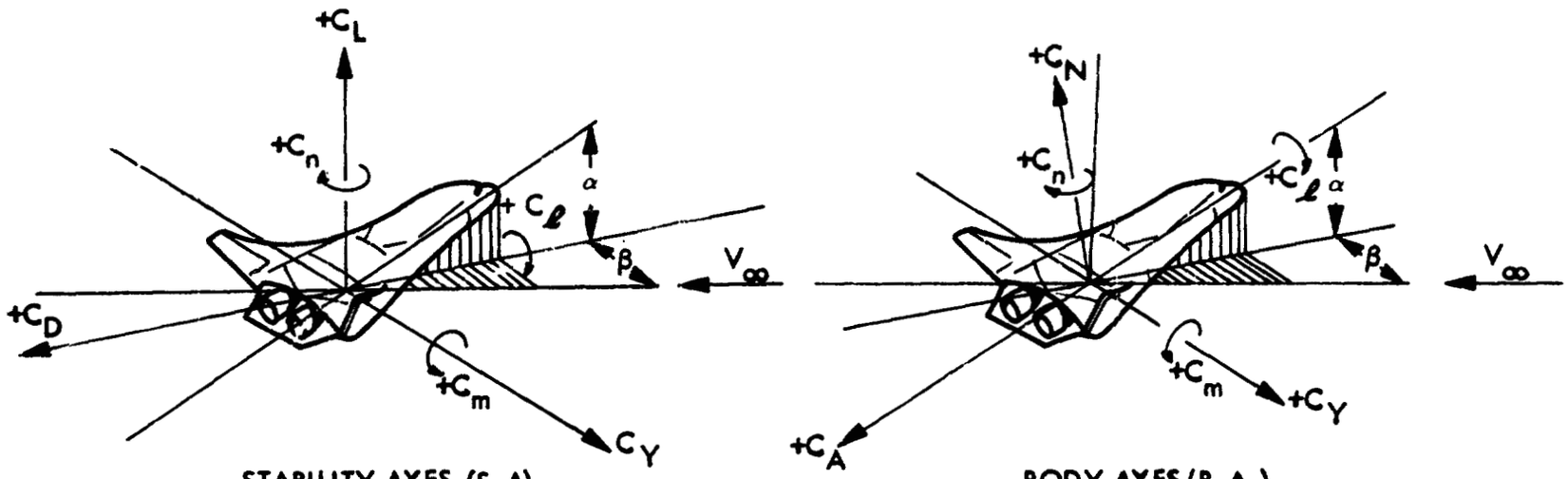

STABILITY AXES (S.A) BODY AXES (B.A.)

FIG. 12

$$C_{n_\beta}{}_{S.A} = C_{n_\beta}{}_{B.A.} \cos\alpha - C_{\ell_\beta}{}_{B.A.} \sin\alpha$$

$$C_{n_\beta}{}_{DYNAMIC} = C_{n_\beta}{}_{B.A.} \cos\alpha - C_{\ell_\beta}{}_{B.A.} \frac{I_{zz}}{I_{xx}} \sin\alpha$$

NOTING THAT UNDAMPED NATURAL FREQUENCY OF THE DUTCH ROLL MODE (ω_D)

$$\omega_D = \left[(q_\infty A_{REF} L_{REF} / I_{zz}) C_{n_\beta}{}_{DYNAMIC} \right]^{1/2}$$

D02812

fav

DIRECTIONAL STABILITY

$M_\infty = 0.23^{**}$

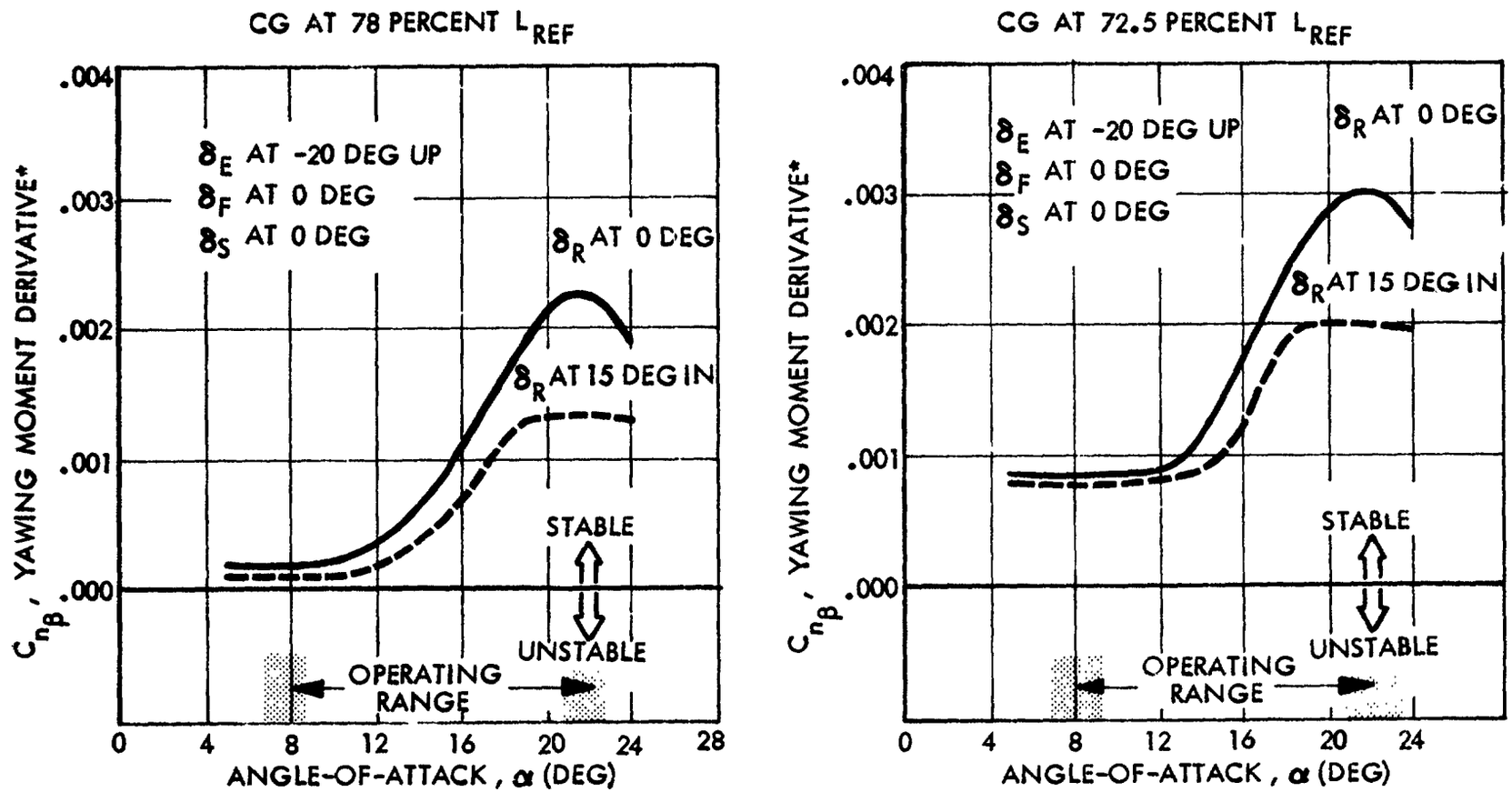

FIG. 13

*STABILITY AXIS, BASED ON L_{REF}

**LOCKHEED 8 FT X 12 FT WIND TUNNEL TEST NO. L-324

D03353

DIRECTIONAL STABILITY

$M_\infty = 0.23$*

δ_E AT 20 DEG UP
δ_F AT 0 DEG
δ_S AT 0 DEG

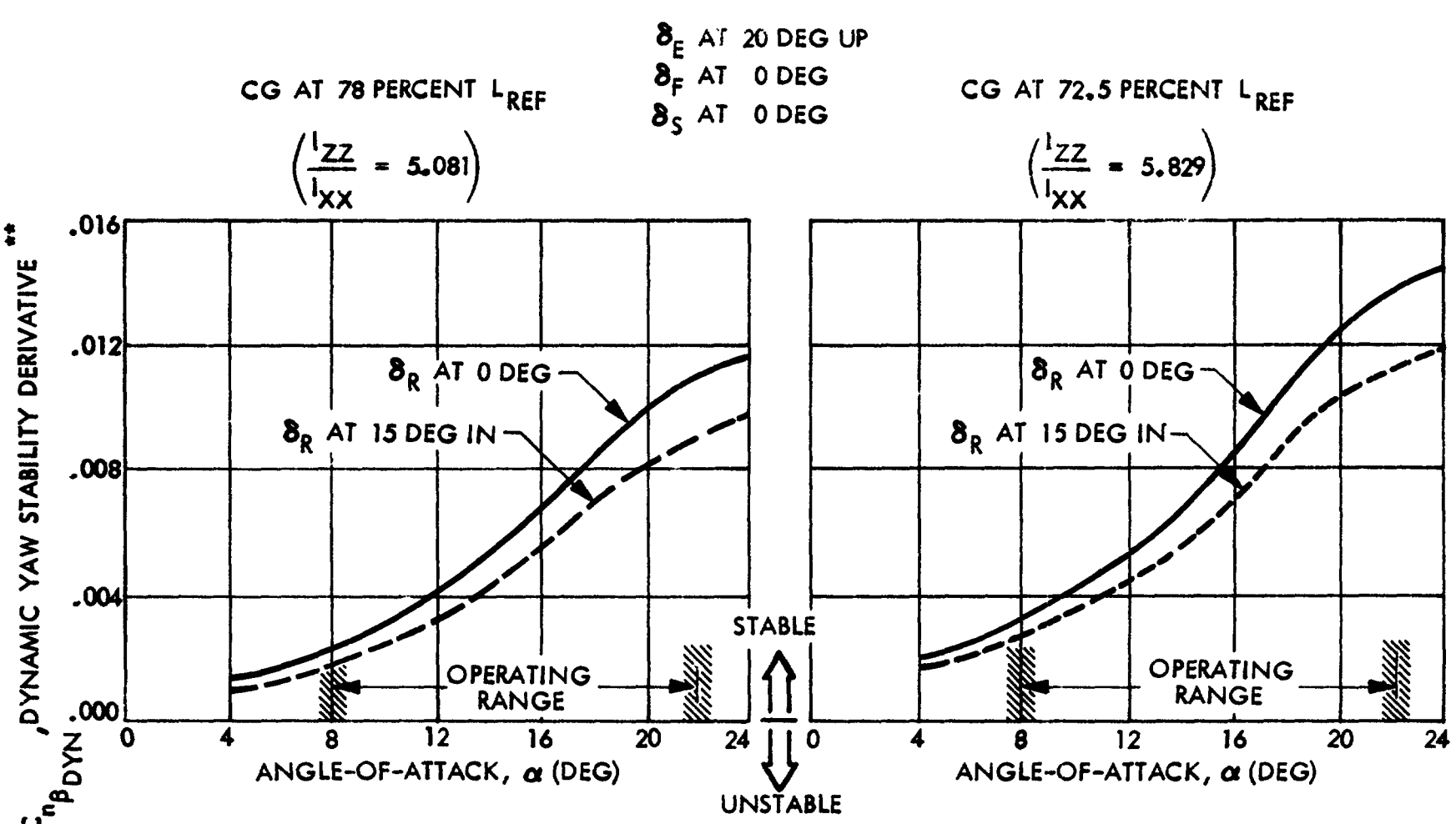

*LOCKHEED 8 FT X 12 FT WIND TUNNEL TEST NO. L-324
**BASED ON L_{REF}

D03354

FIG. 14
6-15

SIDE FORCE AND ROLLING MOMENT DERIVATIVES

$M_\infty = 0.23$*

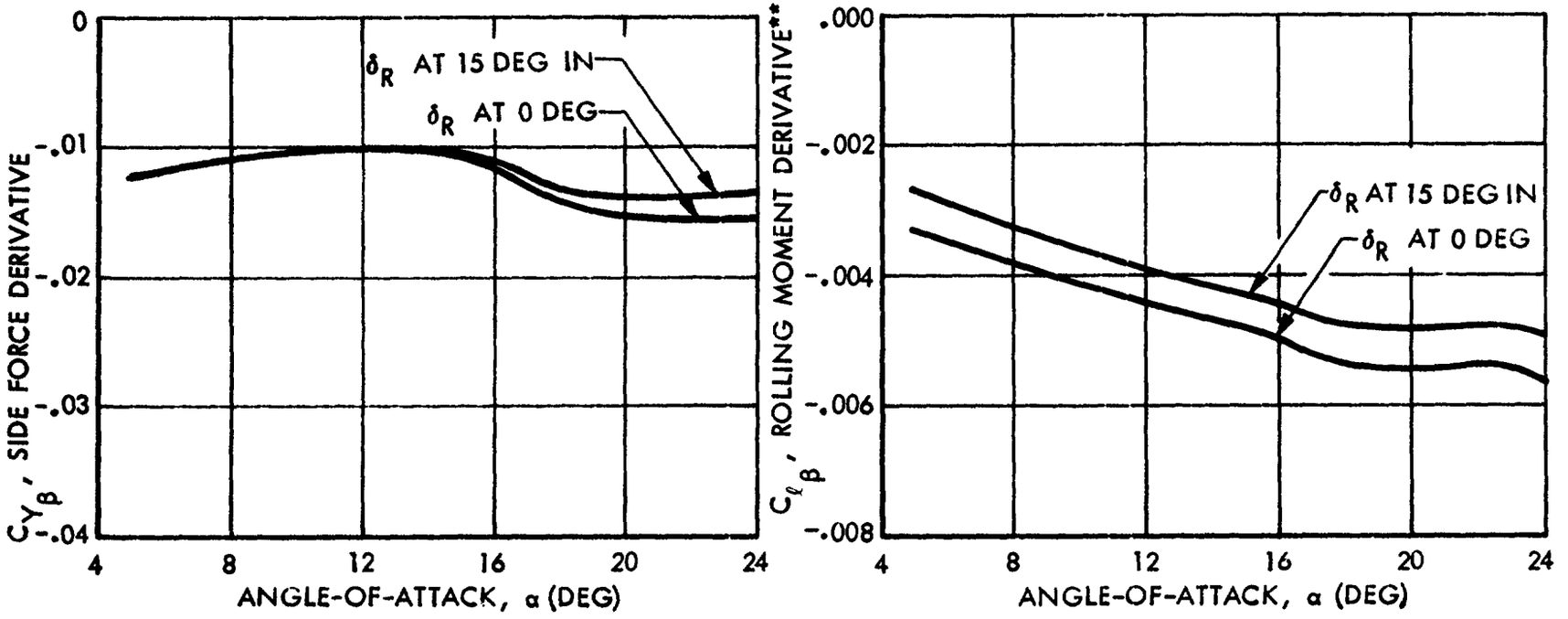

FIG. 15
6-16

*LOCKHEED 8 FT X 12 FT WIND TUNNEL TEST NO. L-324
**STABILITY AXIS, BASED ON L_{REF}

D03355

UPPER ELEVON ROLL-YAW COUPLING

$M_\infty = 0.23$*

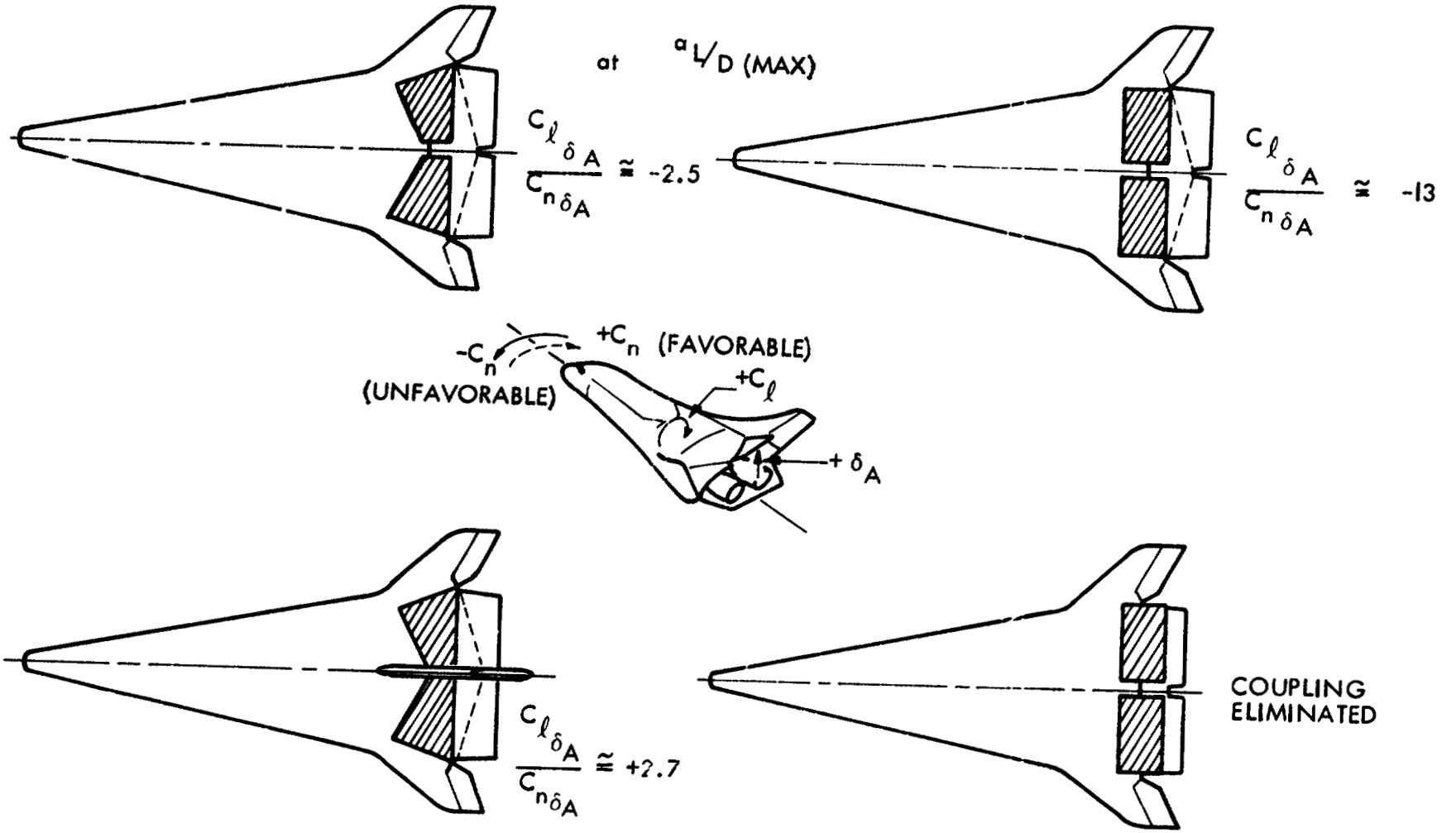

*LOCKHEED 8 FT X 12 FT WIND TUNNEL TEST NO. L-324

D02705

fav

FIG. 16
A-17

DELTA-BODY SUBSONIC FLOW VISUALIZATION

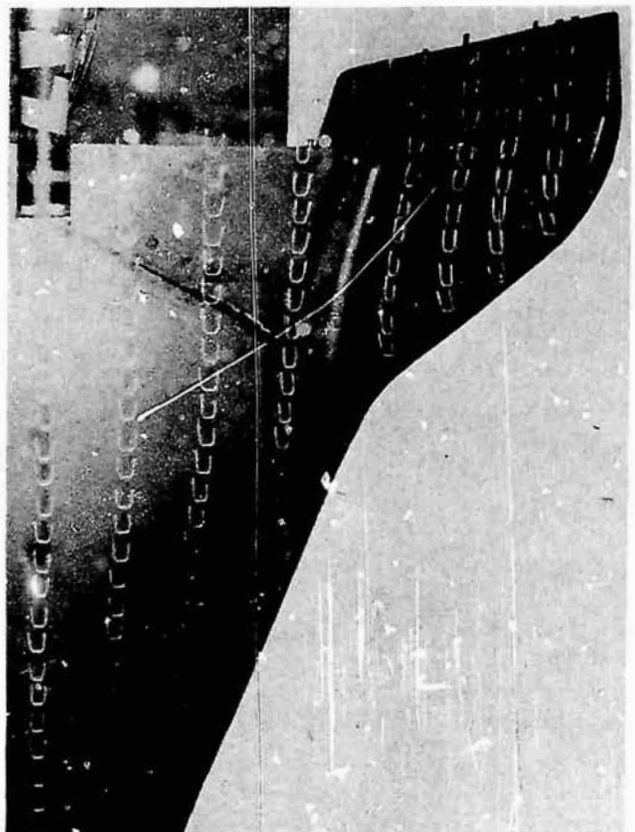

α = 5 DEG

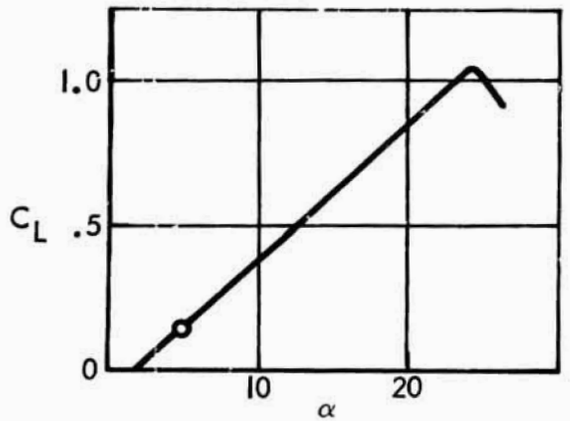

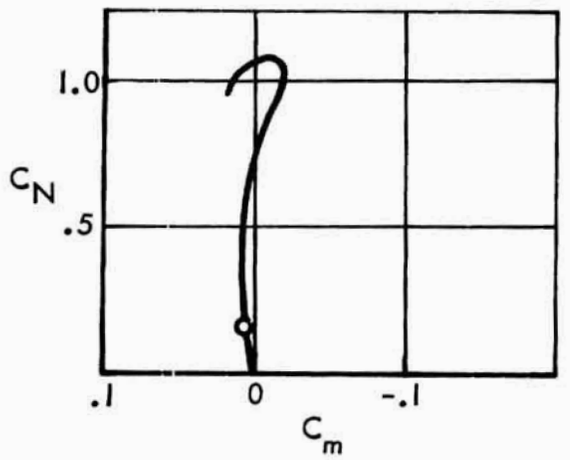

FIG. 17

D02698
fav
4-1-71

DELTA-BODY SUBSONIC FLOW VISUALIZATION

α = 10 DEG

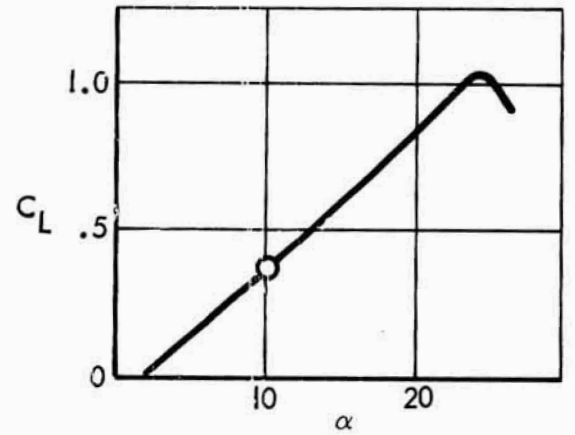

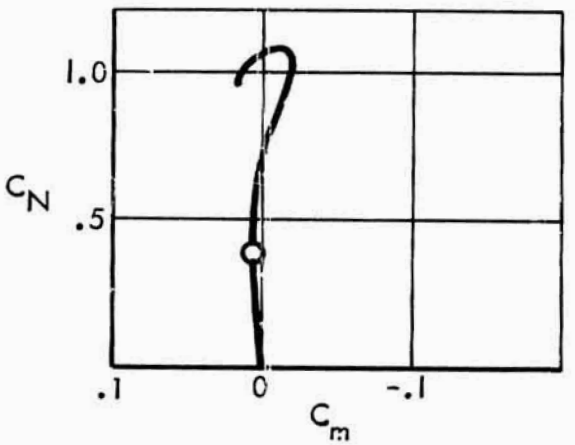

FIG. 18

D02699
fav
4-1-71

DELTA-BODY SUBSONIC FLOW VISUALIZATION

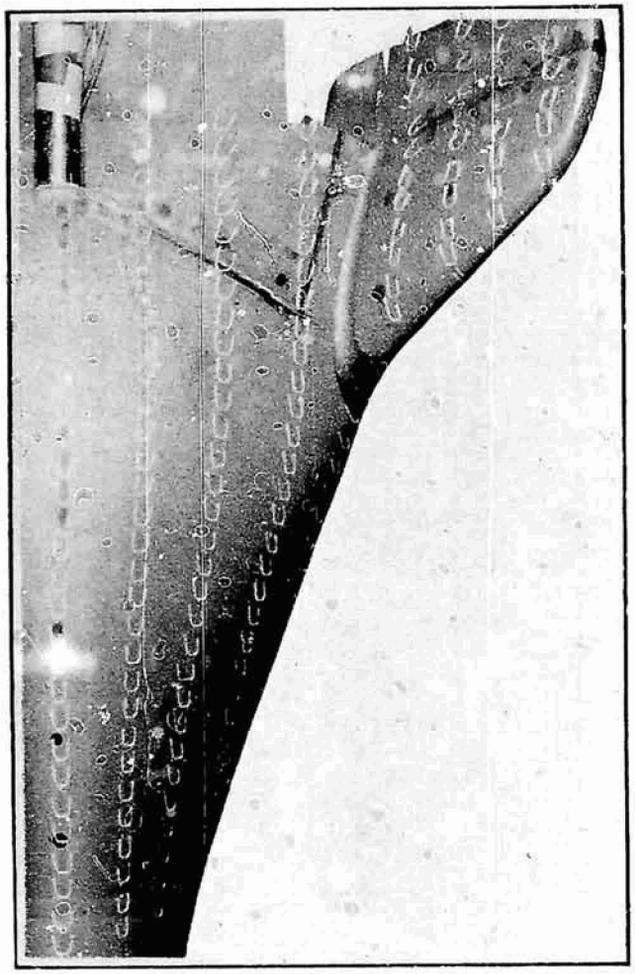

α = 15 DEG

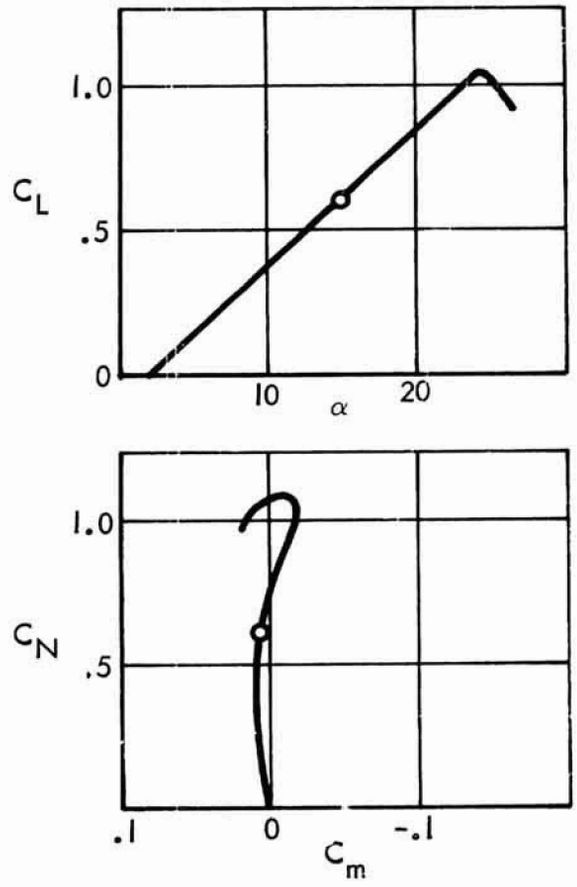

FIG. 19

D02702
fav
4-1-71

DELTA-BODY SUBSONIC FLOW VISUALIZATION

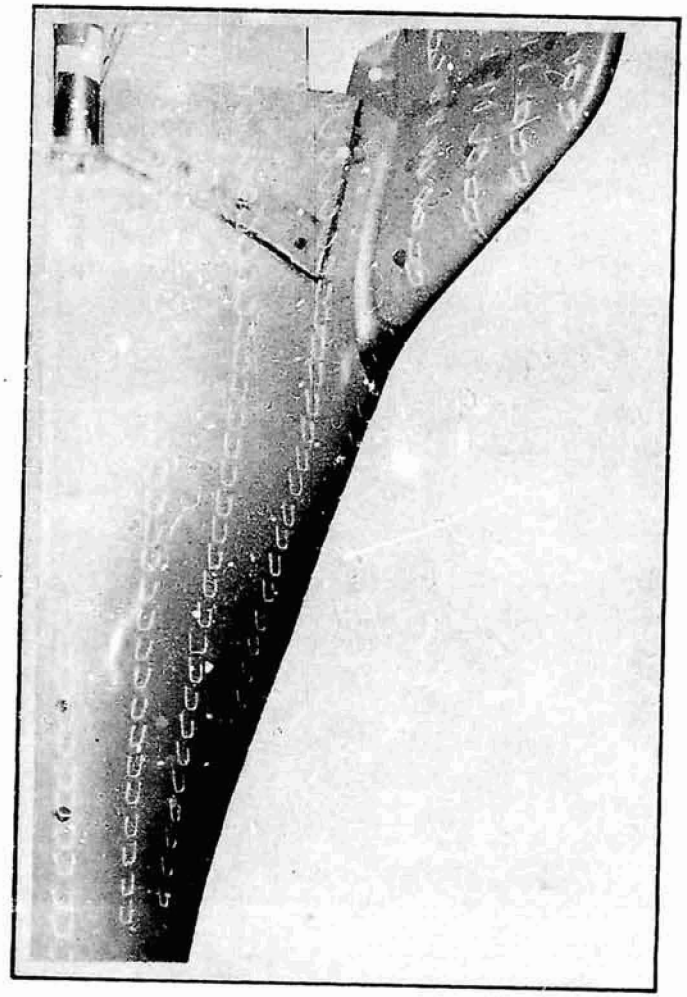

α = 20 DEG

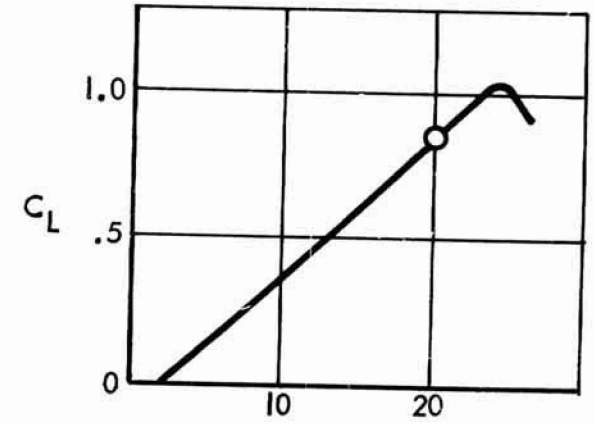

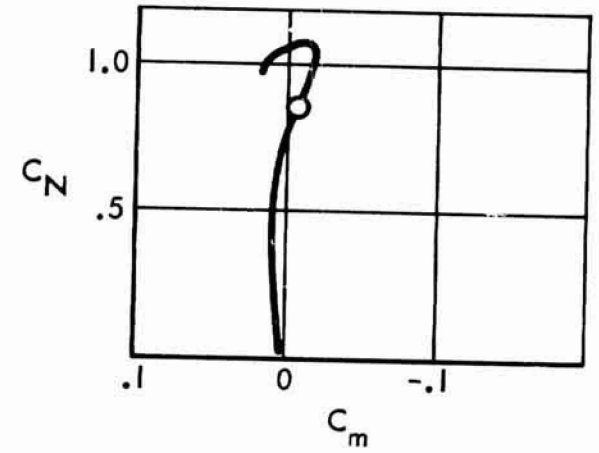

FIG. 20

6-21

D02700
fav
4-1-71

DELTA-BODY SUBSONIC FLOW VISUALIZATION

α = 25 DEG

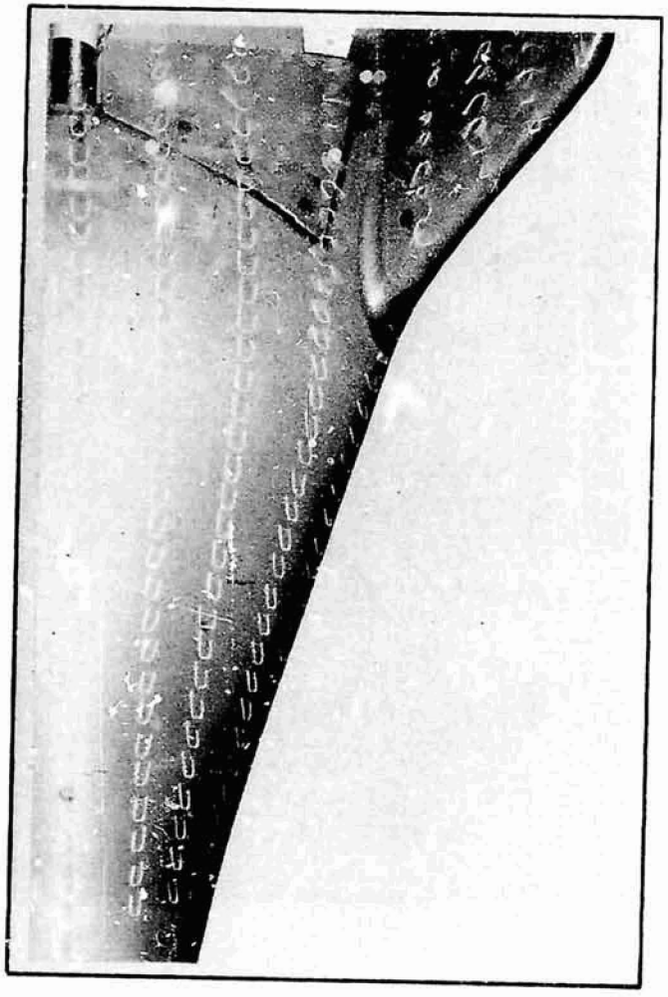

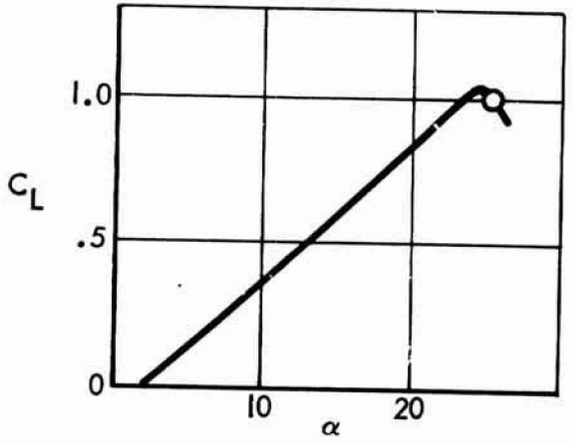

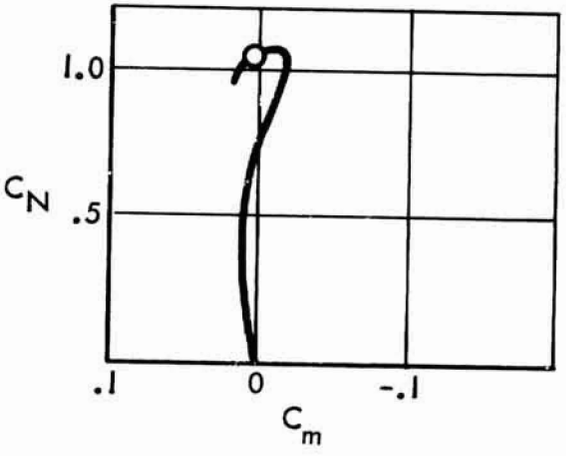

FIG. 21
6-22

D02701
fav
4-1-71

LOCKHEED MISSILES & SPACE COMPANY

ORBITER CONFIGURATION

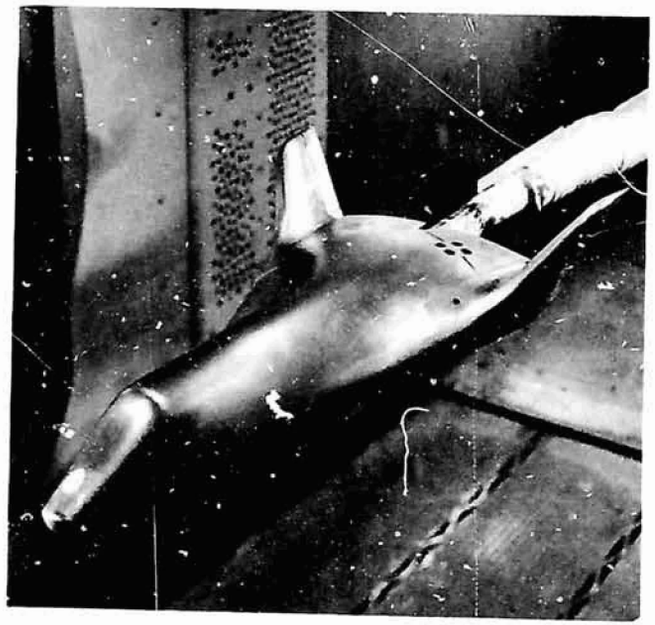

FIG. 22

	ORBITER	
TEST FACILITY	AMES 6 x 6 FT	LaRC-UPWT
RUNS	67	84
MACH NUMBER	0.60 to 2.0	2.3 TO 4.6
ANGLE-OF-ATTACK (DEG)	-4 TO 22	0 TO 60
SIDESLIP ANGLE (DEG)	-4 TO 10	-4 TO 10
REYNOLDS NUMBER PER FOOT	2.5×10^6 TO 4.0×10^6	2.5×10^6 TO 4.5×10^6

LONGITUDINAL STABILITY AND TRIM

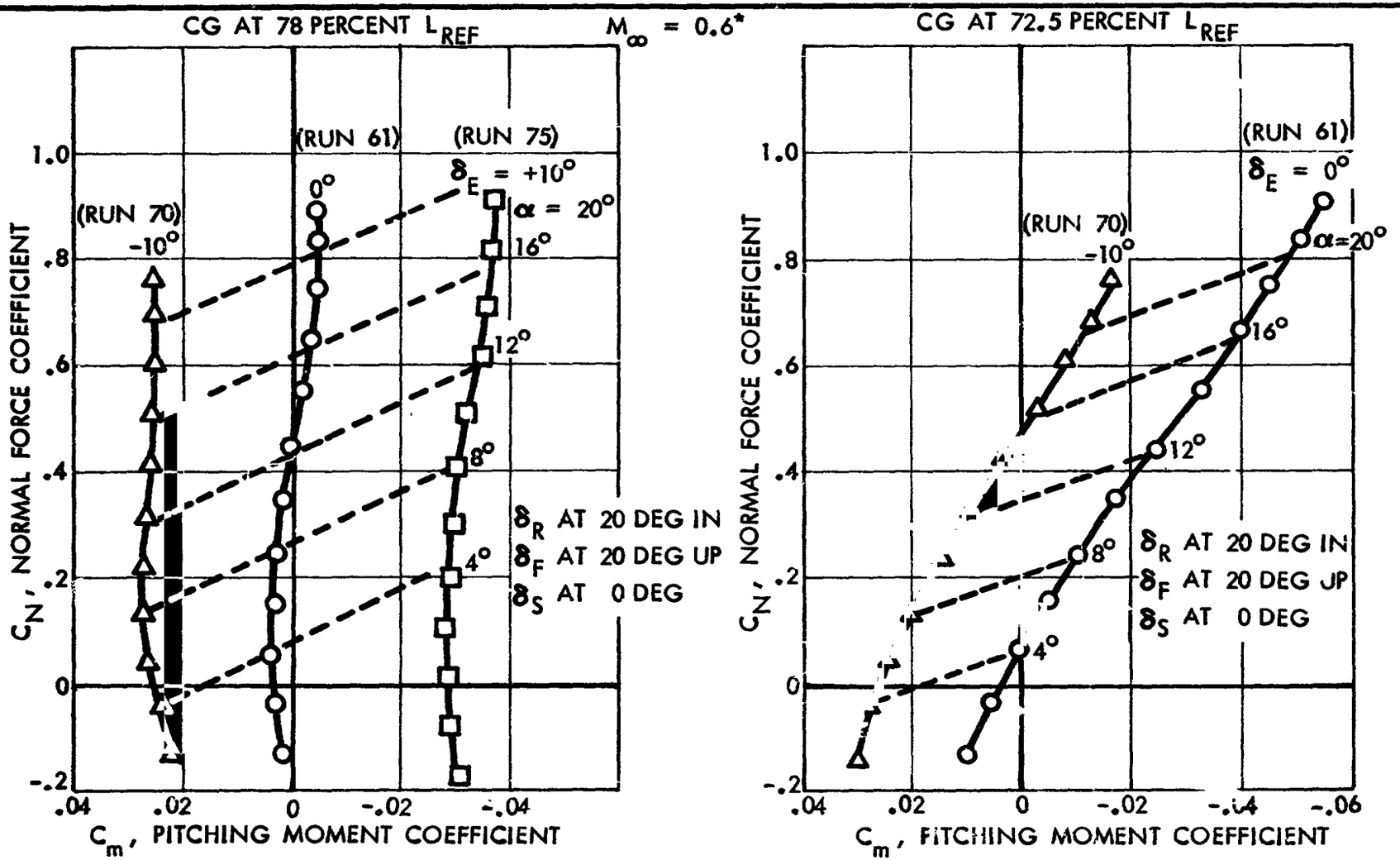

FIG. 23

*AMES 6 FT X 6 FT WIND TUNNEL TEST NO. 542

D03268

LONGITUDINAL STABILITY AND TRIM

$M_\infty = 0.9$*

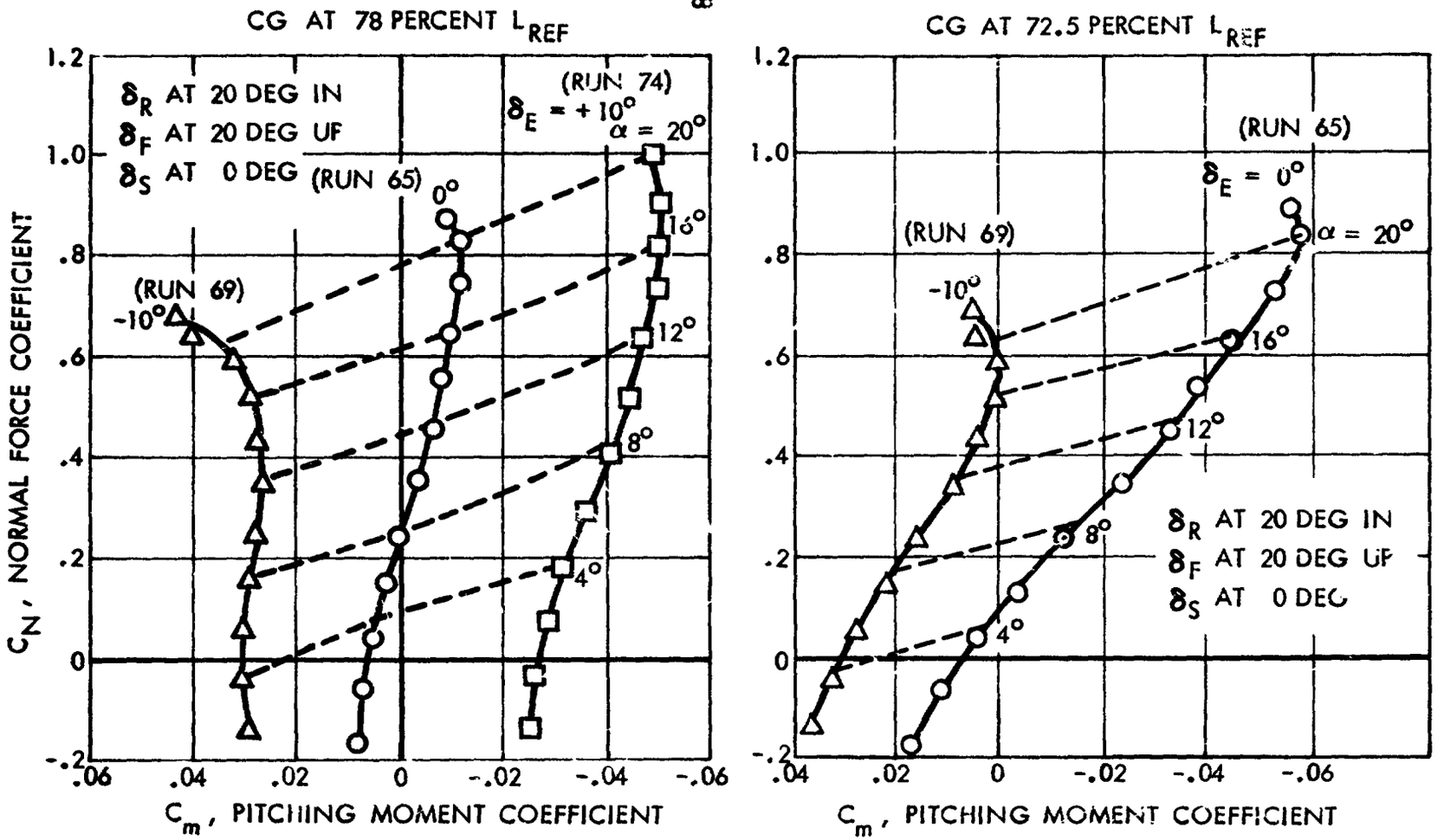

FIG. 24
6-25

*AMES 6 FT X 6 FT WIND TUNNEL TEST NO. 542

D03269

LONGITUDINAL STABILITY AND TRIM

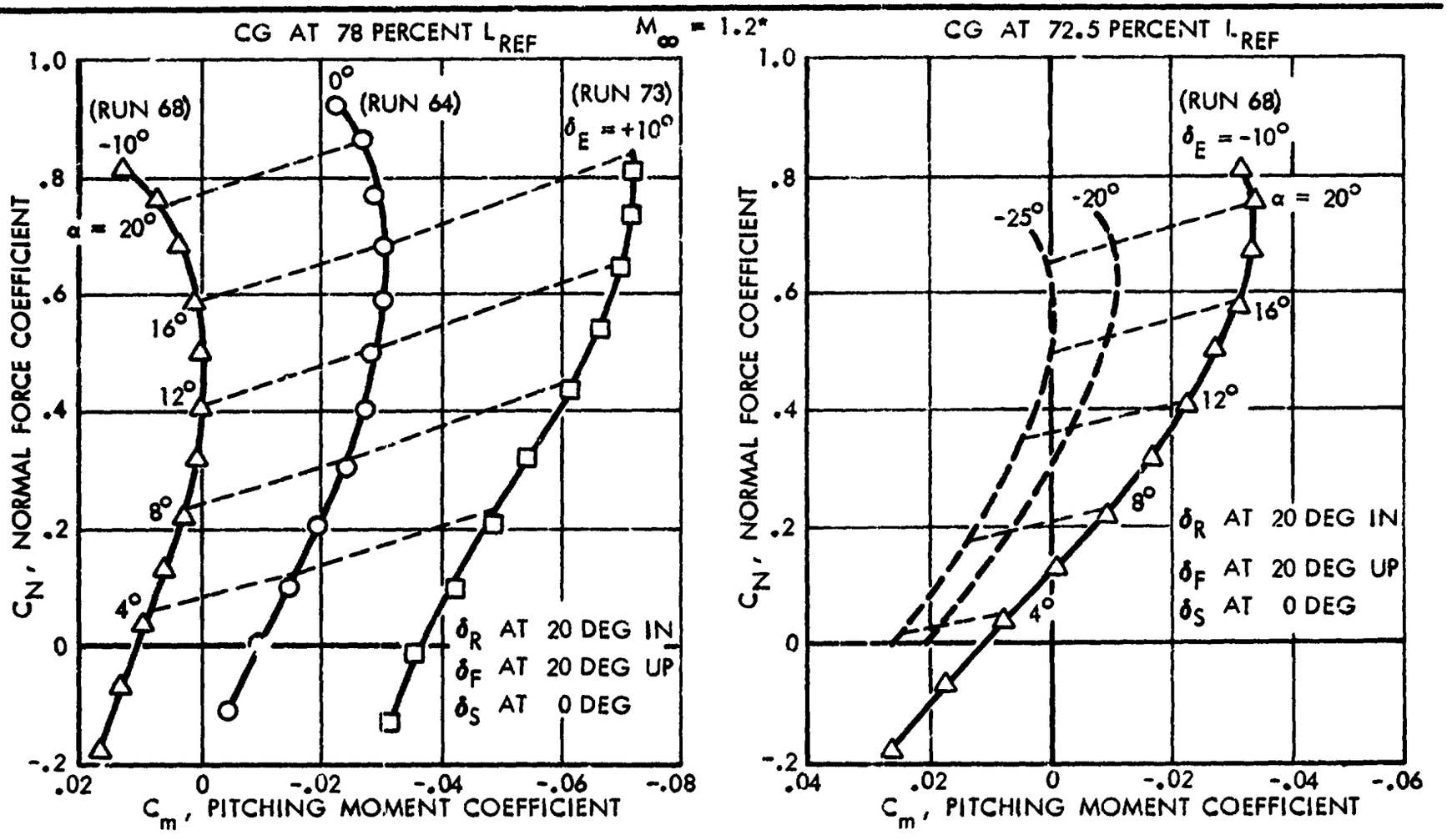

*AMES 6 FT X 6 FT WIND TUNNEL TEST NO. 542

FIG. 25

D03270

LONGITUDINAL STABILITY AND TRIM

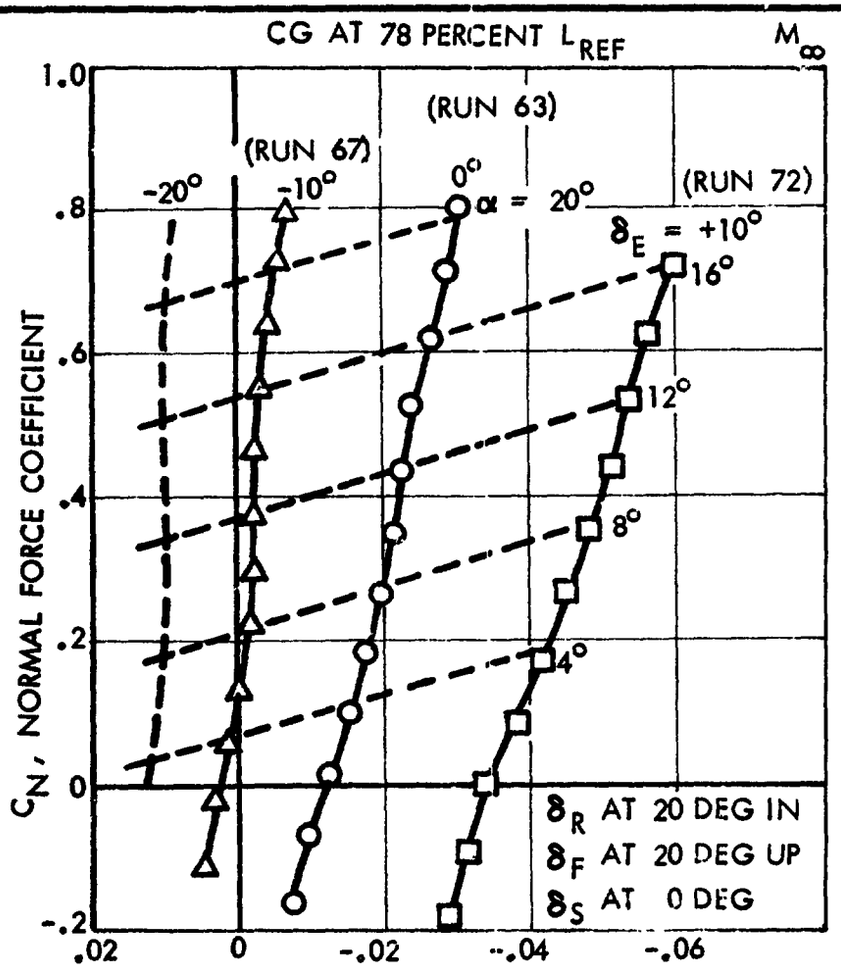

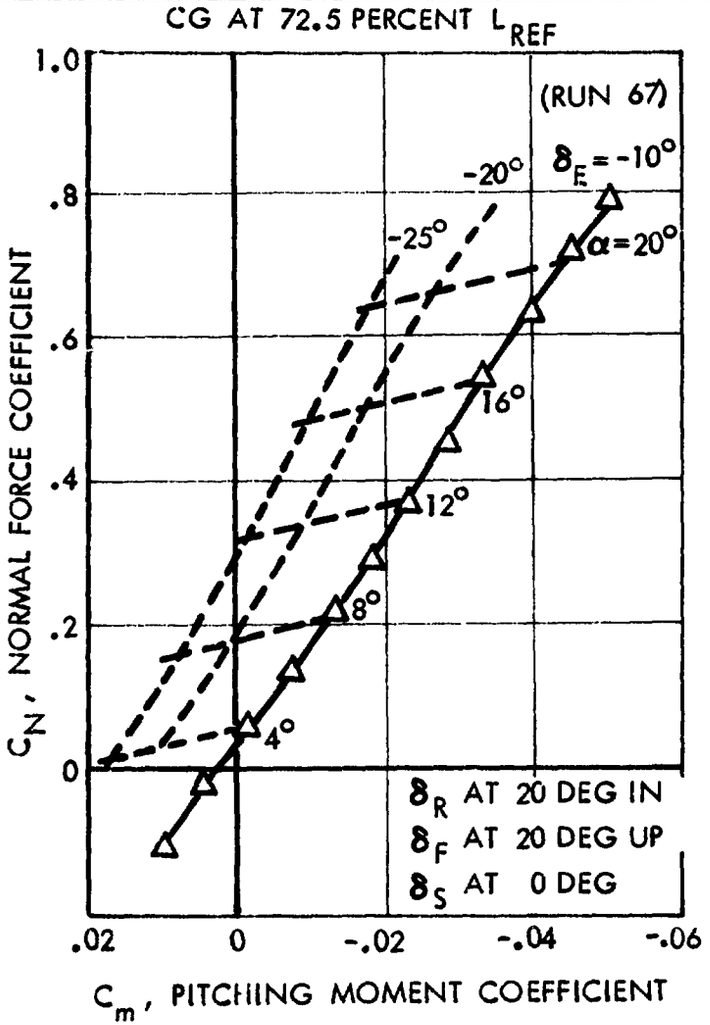

*AMES 6 FT X 6 FT WIND TUNNEL TEST NO. 542

D03271

FIG. 26

$M_\infty = 2.0$*

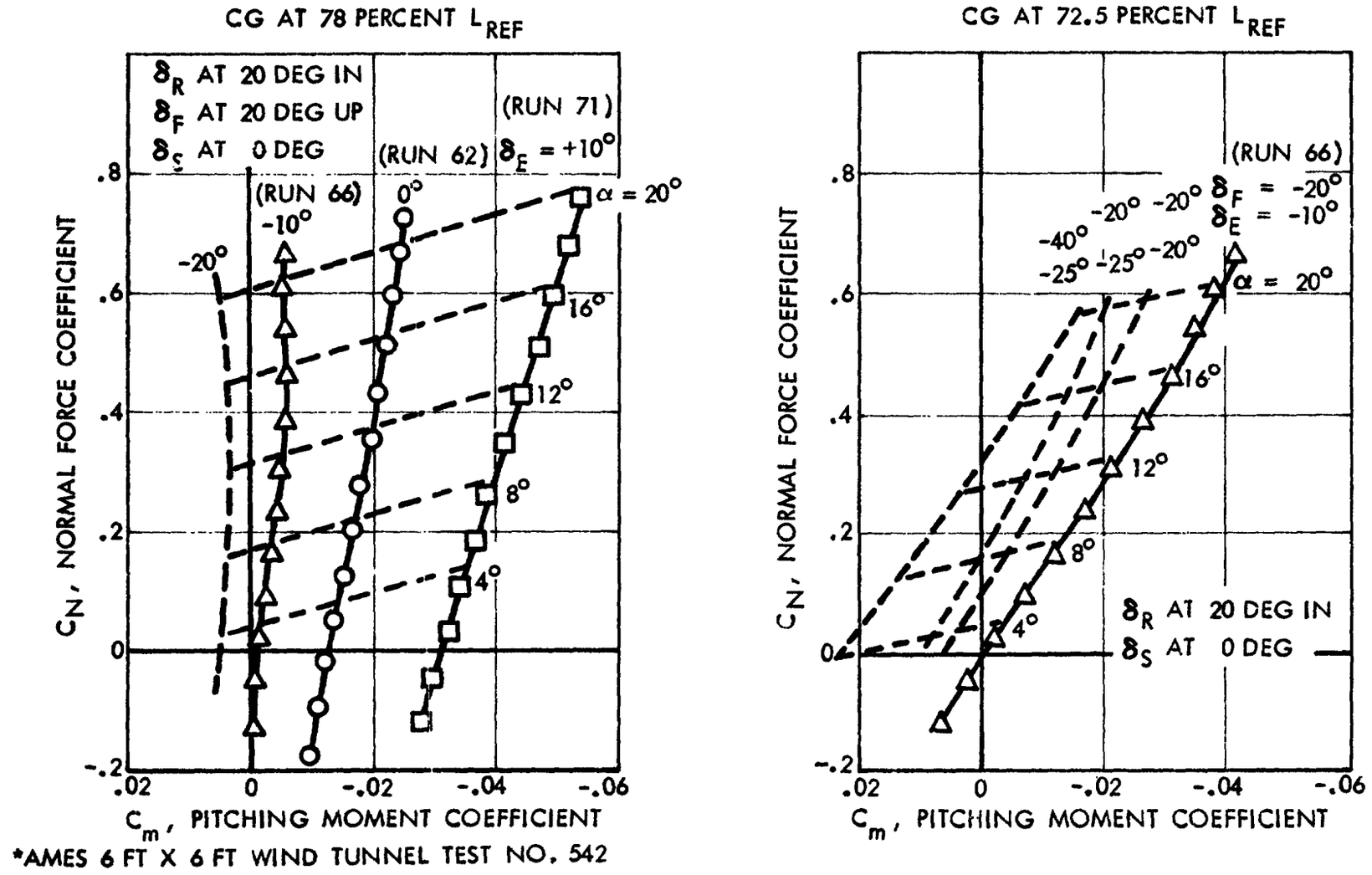

*AMES 6 FT X 6 FT WIND TUNNEL TEST NO. 542

D03272

FIG. 27

DIRECTIONAL STABILITY

α = 7.6 DEG

REFERENCE: AMES 6 X 6 TUNNEL
TEST NO. 542
δ_E AT 0 DEG
δ_F AT 20 DEG UP
δ_S AT 0 DEG
CG AT 78 PERCENT L_{REF}

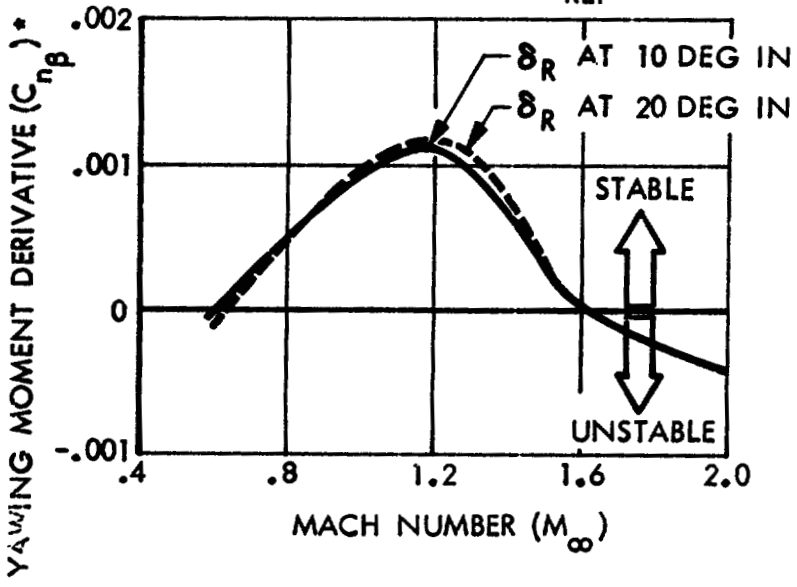

*STABILITY AXIS, BASED ON L_{REF}

REFERENCE: AMES 6 X 6 TUNNEL
TEST NO. 542
δ_E AT 0 DEG
δ_F AT 20 DEG UP
δ_S AT 0 DEG
CG AT 72.5 PERCENT L_{REF}

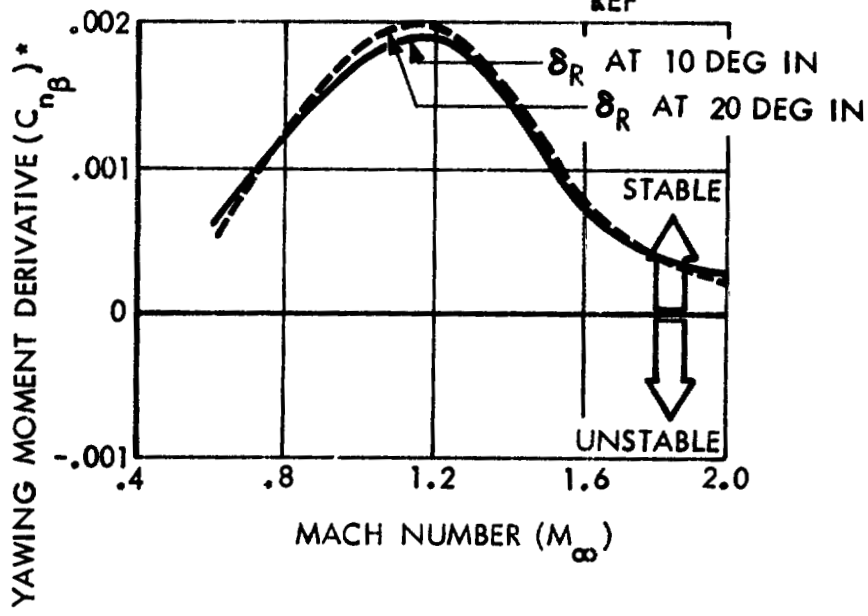

*STABILITY AXIS, BASED ON L_{REF}

D03229

FIG. 28

DIRECTIONAL STABILITY

α = 7.6 DEG*

δ_E AT 0 DEG
δ_F AT 20 DEG UP
δ_S AT 0 DEG

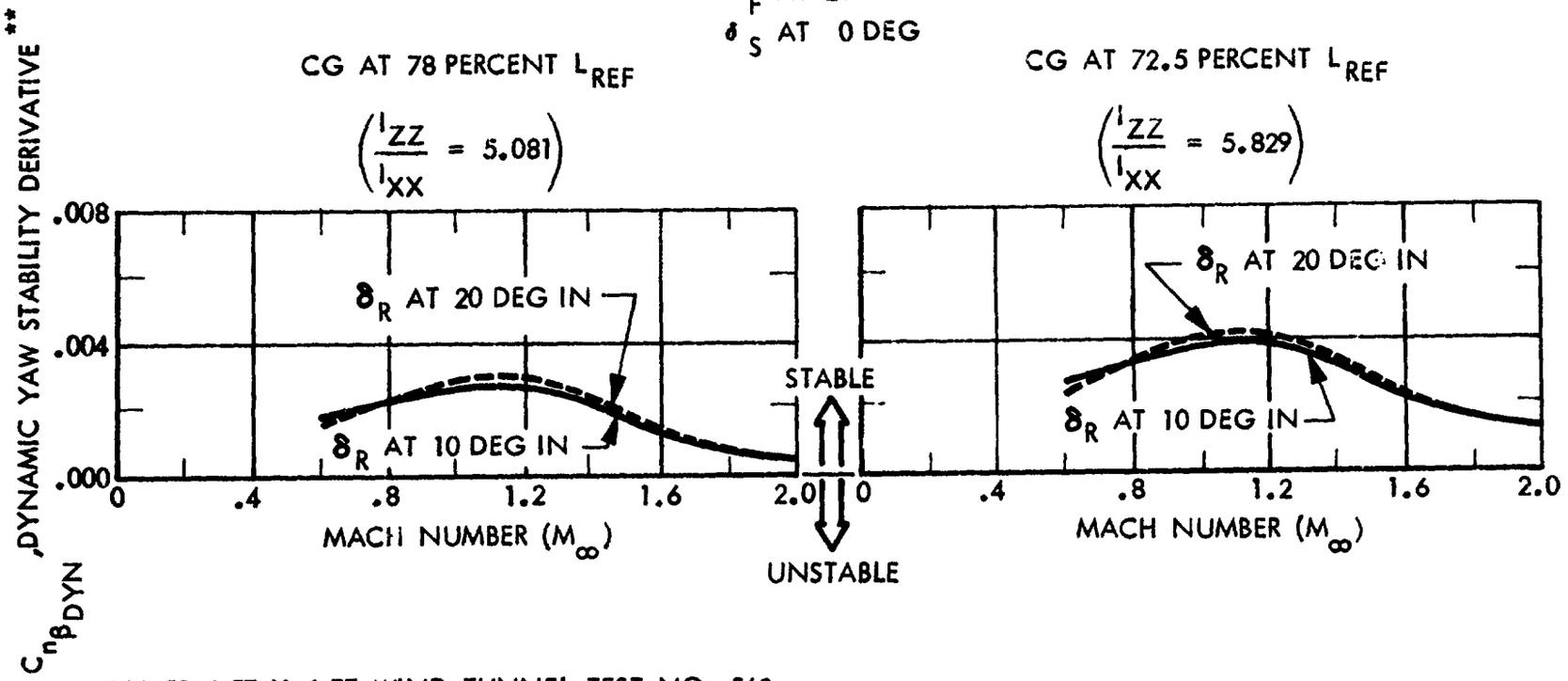

FIG. 29

*AMES 6 FT X 6 FT WIND TUNNEL TEST NO. 542
**BASED ON L_{REF}

D03356

SIDE FORCE AND ROLLING MOMENT DERIVATIVES

α = 7.6 DEG

δ_E AT 0 DEG

δ_F AT 20 DEG UP

δ_S AT 0 DEG

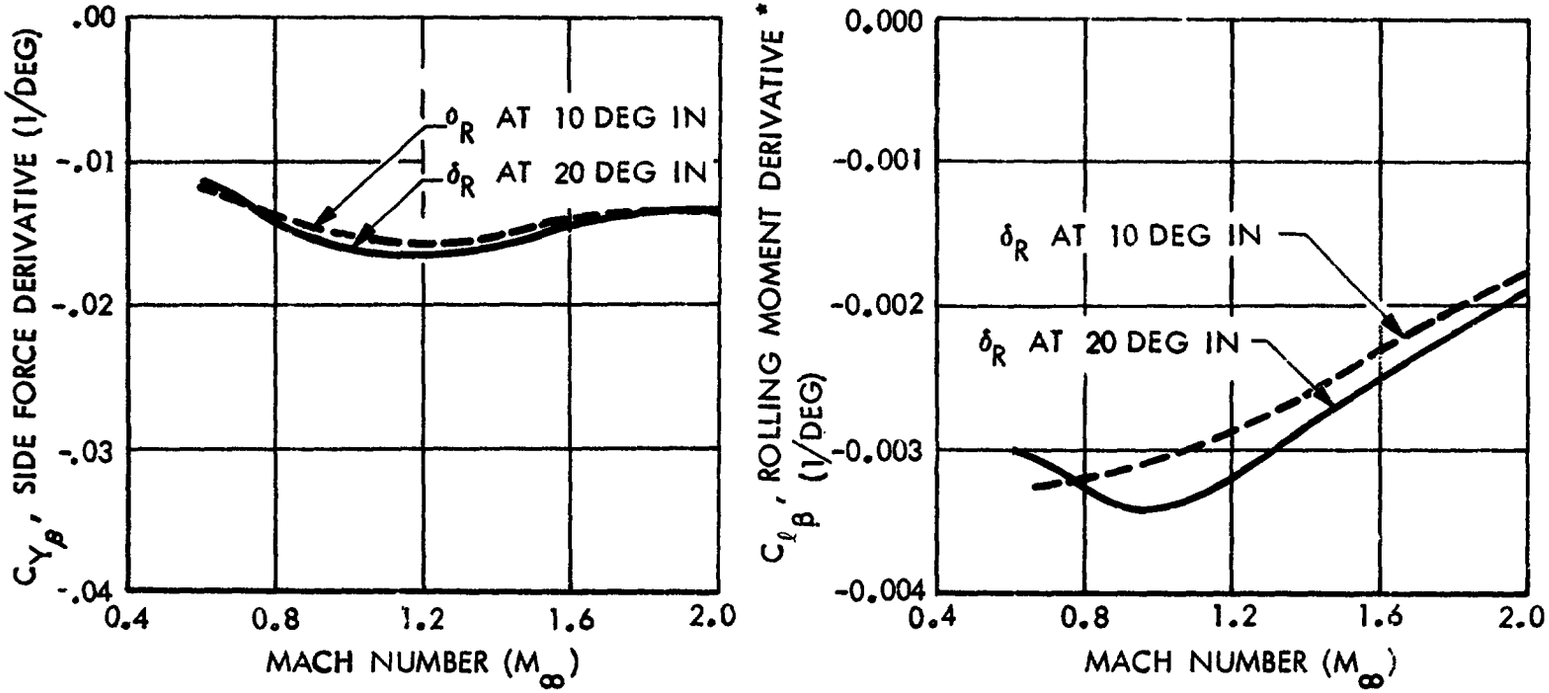

AMES 6 X 6 FT WIND TUNNEL TEST NO. 542

*STABILITY AXIS, BASED ON L_{REF}

FIG. 30

D03357

DIRECTIONAL STABILITY

α = 15.3 DEG

CG AT 78% L_{REF}

REFERENCE: AMES 6 X 6 TUNNEL
TEST NO. 542

δ_E AT 0 DEG
δ_F AT 20 DEG UP
δ_S AT 0 DEG

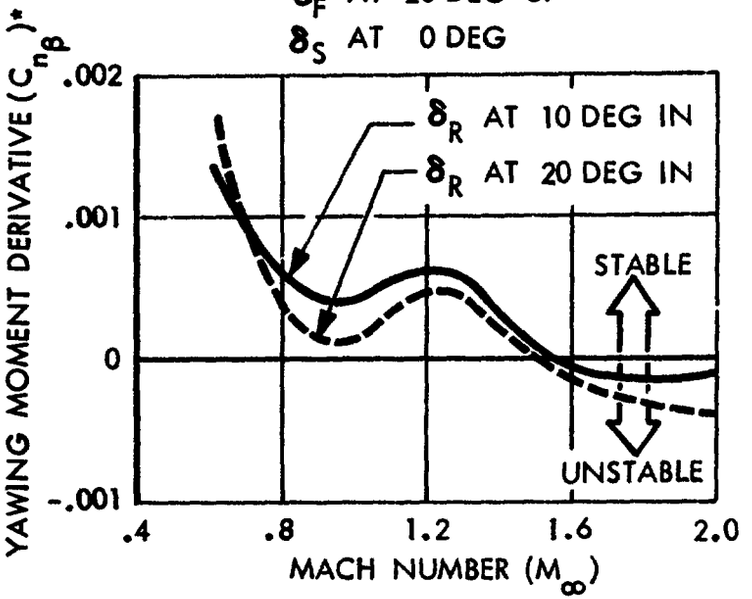

*STABILITY AXIS, BASED ON L_{REF}

CG AT 72.5% L_{REF}

REFERENCE: AMES 6 X 6 TUNNEL
TEST NO. 542

δ_E AT 0 DEG
δ_F AT 20 DEG UP
δ_S AT 0 DEG

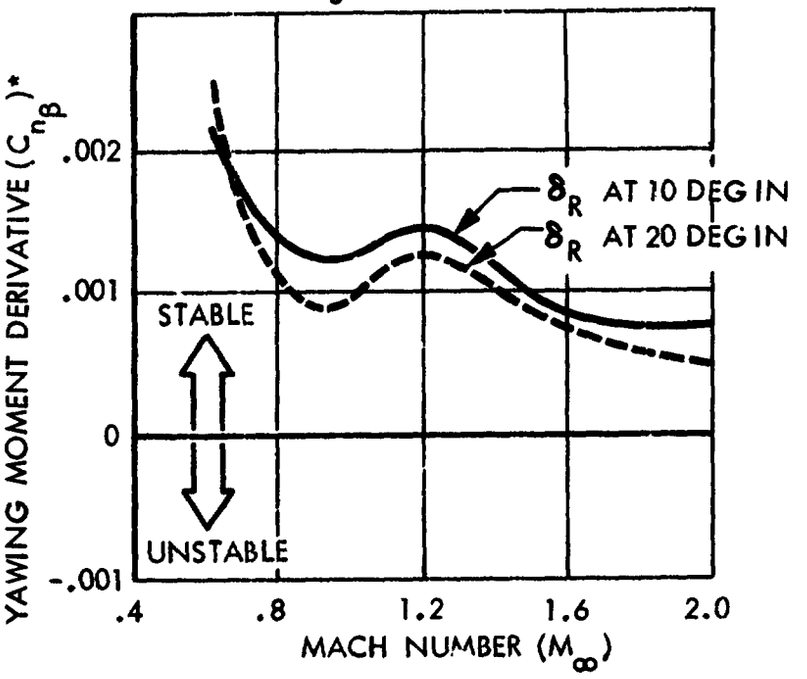

*STABILITY AXIS, BASED ON L_{REF}

D03358

FIG. 31
6-32

DIRECTIONAL STABILITY

α = 15.3 DEG*

δ_E AT 0 DEG
δ_F AT 20 DEG UP
δ_S AT 0 DEG

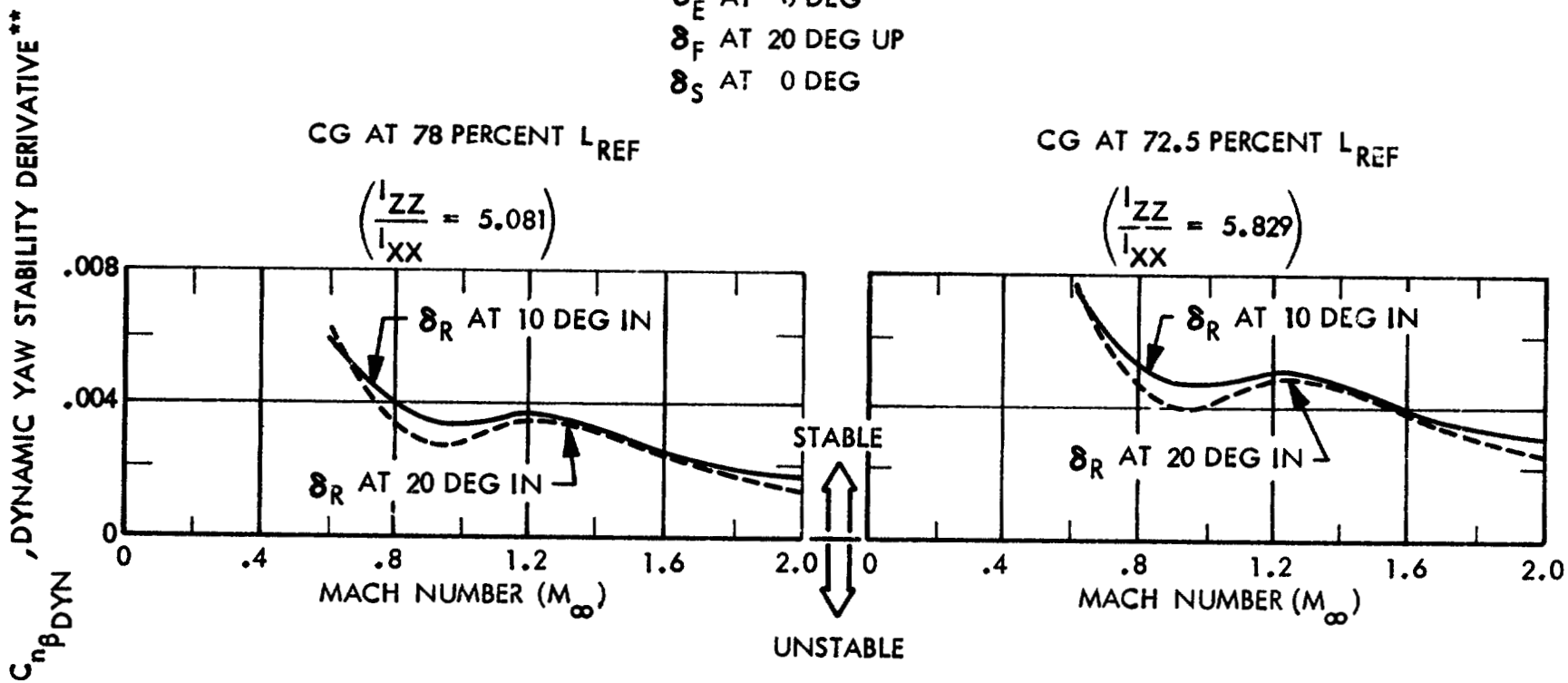

*AMES 6 FT X 6 FT WIND TUNNEL TEST NO. 542
**BASED ON L_{REF}

D03359

SIDE FORCE AND ROLLING MOMENT DERIVATIVES

α = 15.3 DEG **

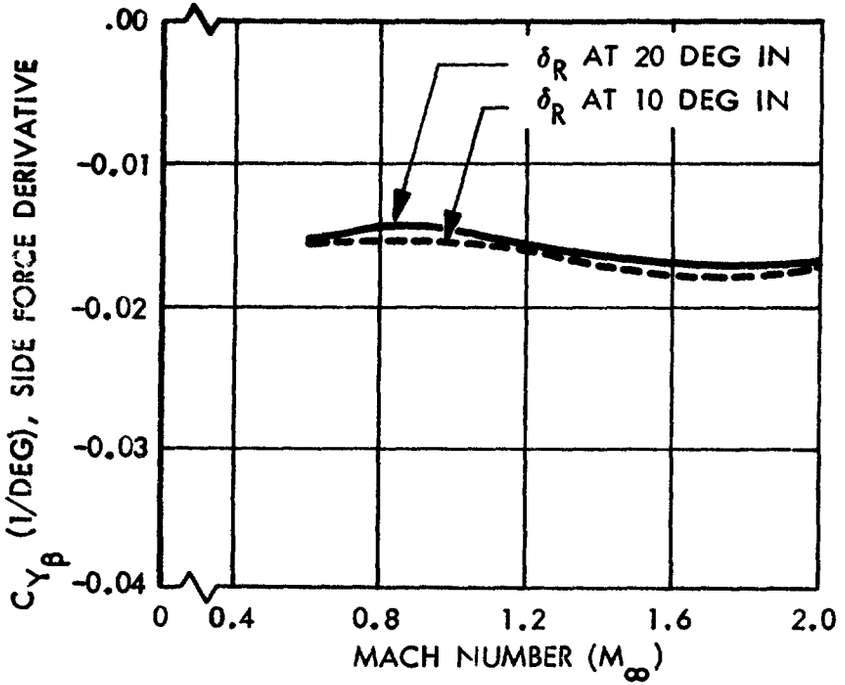

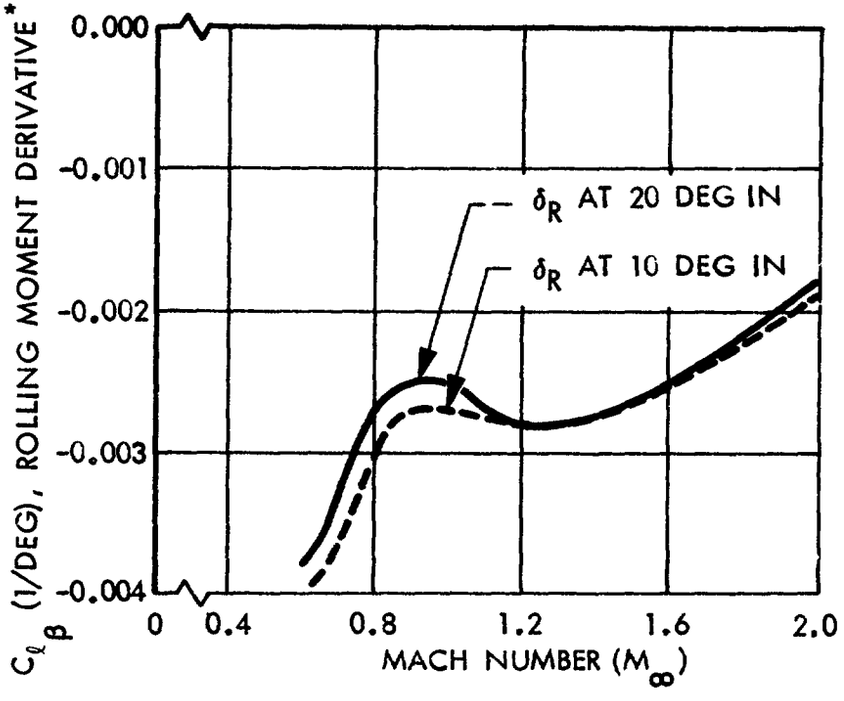

*STABILITY AXIS, BASED ON L_{REF}

**AMES 6 FT X 6 FT WIND TUNNEL TEST NO. 542

FIG. 33

D03360

$M_\infty = 2.3$*

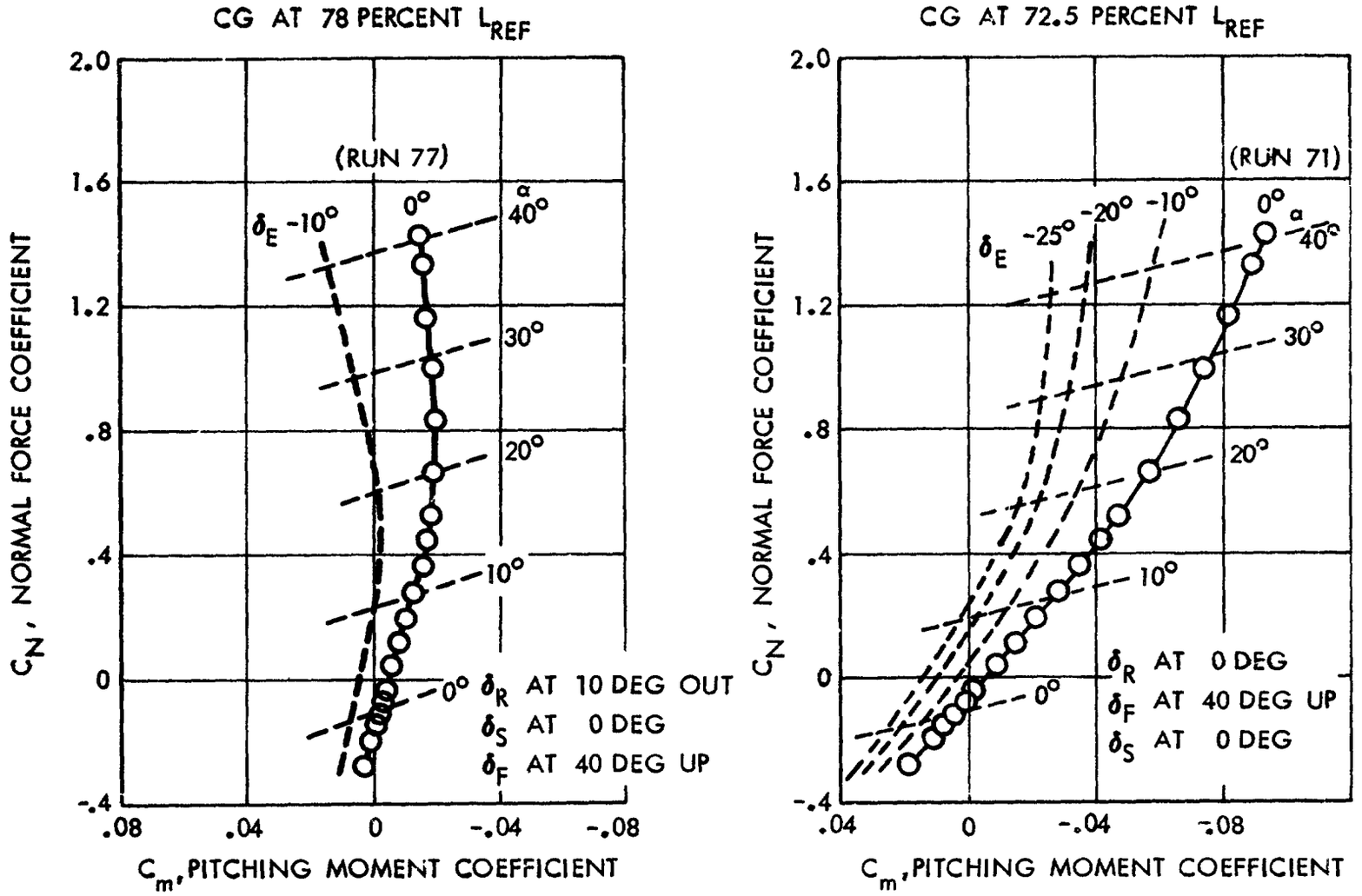

*LANGLEY UNITARY WIND TUNNEL TEST NO. 955

D03273

FIG. 34

LONGITUDINAL STABILITY AND TRIM

$M_\infty = 3.0$*

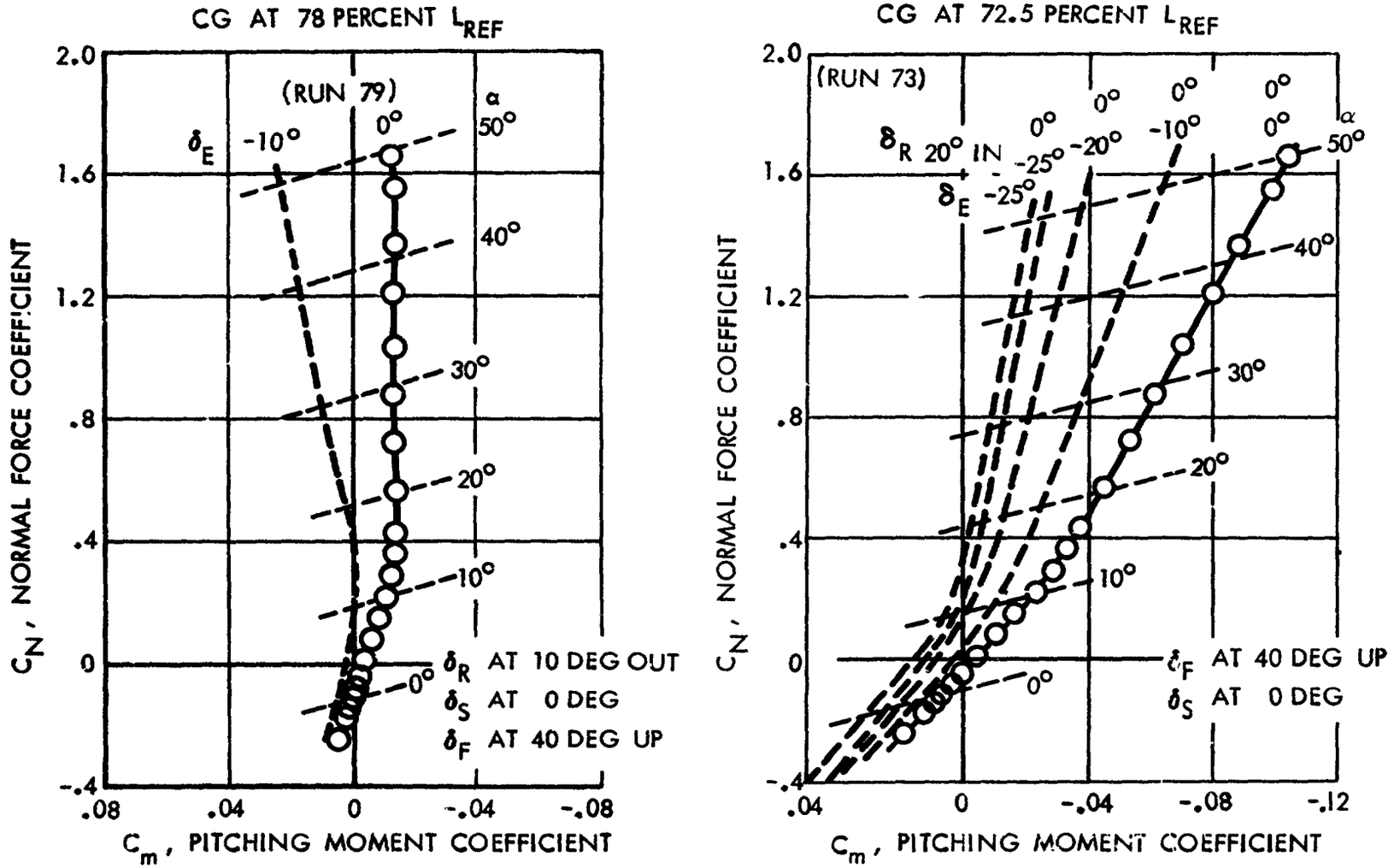

FIG. 35

*LANGLEY UNITARY WIND TUNNEL TEST NO. 955

D03274

LONGITUDINAL STABILITY AND TRIM

M_∞ = 4.0*

CG AT 78 PERCENT L_{REF}

(RUN 81)

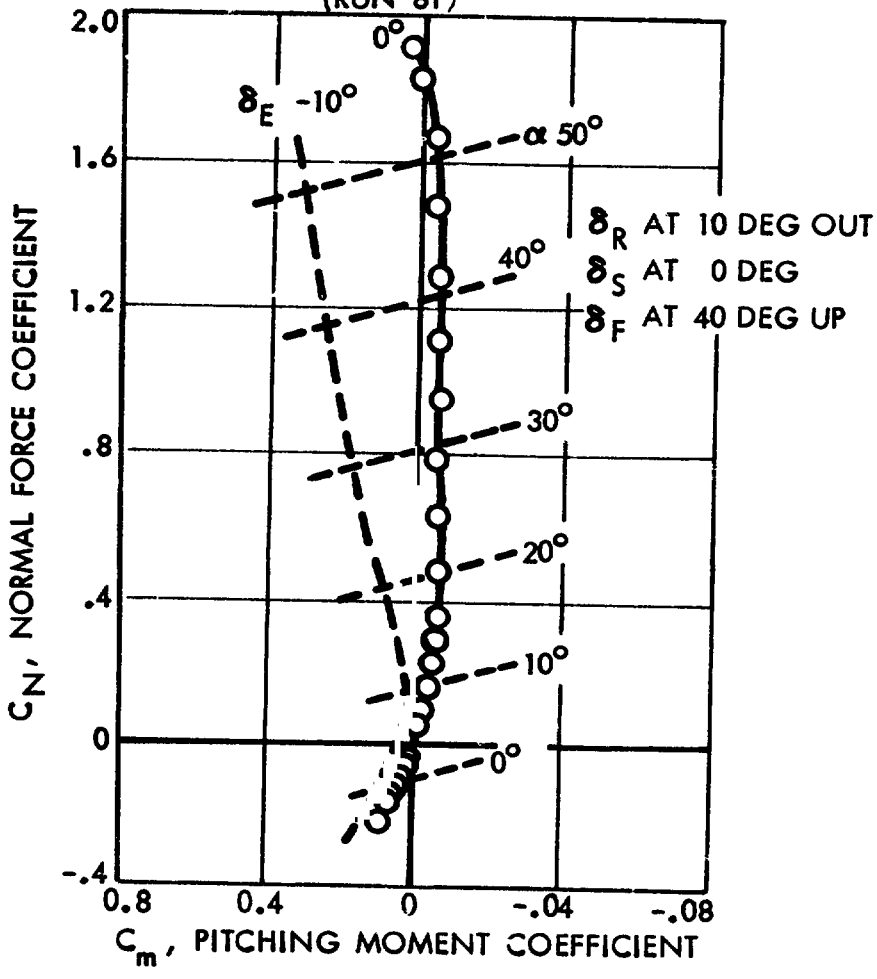

CG AT 72.5 PERCENT L_{REF}

(RUN 74)

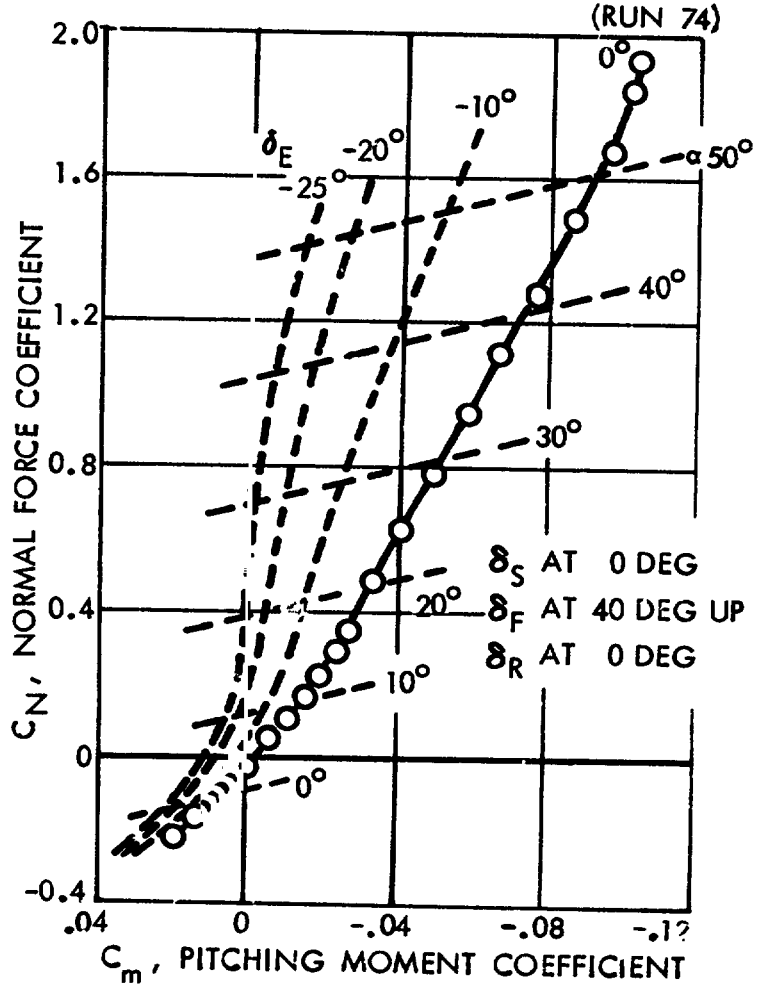

*LANGLEY UNITARY WIND TUNNEL TEST NO. 955

D03275

FIG. 36

MACH 4.6*

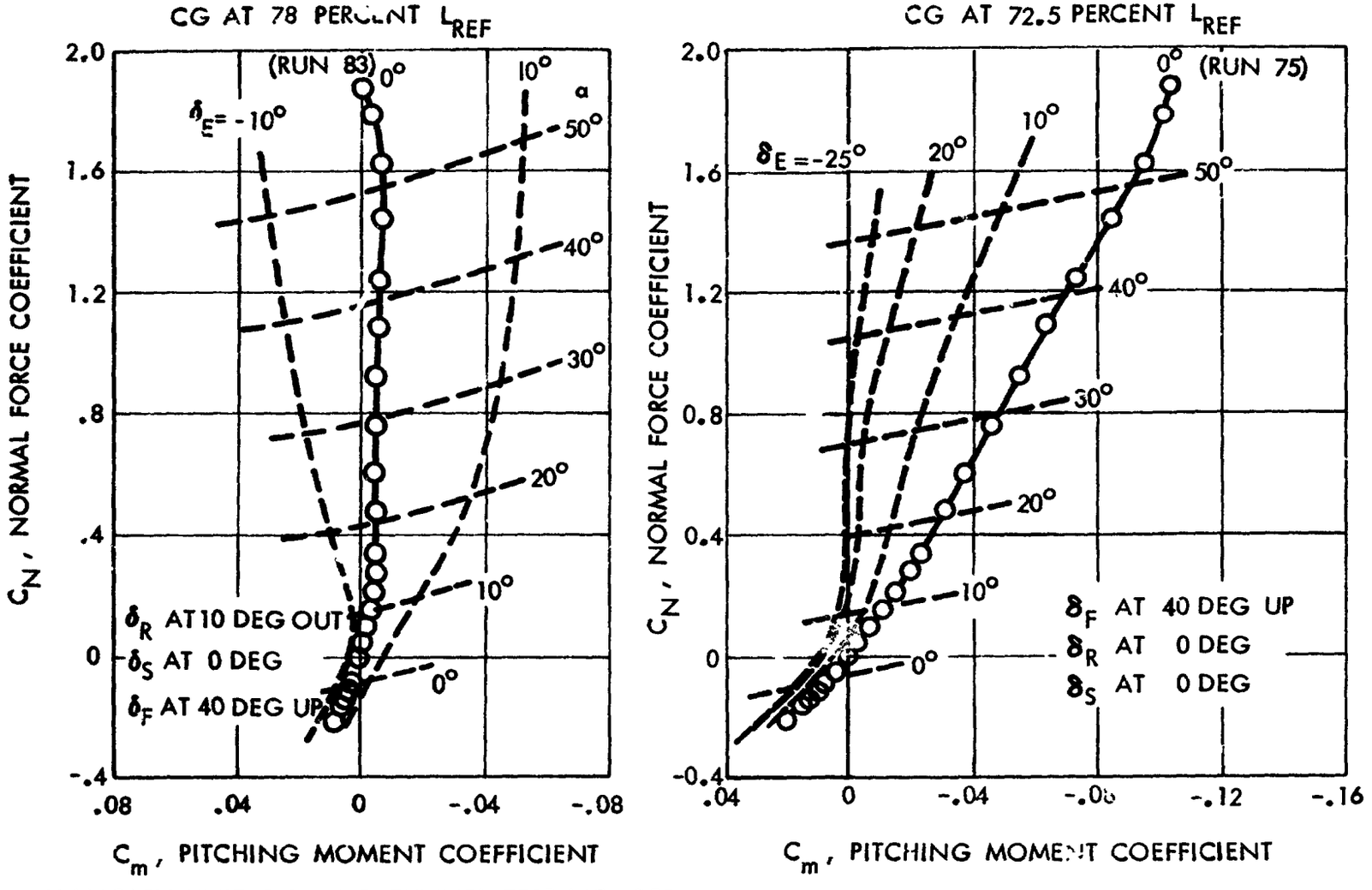

FIG. 37

*LANGLEY UNITARY WIND TUNNEL TEST NO. 955

DIRECTIONAL STABILITY

$M_\infty = 2.3$**

δ_F AT 40 DEG UP
δ_S AT 0 DEG
δ_E AT 0 DEG

CG AT 78 PERCENT L_{REF}

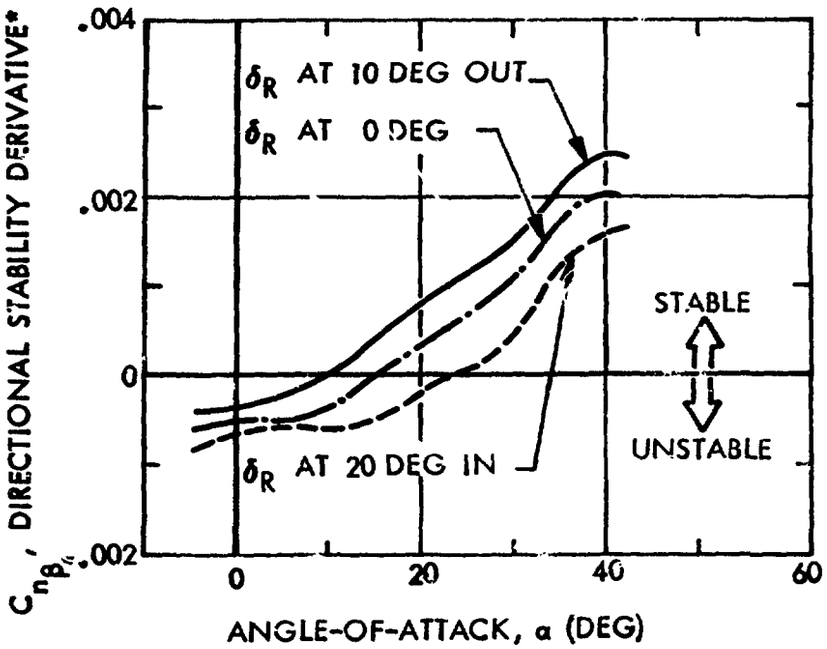

CG AT 72.5 PERCENT L_{REF}

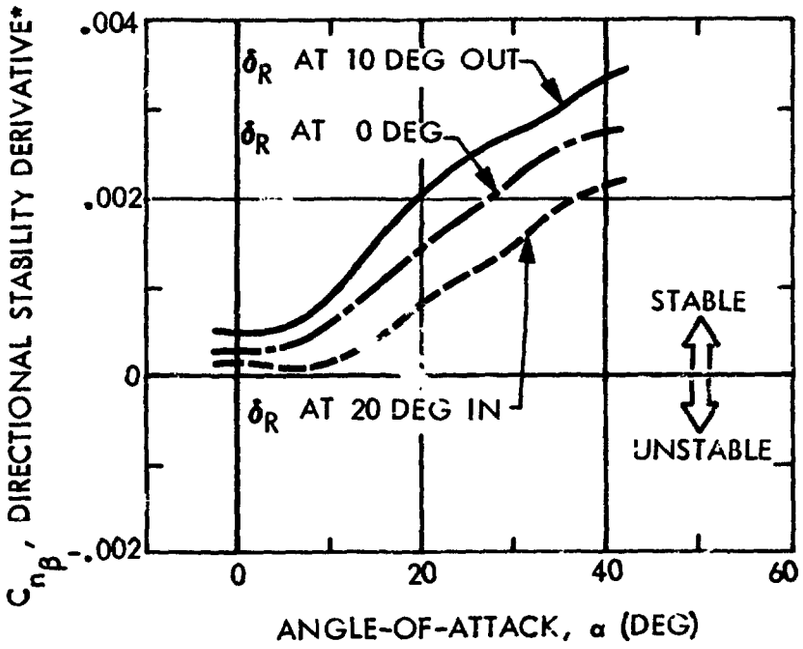

*STABILITY AXIS, BASED ON L_{REF}

**LANGLEY UNITARY PLAN WIND TUNNEL TEST NO. 955

D03361

DIRECTIONAL STABILITY

$M_\infty = 2.3^*$

δ_E AT 0 DEG
δ_F AT 40 DEG UP
δ_S AT 0 DEG

CG AT 78 PERCENT L_{REF} $\left(\frac{I_{ZZ}}{I_{XX}} = 5.081\right)$

CG AT 72.5 PERCENT L_{REF} $\left(\frac{I_{ZZ}}{I_{XX}} = 5.829\right)$

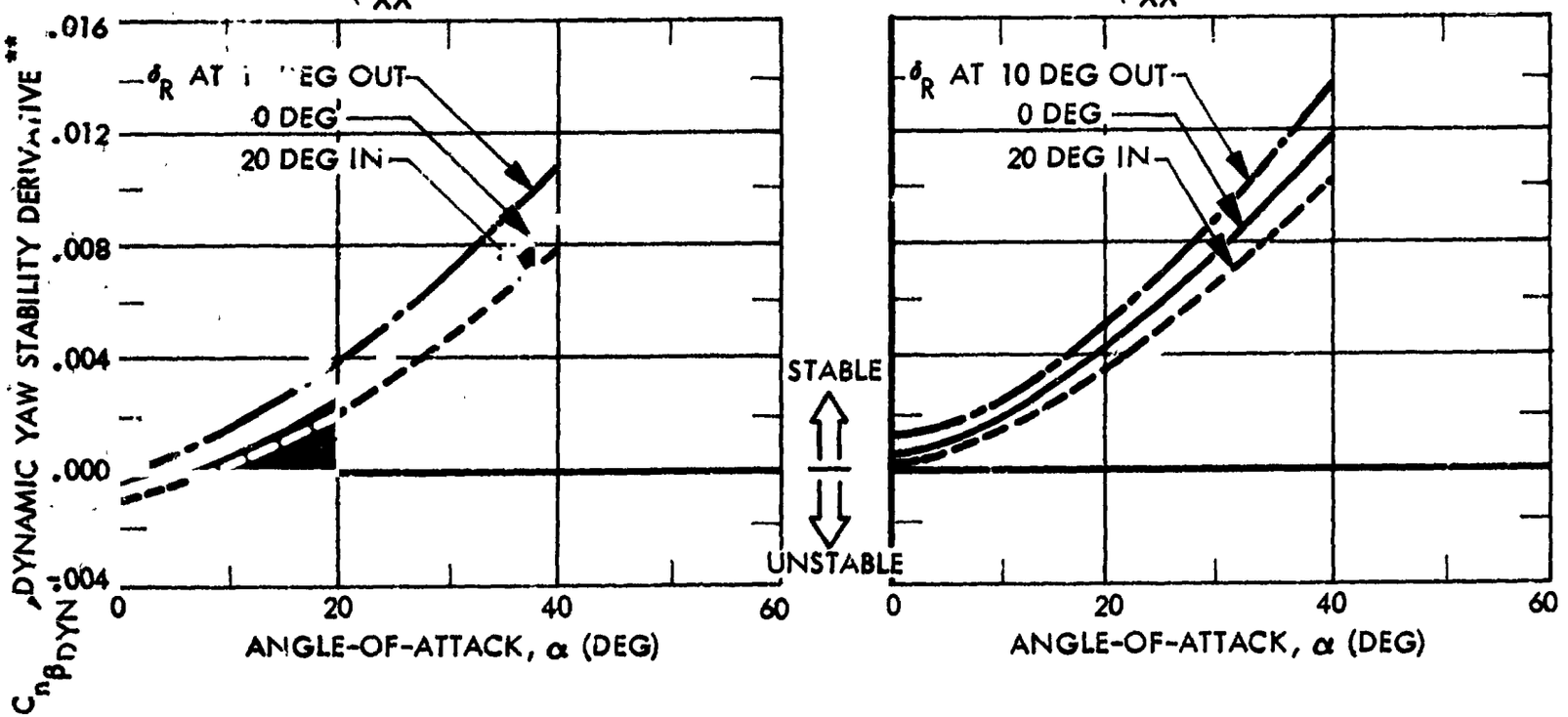

*LANGLEY UNITARY PLAN WIND TUNNEL TEST NO. 955
**BASED ON L_{REF}

D03362(1)

FIG. 39
6-40

SIDE FORCE AND ROLLING MOMENT DERIVATIVE

$M_\infty = 2.3$**

δ_F AT 40 DEG UP
δ_S AT 0 DEG
δ_E AT 0 DEG

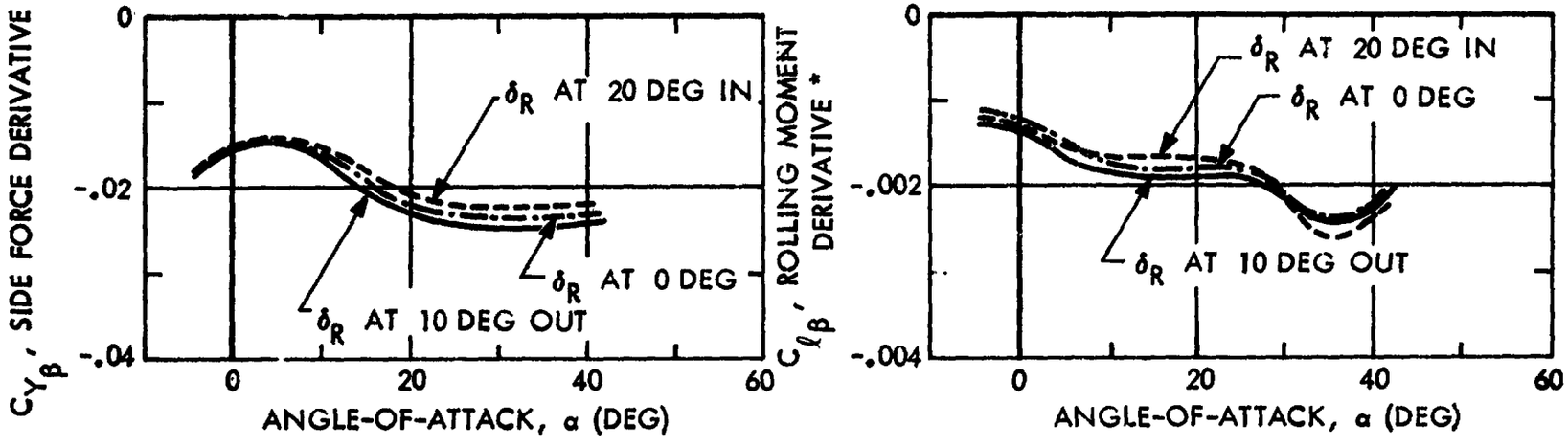

*STABILITY AXIS, BASED ON L_{REF}

**LANGLEY UNITARY PLAN WIND TUNNEL TEST NO. 955

D03363

DIRECTIONAL STABILITY

M_∞ = 3.0**
δ_E AT 0 DEG
δ_F AT 40 DEG UP
δ_S AT 0 DEG

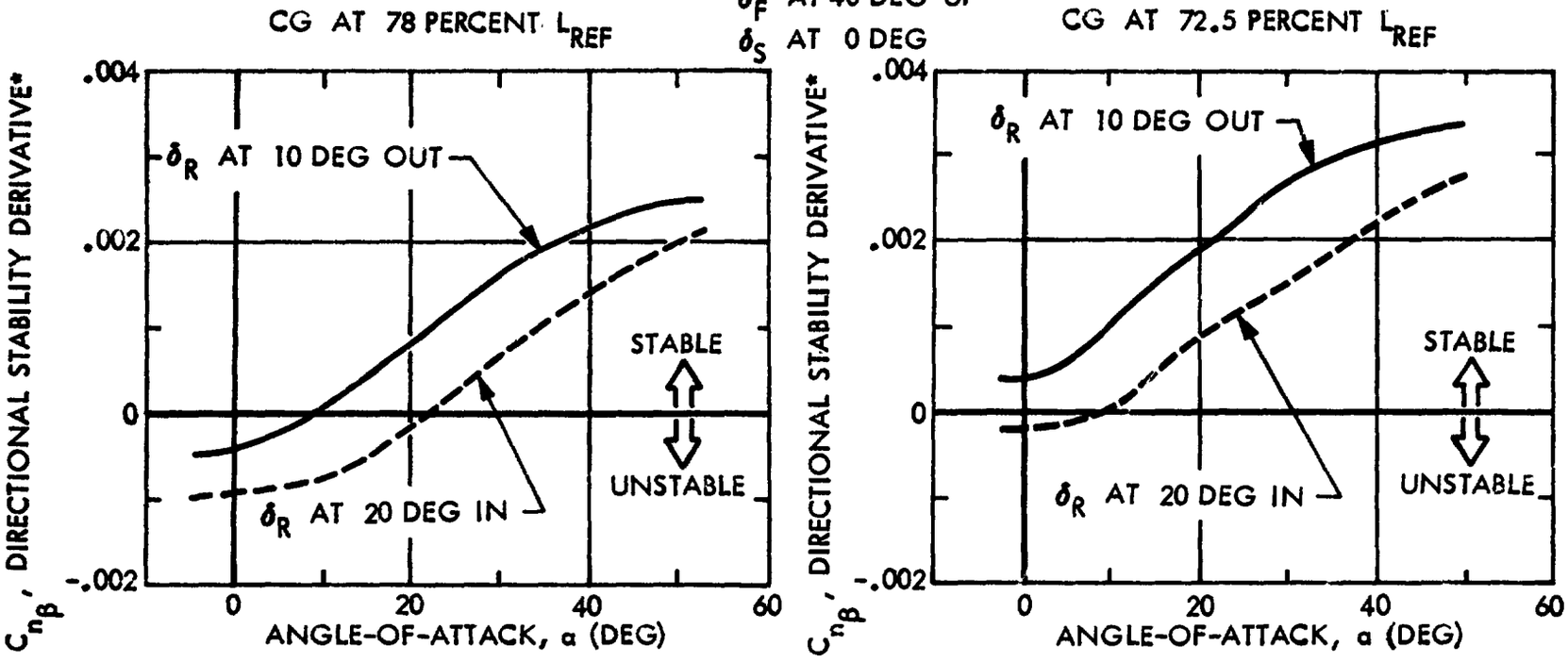

FIG. 41
6-42

*STABILITY AXIS, BASED ON L_{REF}

**LANGLEY UNITARY PLAN WIND TUNNEL TEST NO. 955

D03364

DIRECTIONAL STABILITY

$M_\infty = 3.0^*$

δ_E AT 0 DEG
δ_F AT 40 DEG UP
δ_S AT 0 DEG

CG AT 78 PERCENT L_{REF} $\left(\frac{I_{ZZ}}{I_{XX}} = 5.081\right)$

CG AT 72.5 PERCENT L_{REF} $\left(\frac{I_{ZZ}}{I_{XX}} = 5.829\right)$

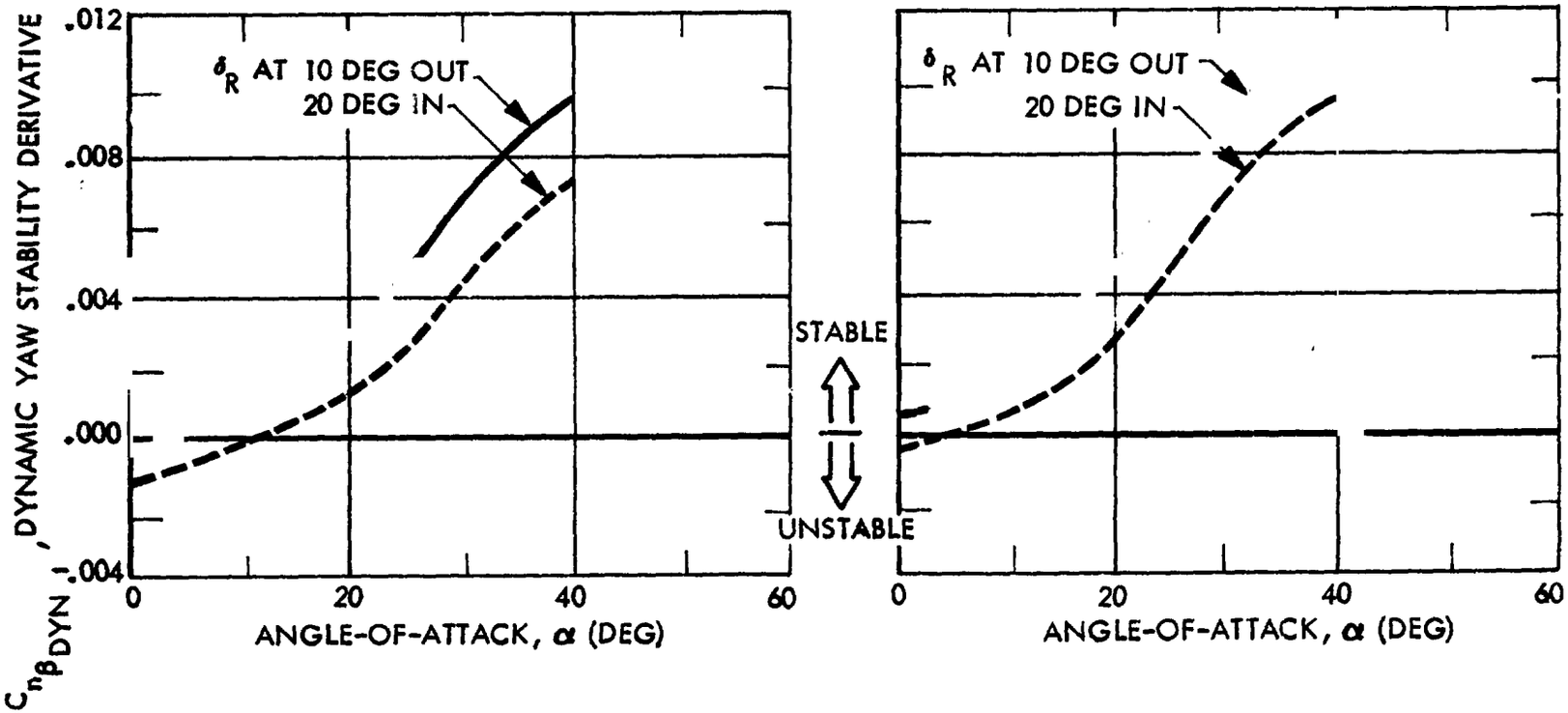

*LANGLEY UNITARY PLAN WIND TUNNEL TEST NO. 955
**BASED ON L_{REF}

D03365(1)

FIG. 42
6-43

SIDE FORCE AND ROLLING MOMENT DERIVATIVE

M_∞ = 3.0**
δ_F AT 40 DEG UP
δ_S AT 0 DEG
δ_E AT 0 DEG

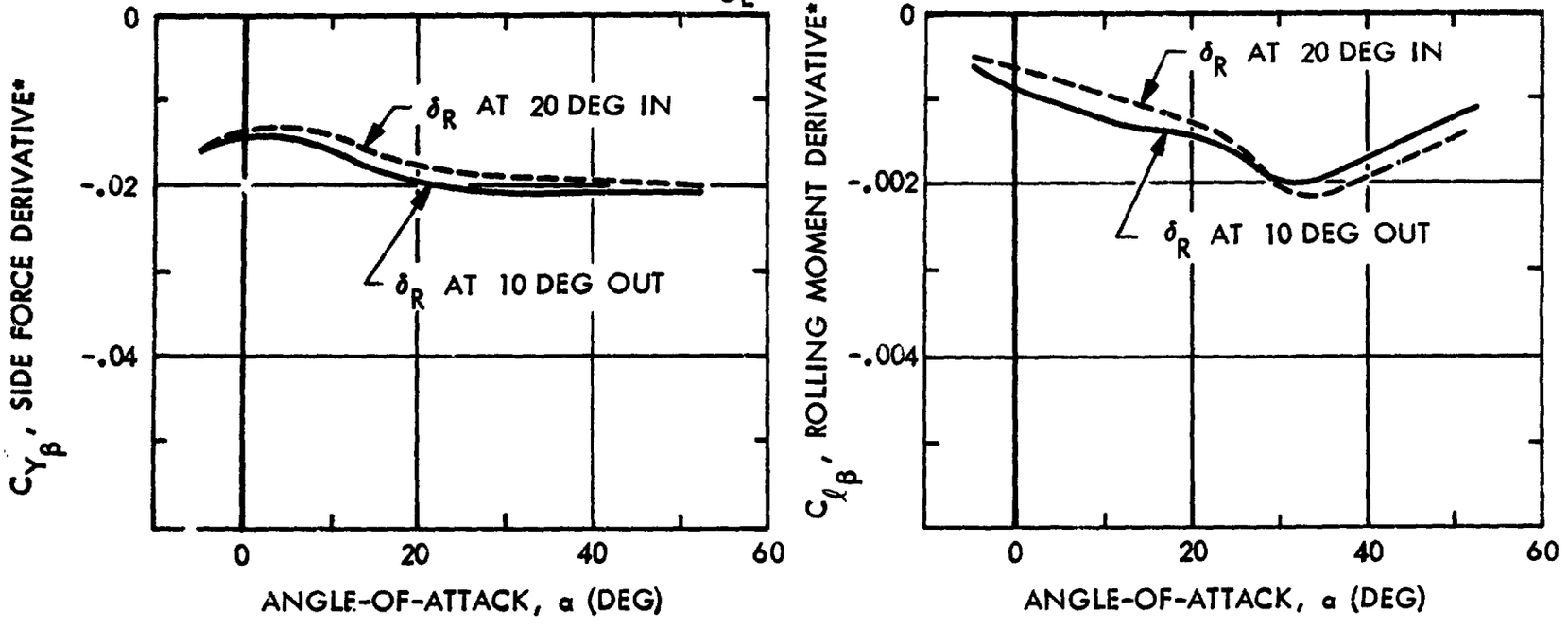

FIG. 43
6-44

*STABILITY AXIS, BASED ON L_{REF}

**LANGLEY UNITARY PLAN WIND TUNNEL TEST NO. 955

D03366

DIRECTIONAL STABILITY

$M_\infty = 4.0^{**}$

δ_F AT 40 DEG UP

δ_S AT 0 DEG

δ_E AT 0 DEG

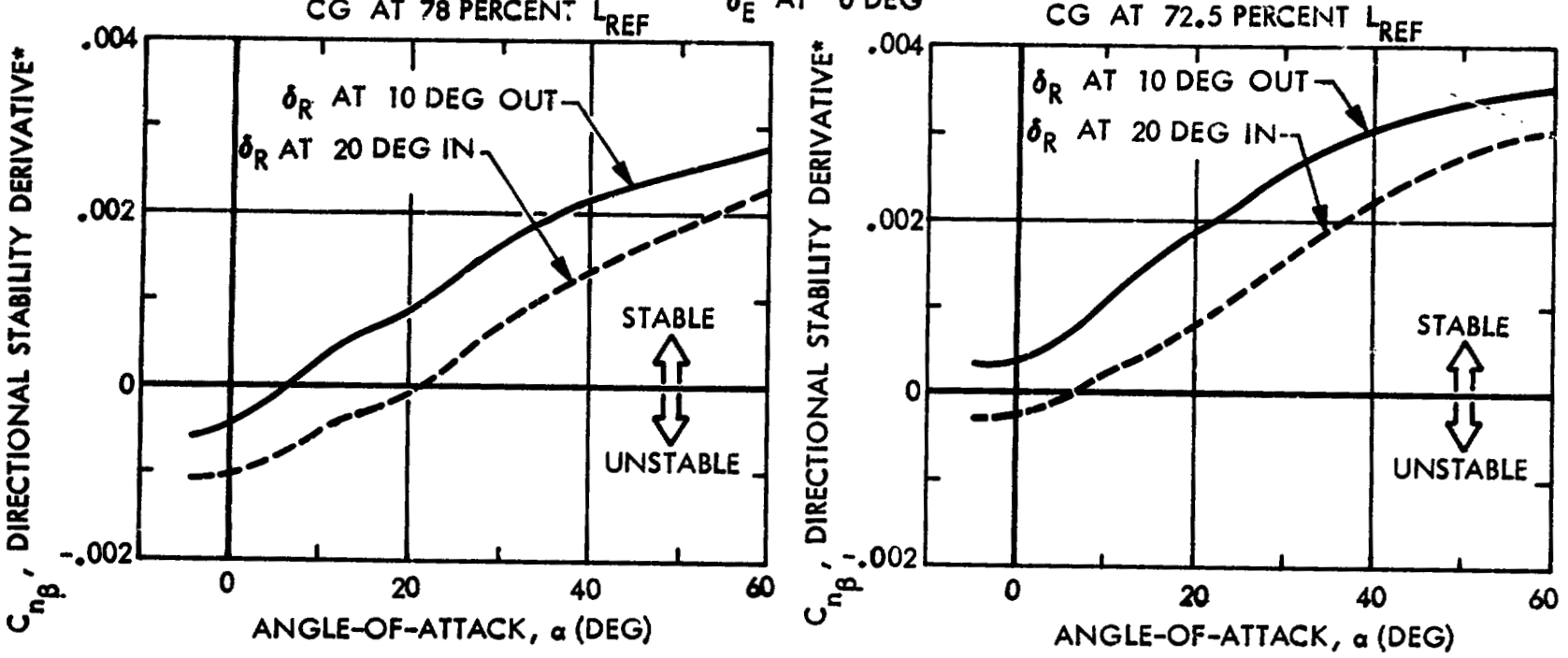

FIG. 44

6-45

*STABILITY AXIS, BASED ON L_{REF}

**LANGLEY UNITARY PLAN WIND TUNNEL TEST NO. 955

D03367

DIRECTIONAL STABILITY

$M_\infty = 4.0$*

δ_F AT 20 DEG UP

δ_S AT 0 DEG

δ_E AT 0 DEG

CG AT 78 PERCENT L_{REF} $\left(\frac{I_{ZZ}}{I_{XX}} = 5.081\right)$

CG AT 72.5 PERCENT L_{REF} $\left(\frac{I_{ZZ}}{I_{XX}} = 5.829\right)$

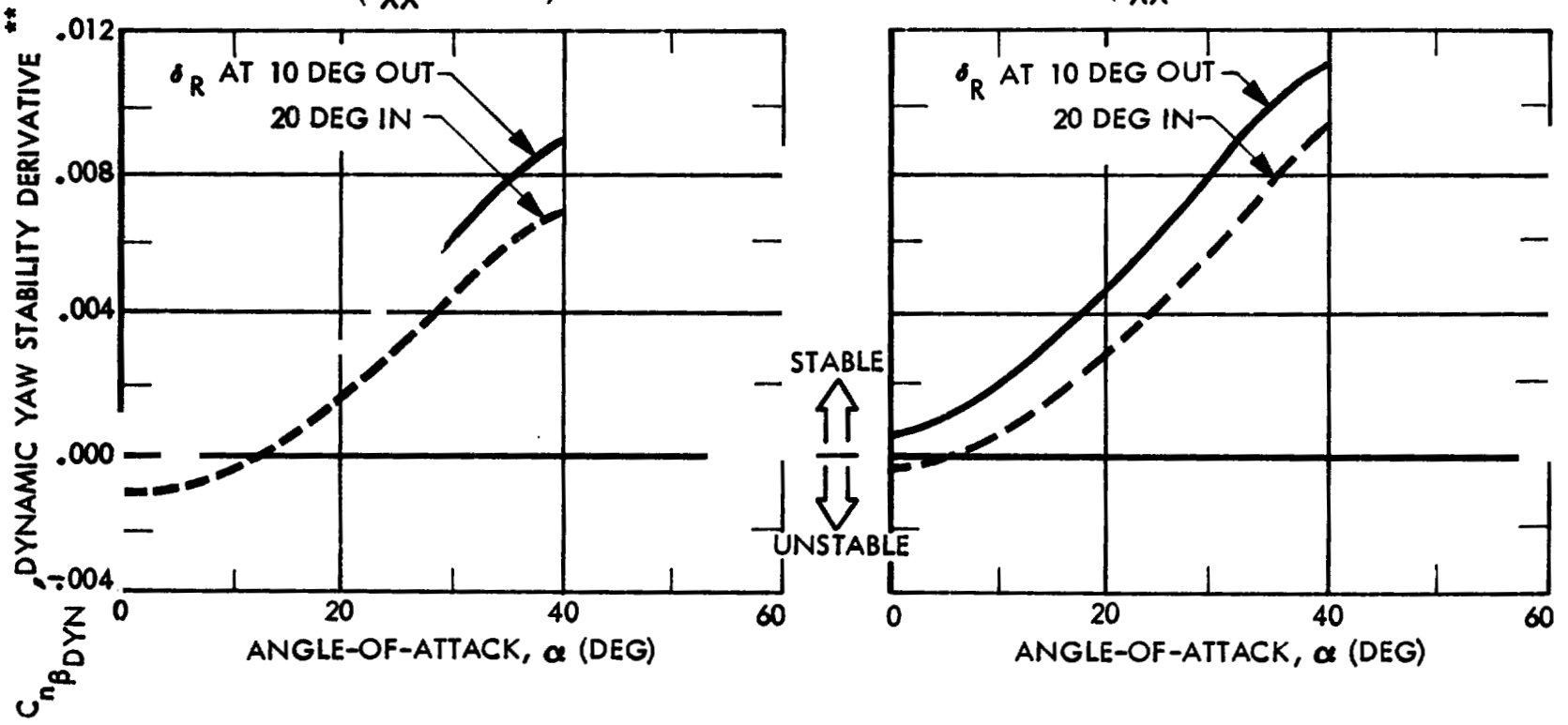

FIG. 45
6-46

*LANGLEY UNITARY PLAN WIND TUNNEL TEST NO. 955

**BASED ON L_{REF}

D03368 (1)

SIDE FORCE AND ROLLING MOMENT DERIVATIVE

$M_\infty = 4.0$**

δ_E AT 0 DEG
δ_F AT 40 DEG UP
δ_S AT 0 DEG

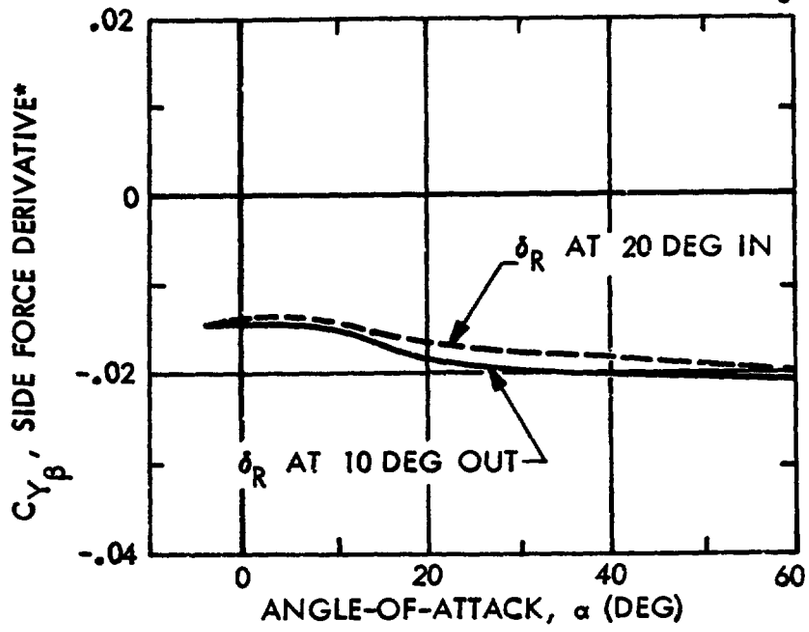

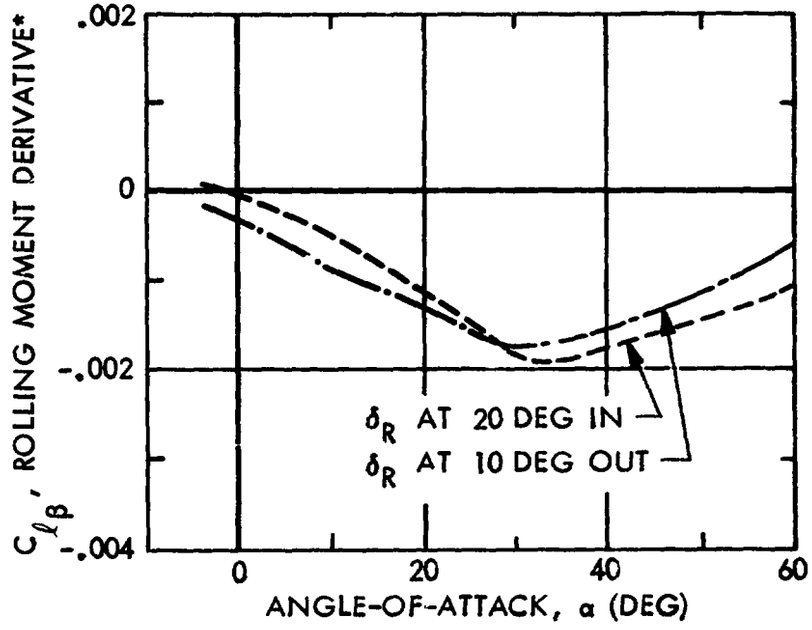

*STABILITY AXIS, BASED ON L_{REF}

**LANGLEY UNITARY PLAN WIND TUNNEL TEST NO. 955

D03369

DIRECTIONAL STABILITY

$M_\infty = 4.6$**
δ_F AT ' DEG UP
δ_S AT 0 DEG
δ_E AT 0 DEG

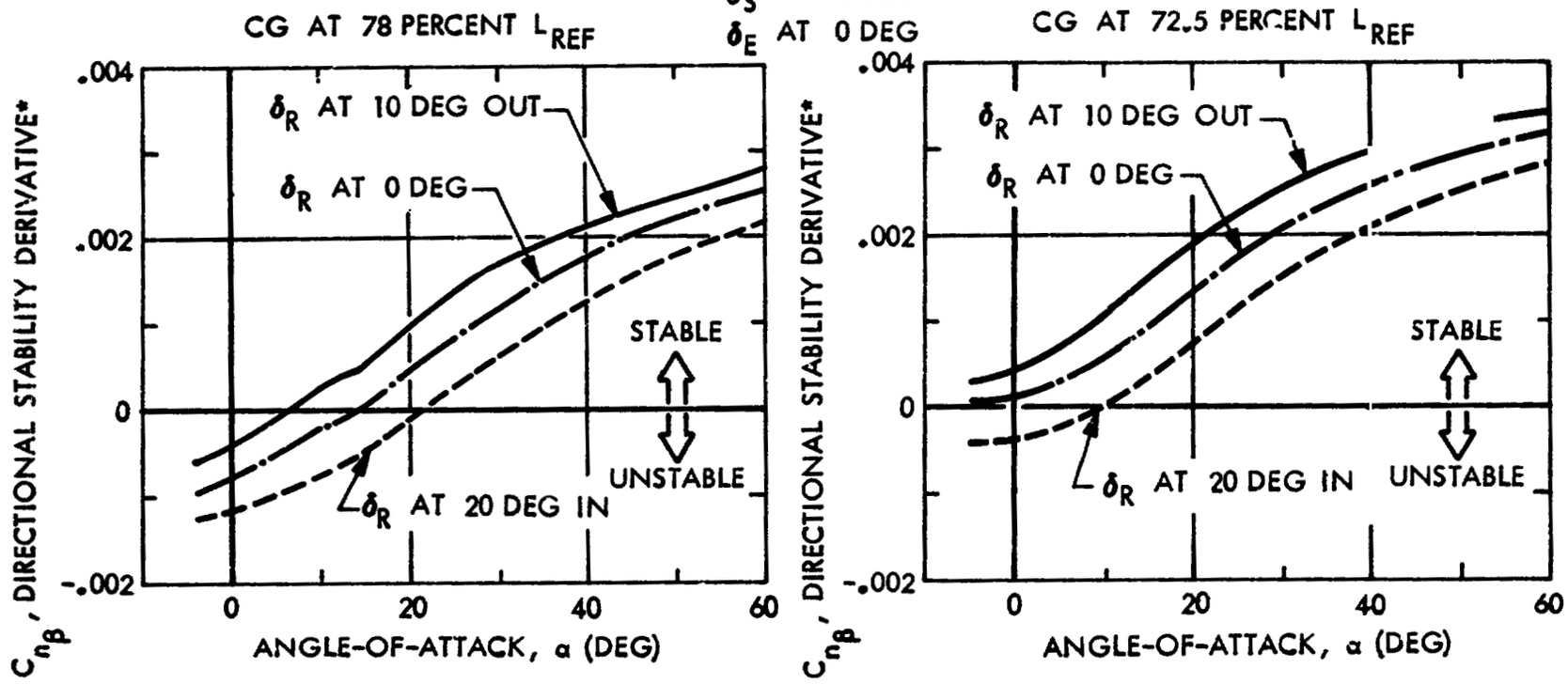

FIG. 47
6-48

*STABILITY AXIS, BASED ON L_{REF}

**LANGLEY UNITARY PLAN WIND TUNNEL TEST NO. 955

D03370

DIRECTIONAL STABILITY

$M_\infty = 4.6^*$

δ_E AT 0 DEG
δ_F AT 40 DEG UP
δ_S AT 0 DEG

CG AT 78 PERCENT L_{REF} $\left(\frac{I_{ZZ}}{I_{XX}} = 5.081\right)$

CG AT 72.5 PERCENT L_{REF} $\left(\frac{I_{ZZ}}{I_{XX}} = 5.829\right)$

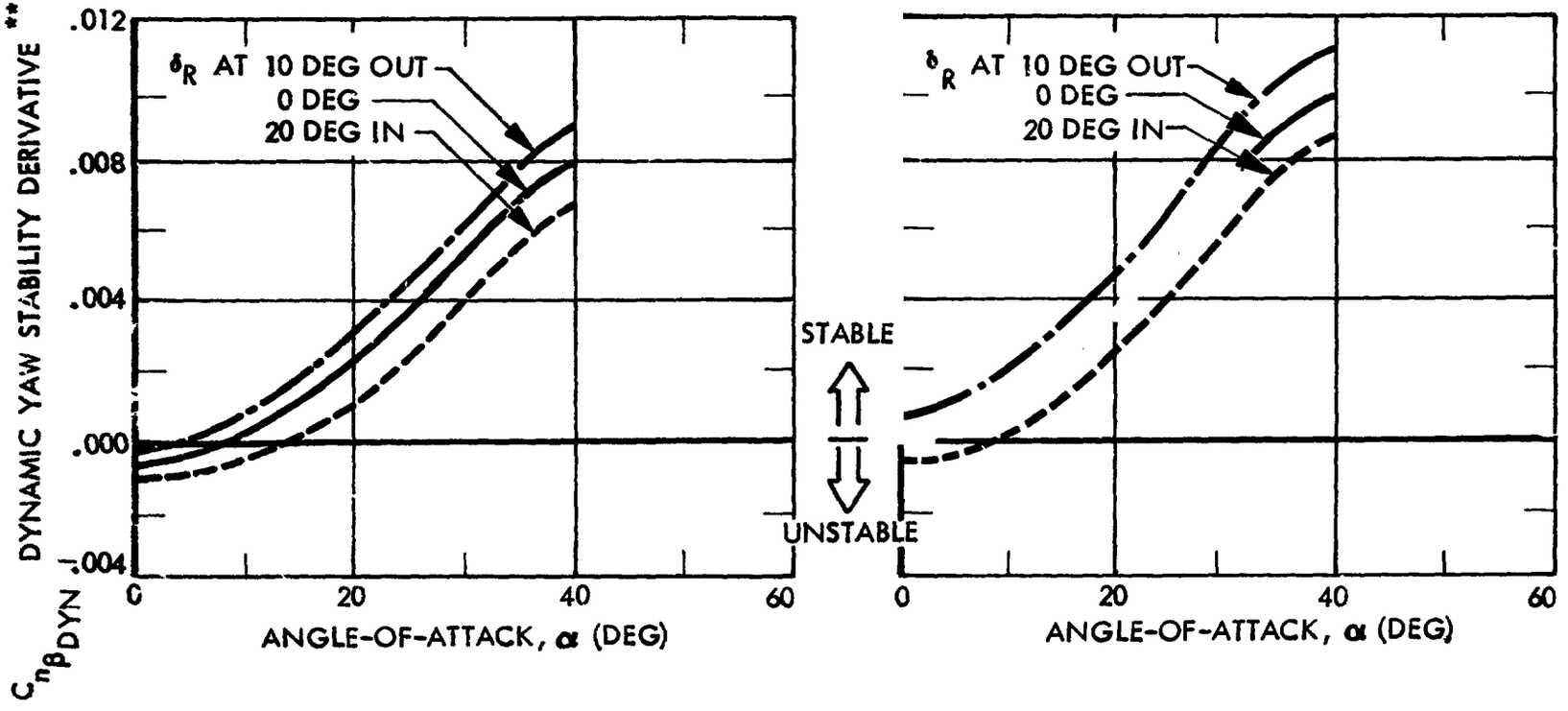

*LANGLEY UNITARY PLAN WIND TUNNEL TEST NO. 955
**BASED ON L_{REF}

D03371 (1)

SIDE FORCE AND ROLLING MOMENT DERIVATIVE

$M_\infty = 4.6$**

δ_E AT 0 DEG
δ_F AT 40 DEG UP
δ_S AT 0 DEG

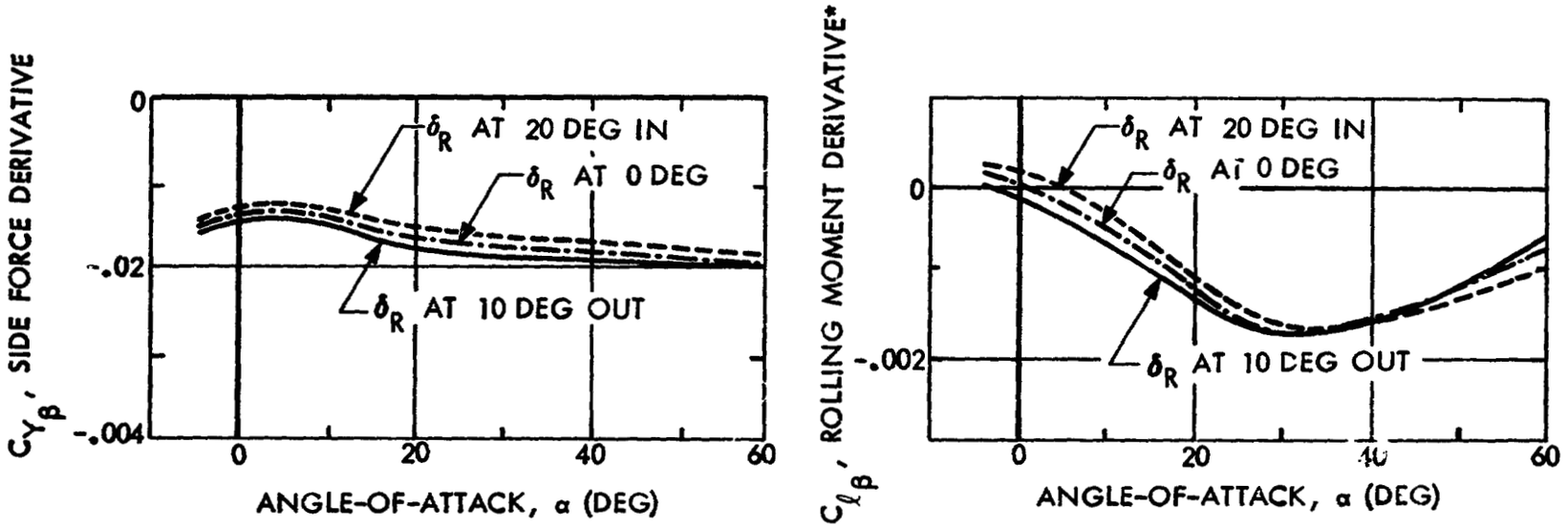

*STABILITY AXIS, BASED ON L_{REF}

**LANGLEY UNITARY PLAN WIND TUNNEL TEST NO. 955

D03372

LOCKHEED

LONGITUDINAL STABILITY AND TRIM

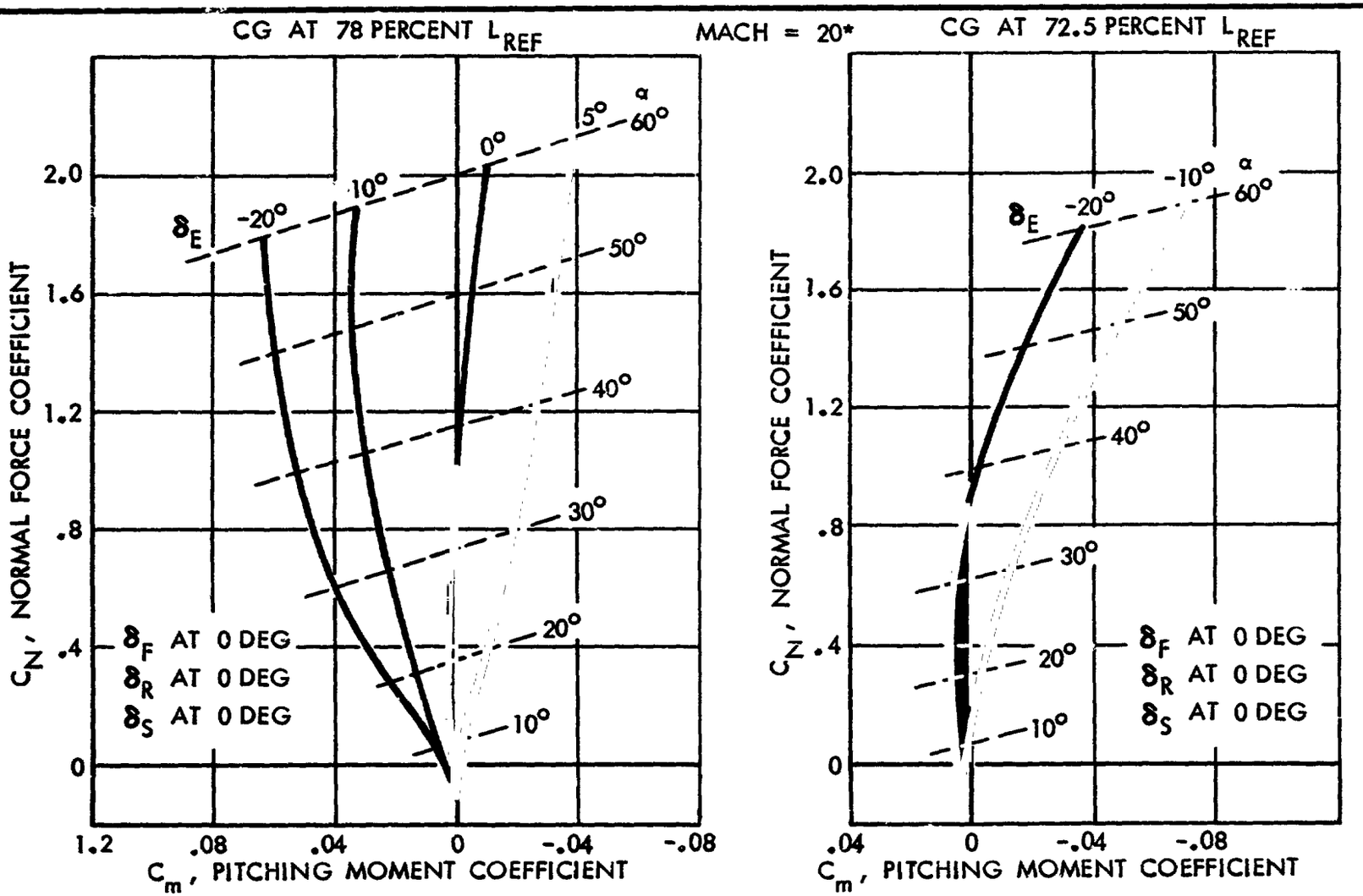

*MODIFIED HYPERSONIC ARBITRARY BODY PROGRAM

D03277

FIG. 50

LIFT AND DRAG CHARACTERISTICS

MACH = 20*

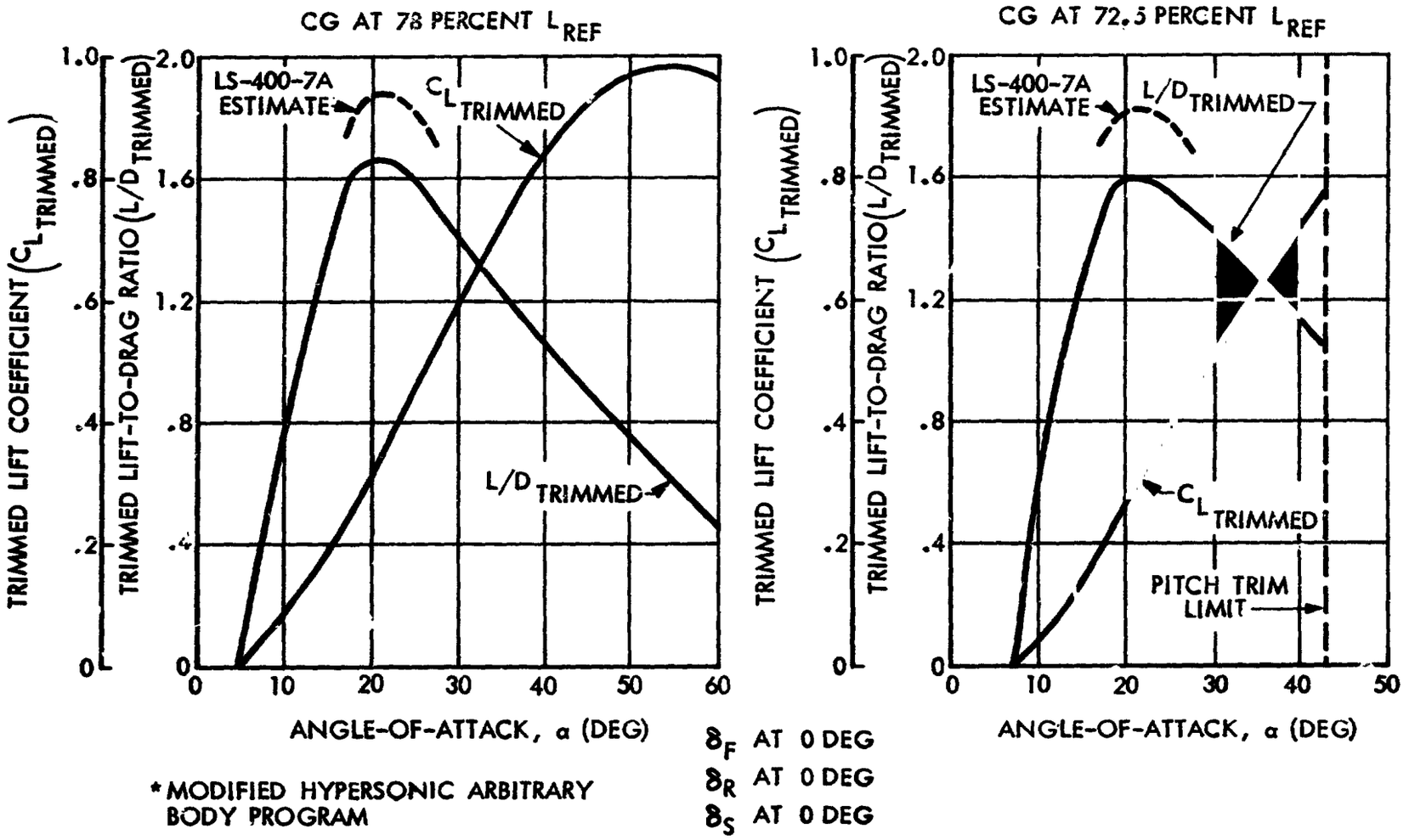

δ_F AT 0 DEG
δ_R AT 0 DEG
δ_S AT 0 DEG

*MODIFIED HYPERSONIC ARBITRARY BODY PROGRAM

D03278

LOCKHEED

AERODYNAMIC LIFT-TO-DRAG RATIO

HYPERSONIC

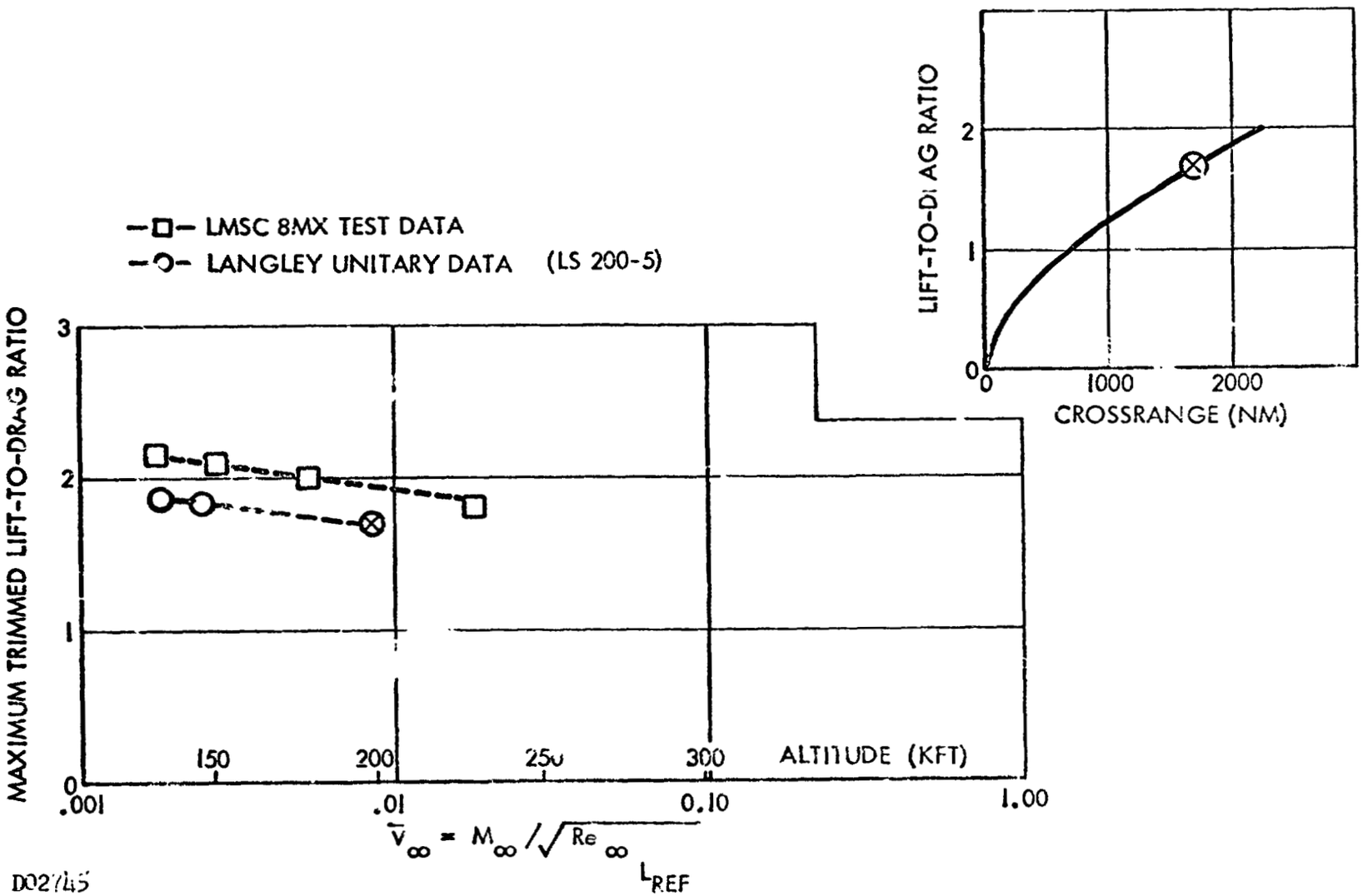

FIG. 52

6-53

D02745

fav

DIRECTIONAL STABILITY SUMMARY

CG AT 78 PERCENT L_{REF}

δ_R AT 20 DEG IN

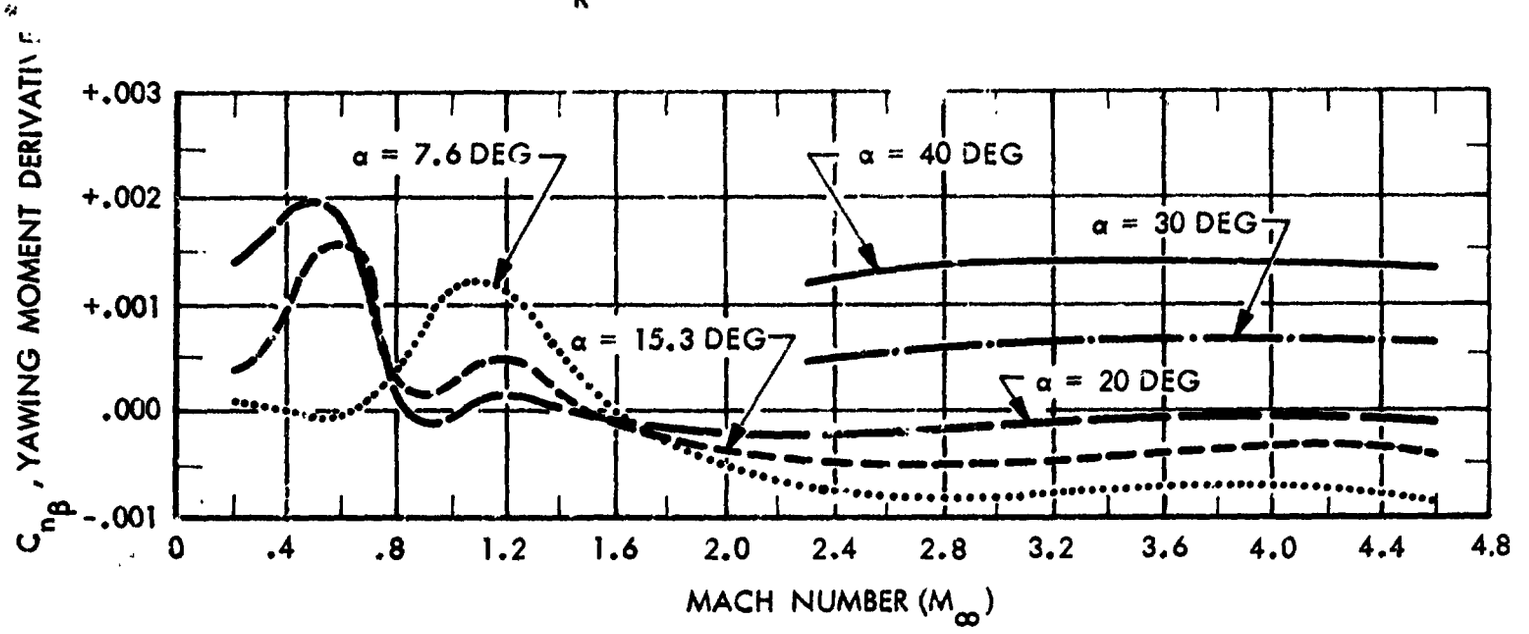

- LOCKHEED 8 FT X 12 FT TEST NO. L-324
- AMES 6 FT X 6 FT TEST NO. 542
- LANGLEY UPWT TEST NO. 955

* STABILITY AXIS, BASED ON L_{REF}

FIG. 53

6-54

D03373

DIRECTIONAL STABILITY SUMMARY

CG AT 78 PERCENT L_{REF}

δ_R AT 0 DEG IN

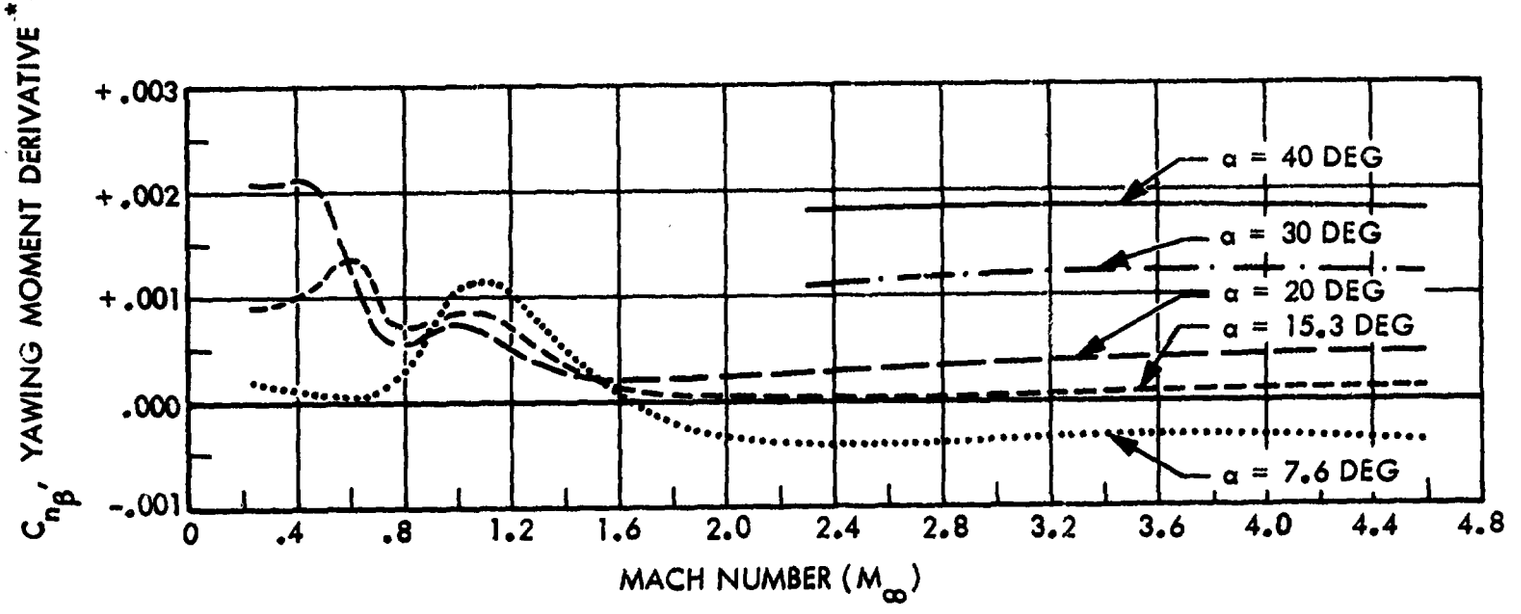

- LOCKHEED 8 FT X 12 FT TEST NO. L-324
- AMES 6 FT X 6 FT TEST NO. 542
- LANGLEY UPWT TEST NO. 955

* STABILITY AXIS, BASED ON L_{REF}

FIG. 54
6-55

D03374

DIRECTIONAL STABILITY SUMMARY

CG AT 78 PERCENT L_{REF}

δ_k AT 10 DEG OUT

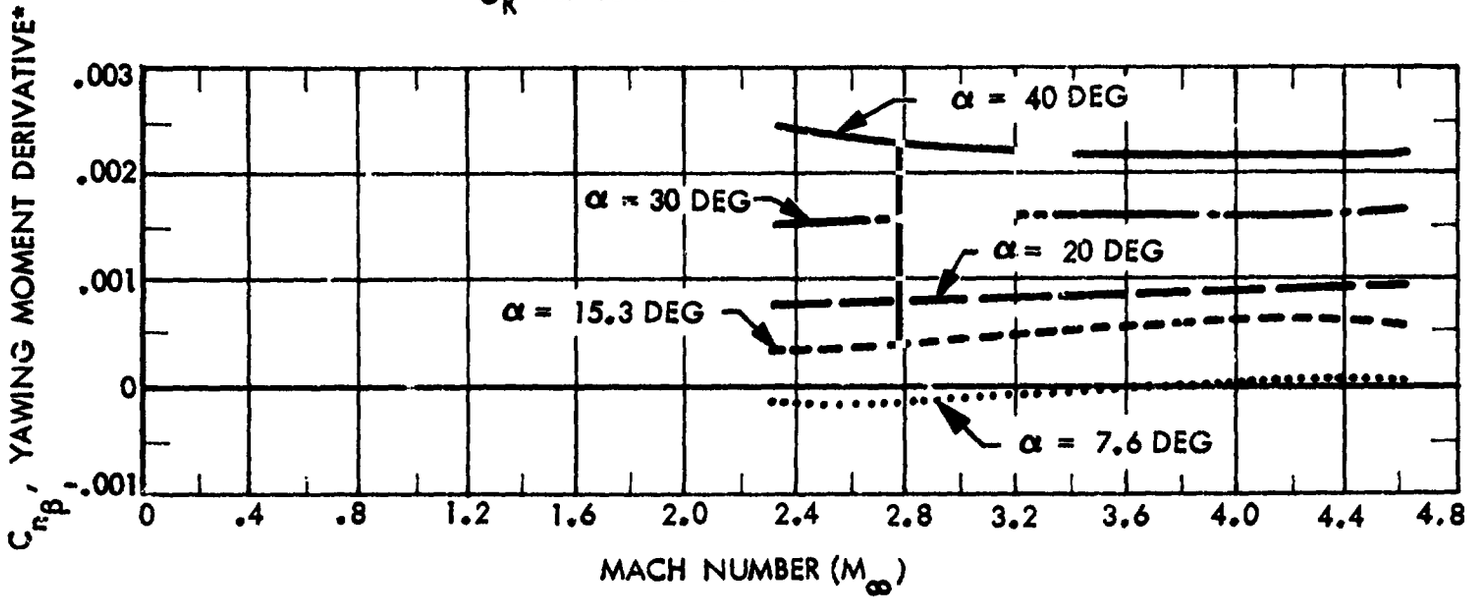

FIG. 55

6-56

- LOCKHEED 8 FT X 12 FT TEST L-324
- AMES 6 FT X 6 FT TEST 542
- LANGLEY UPWT TEST 955

* STABILITY AXIS, BASED ON L_{REF}

D03375

SIDE FORCE DERIVATIVE SUMMARY

δ_R AT 20 DEG IN

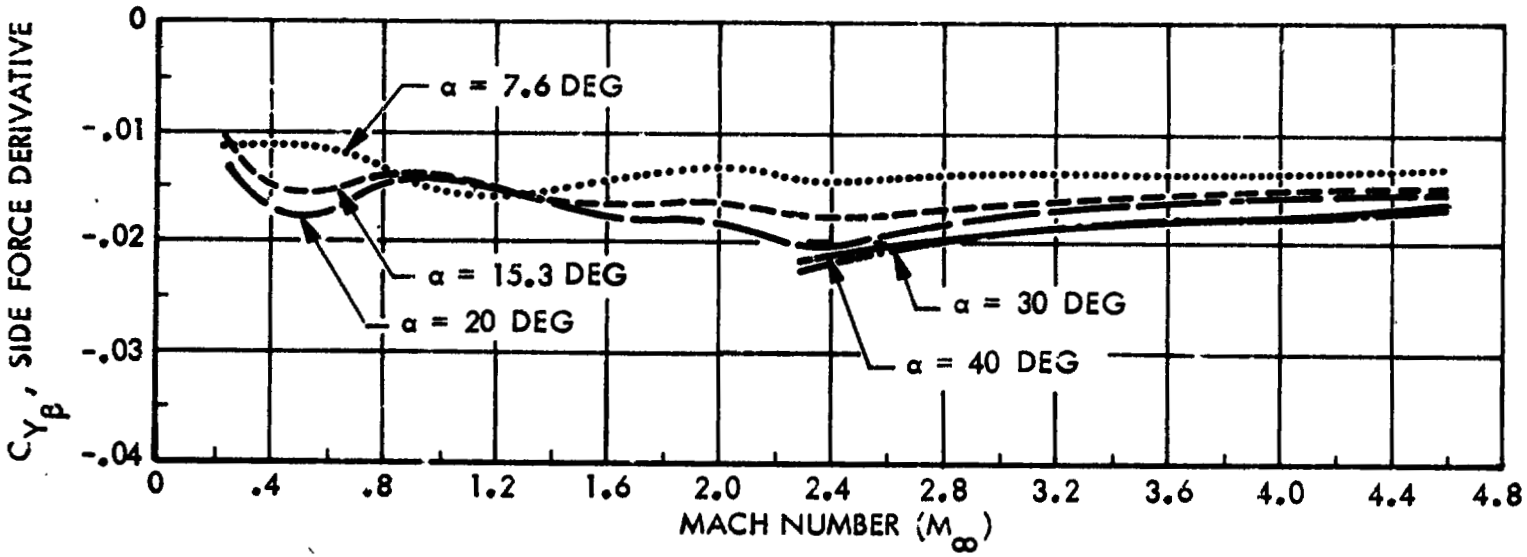

FIG. 56
6-57

- LOCKHEED 8 FT X 12 FT TEST NO. L-324
- AMES 6 FT X 6 FT TEST NO. 542
- LANGLEY UPWT TEST NO. 955

DC3376

SIDE FORCE DERIVATIVE SUMMARY

δ_R AT 0 DEG

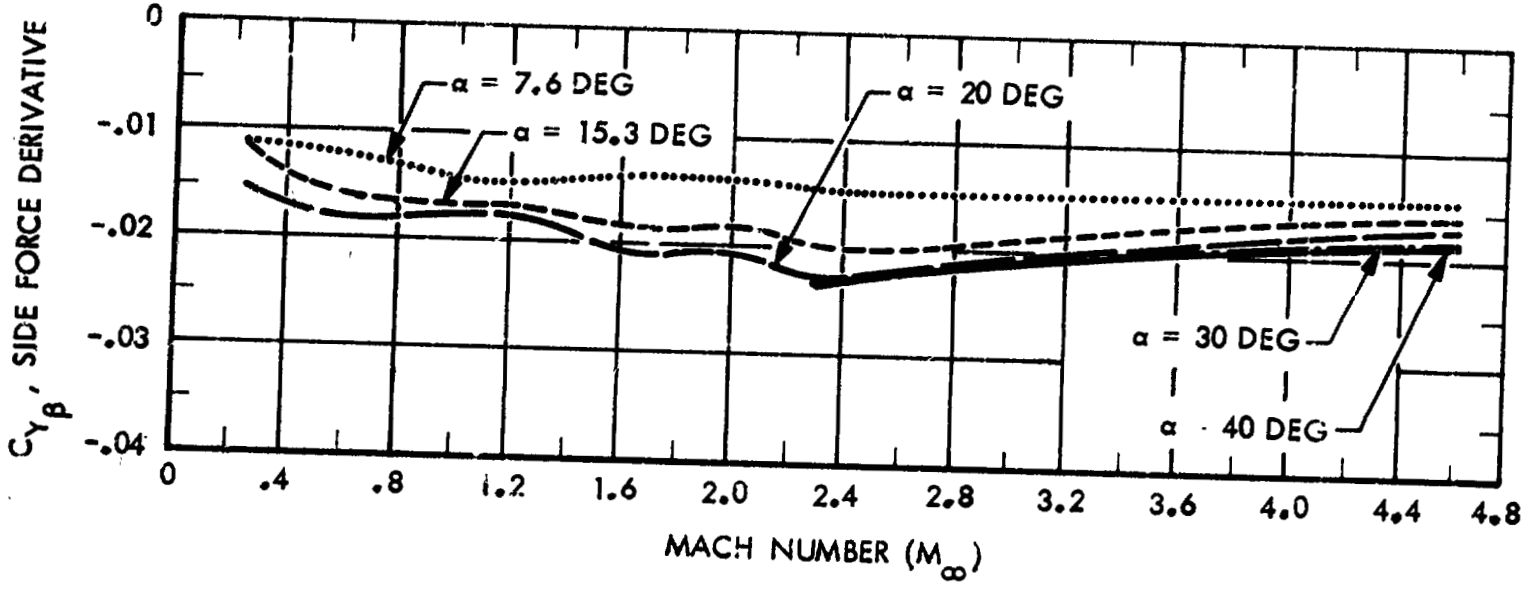

FIG. 57

- LOCKHEED 8 FT X 12 FT TEST NO. L-324
- AMES 6 FT X 6 FT TEST NO. 542
- LANGLEY UPWT TEST NO. 955

D03377

SIDE FORCE DERIVATIVE SUMMARY

δ_R AT 10 DEG OUT

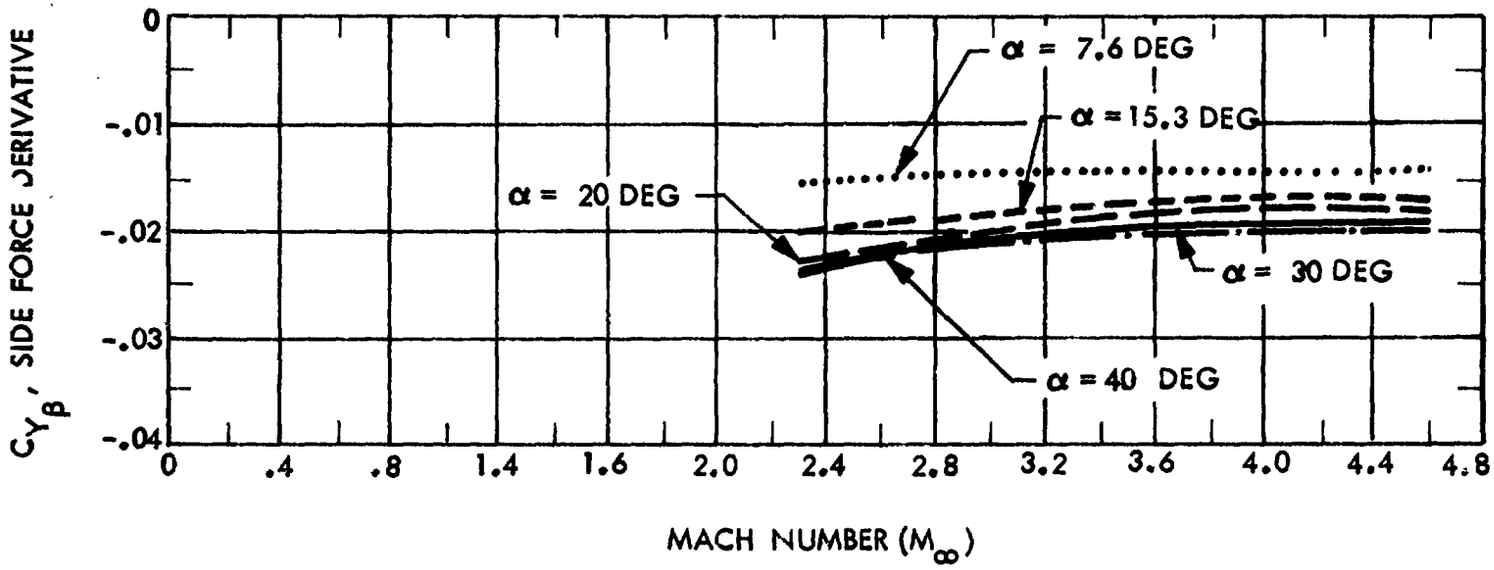

FIG. 58

6-59

REFERENCES:

- LOCKHEED 8 FT X 12 FT TEST L-324
- AMES 6 FT X 6 FT TEST 542
- LANGLEY UPWT TEST 955

D03378

LATERAL STABILITY SUMMARY

δ_R AT 20 DEG IN

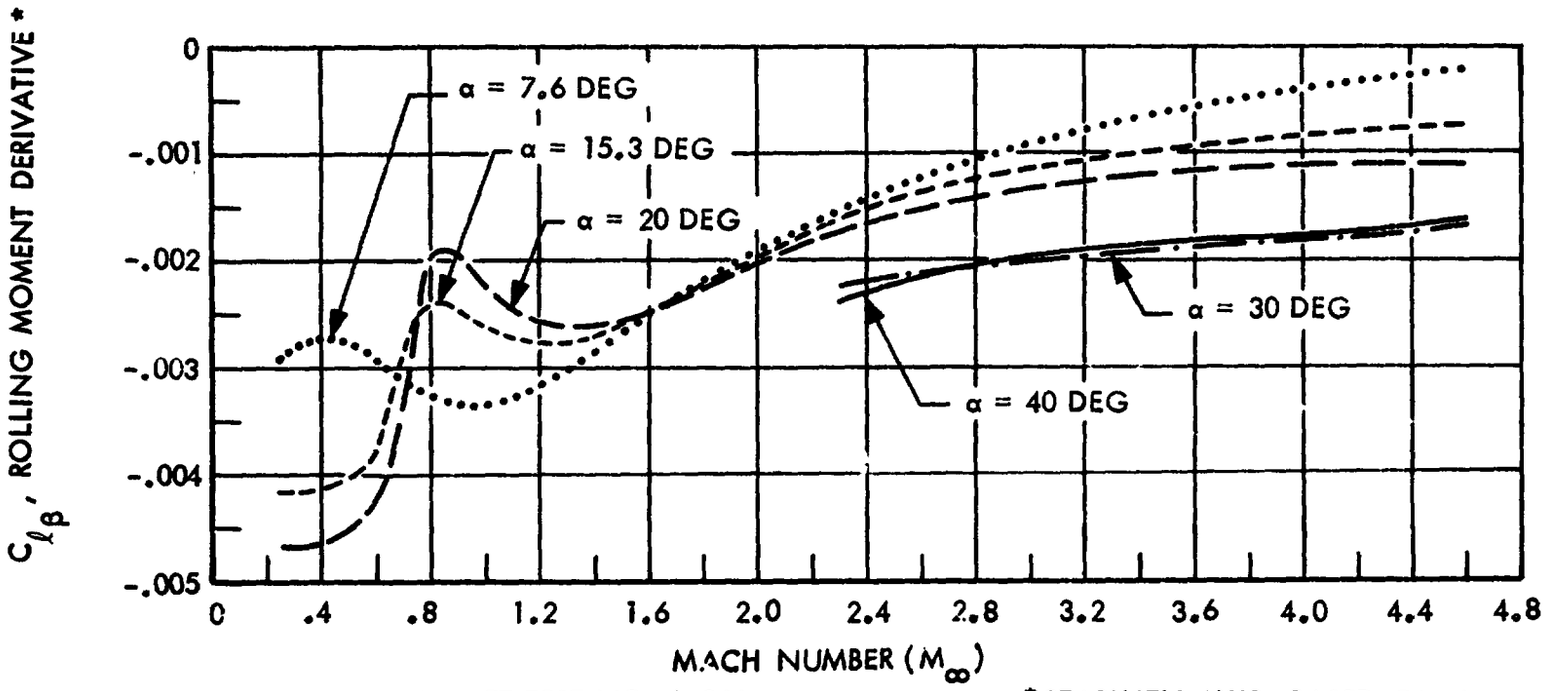

- LOCKHEED 8 FT X 12 FT TEST NO. L-324
- AMES 6 FT X 6 FT TEST NO. 542
- LANGLEY UPWT TEST NO. 955

*STABILITY AXIS. BASED ON L_{REF}

FIG. 59

6-60

D03379

LATERAL STABILITY SUMMARY

δ_R AT 0 DEG

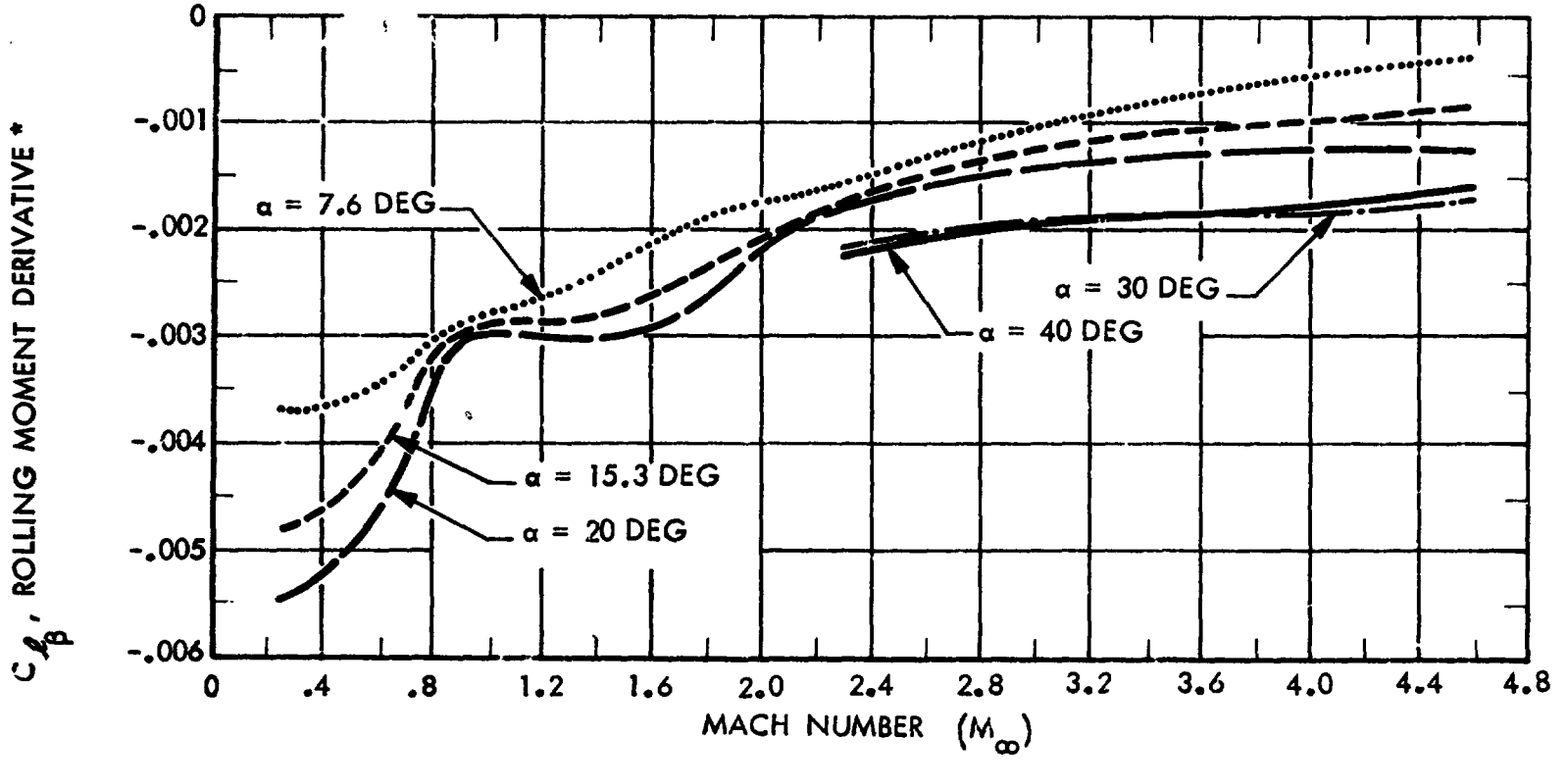

- LOCKHEED 8 FT X 12 FT TEST NO. L-324
- AMES 6 FT X 6 FT TEST NO. 542
- LANGLEY UPWT TEST NO. 955

*STABILITY AXIS, BASED ON L_{REF}

D03380

FIG. 60
6-61

LATERAL STABILITY SUMMARY

δ_R AT 10 DEG OUT

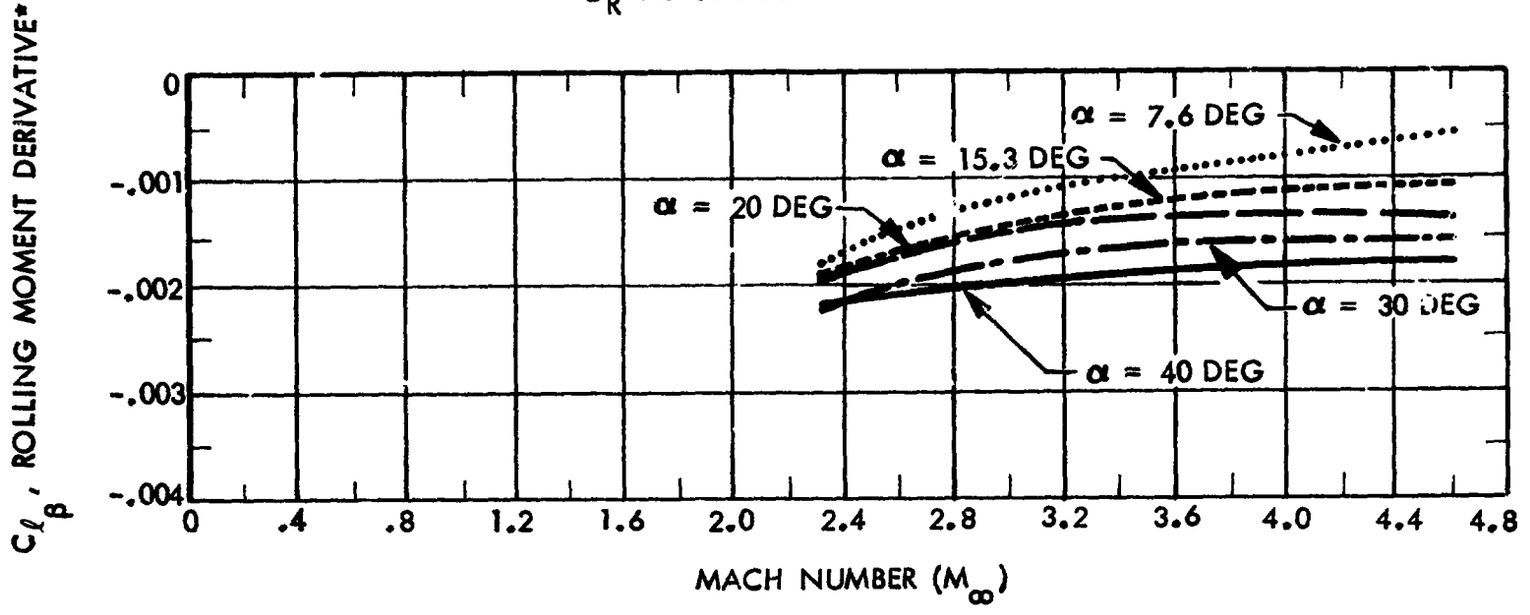

- LOCKHEED 8 FT X 12 FT TEST L-324
- AMES 6 FT X 6 FT TEST 542
- LANGLEY UPWT TEST 955

*STABILITY AXIS, BASED ON L_{REF}

FIG. 61

6-62

D03381

DIRECTIONAL STABILITY SUMMARY

δ_R AT 20 DEG IN

DYNAMIC DIRECTIONAL STABILITY DERIVATIVE*

CG AT 78 PERCENT L_{REF}

$\left(\frac{I_{ZZ}}{I_{XX}} = 5.081\right)$

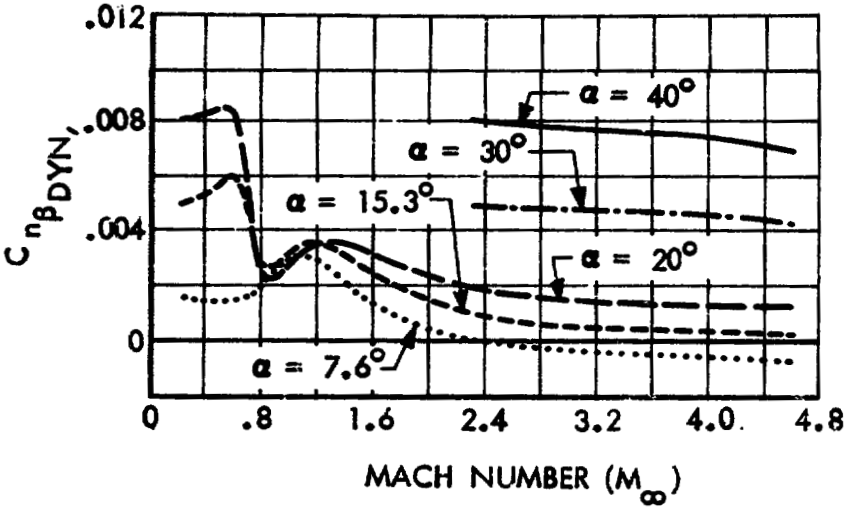

CG AT 72.5 PERCENT L_{REF}

$\left(\frac{I_{ZZ}}{I_{XX}} = 5.829\right)$

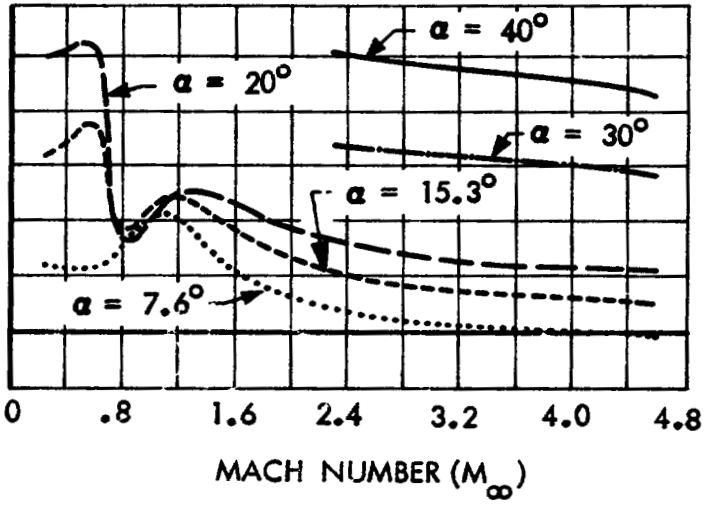

*BASED ON L_{REF}

- LOCKHEED 8 FT X 12 FT TEST L-324
- AMES 6 FT X 6 FT TEST 542
- LANGLEY UPWT TEST 955

DC3279

FIG. 62

DIRECTIONAL STABILITY SUMMARY

δ_R AT 0 DEG

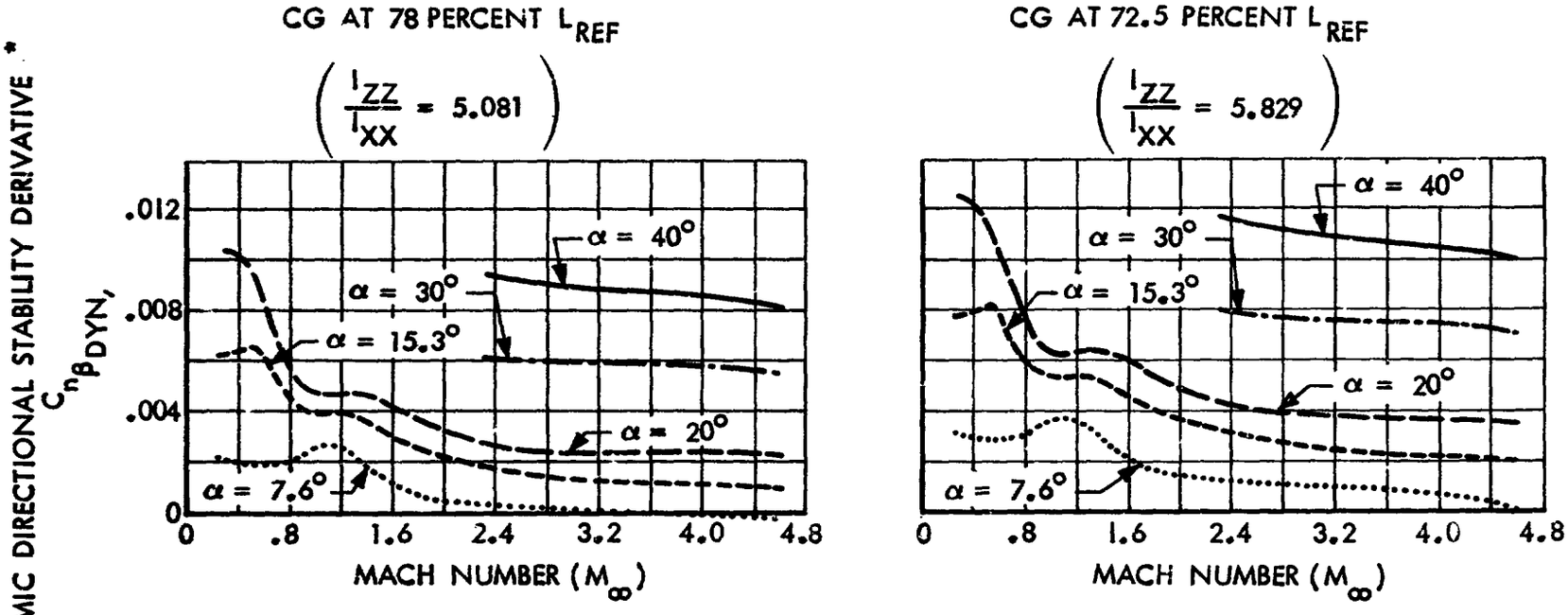

*BASED ON L_{REF}

- LOCKHEED 8 FT X 12 FT TEST L-324
- AMES 6 FT X 6 FT TEST 542
- LANGLEY UPWT TEST 955

D03280

DIRECTIONAL STABILITY SUMMARY

δ_R AT 10 DEG OUT

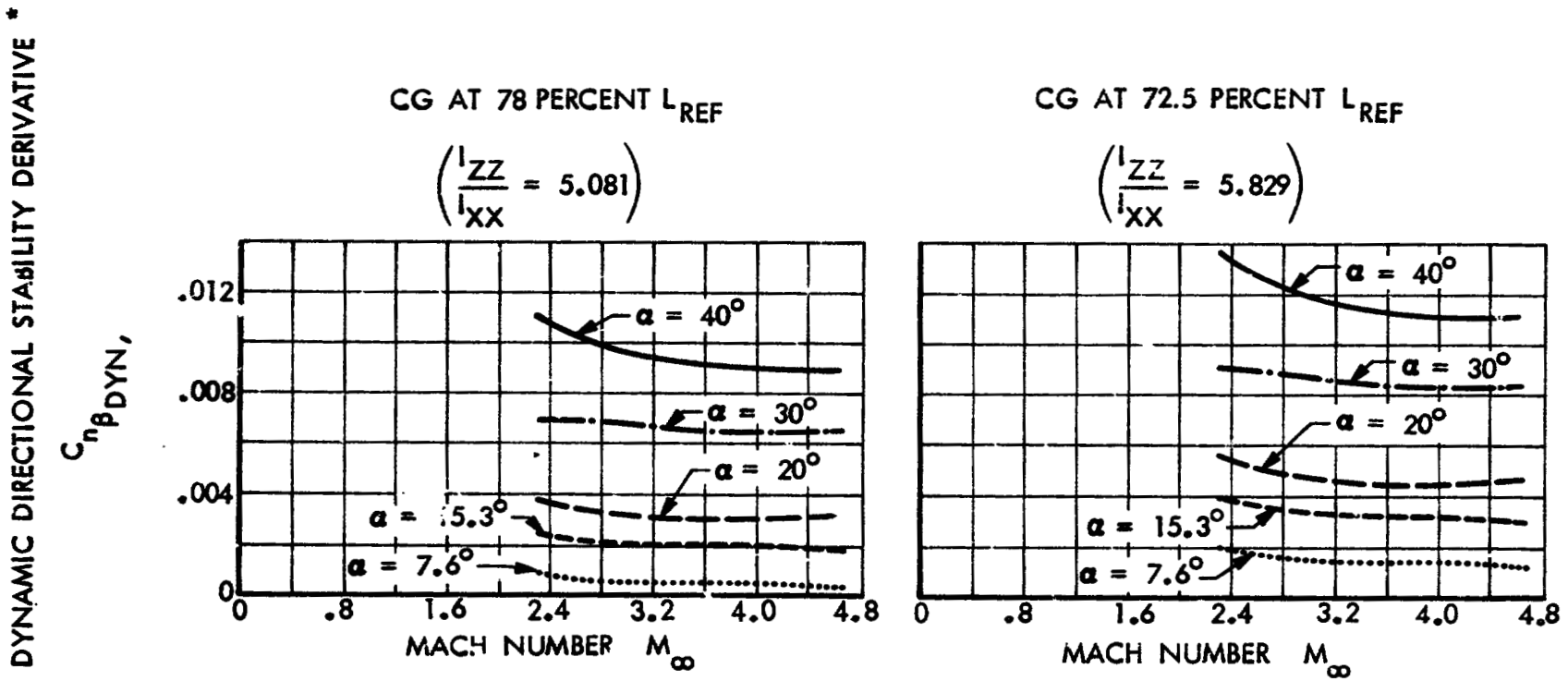

*BASED ON L_{REF}

- LOCKHEED 8 FT X 12 FT TEST L-324
- AMES 6 FT X 6 FT TEST 542
- LANGLEY UPWT TEST 955

D03281

AERODYNAMIC LIFT-TO-DRAG SUMMARY

TWO-STAGE*

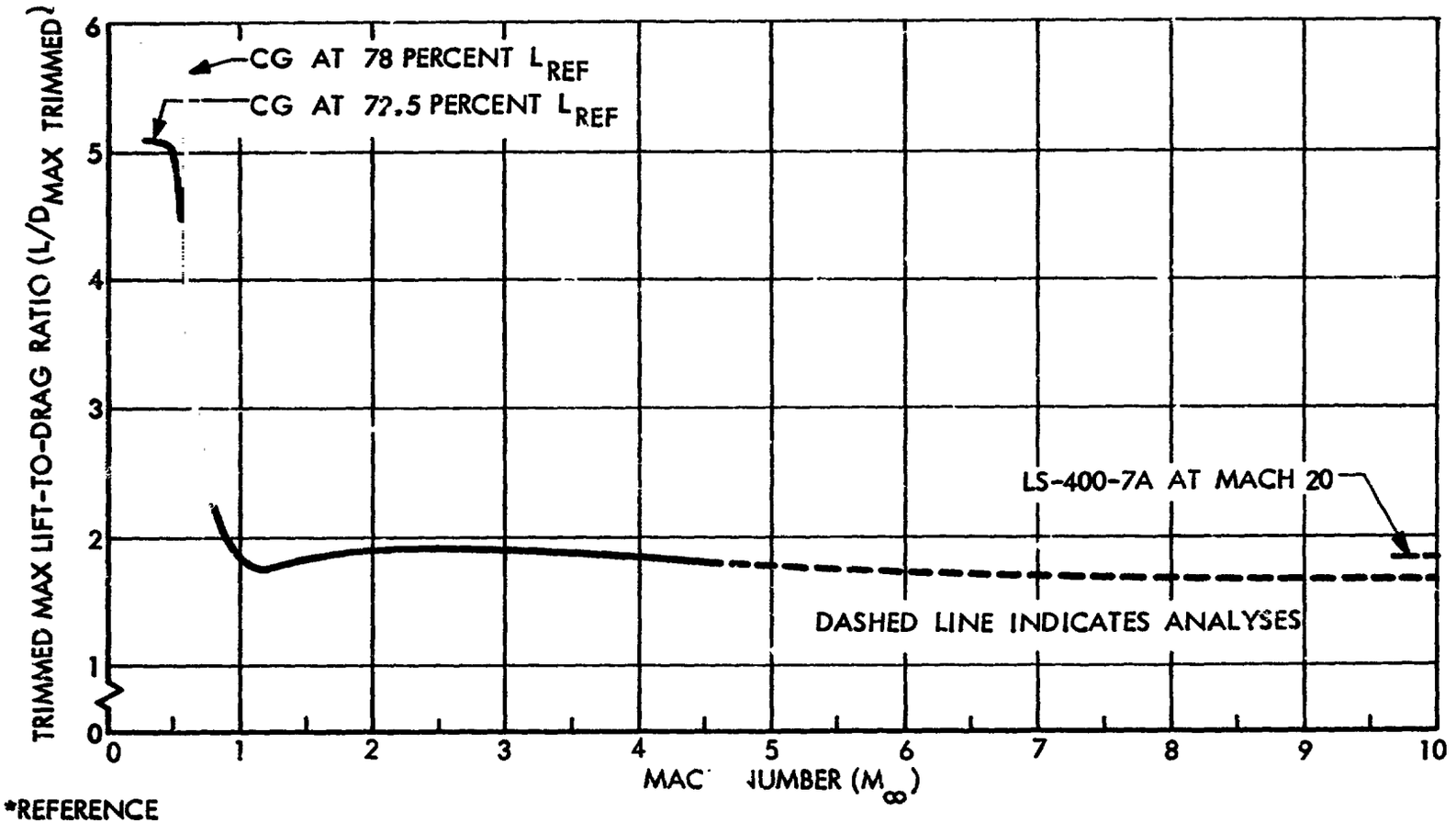

*REFERENCE

- LOCKHEED 8 FT X 12 FT TEST NO. L-324
- AMES 6 FT X 6 FT TEST NO. 542
- LANGLEY UPWT TEST NO. 955

D03066

LOCKHEED

TRIM ANGLE-OF-ATTACK RANGE

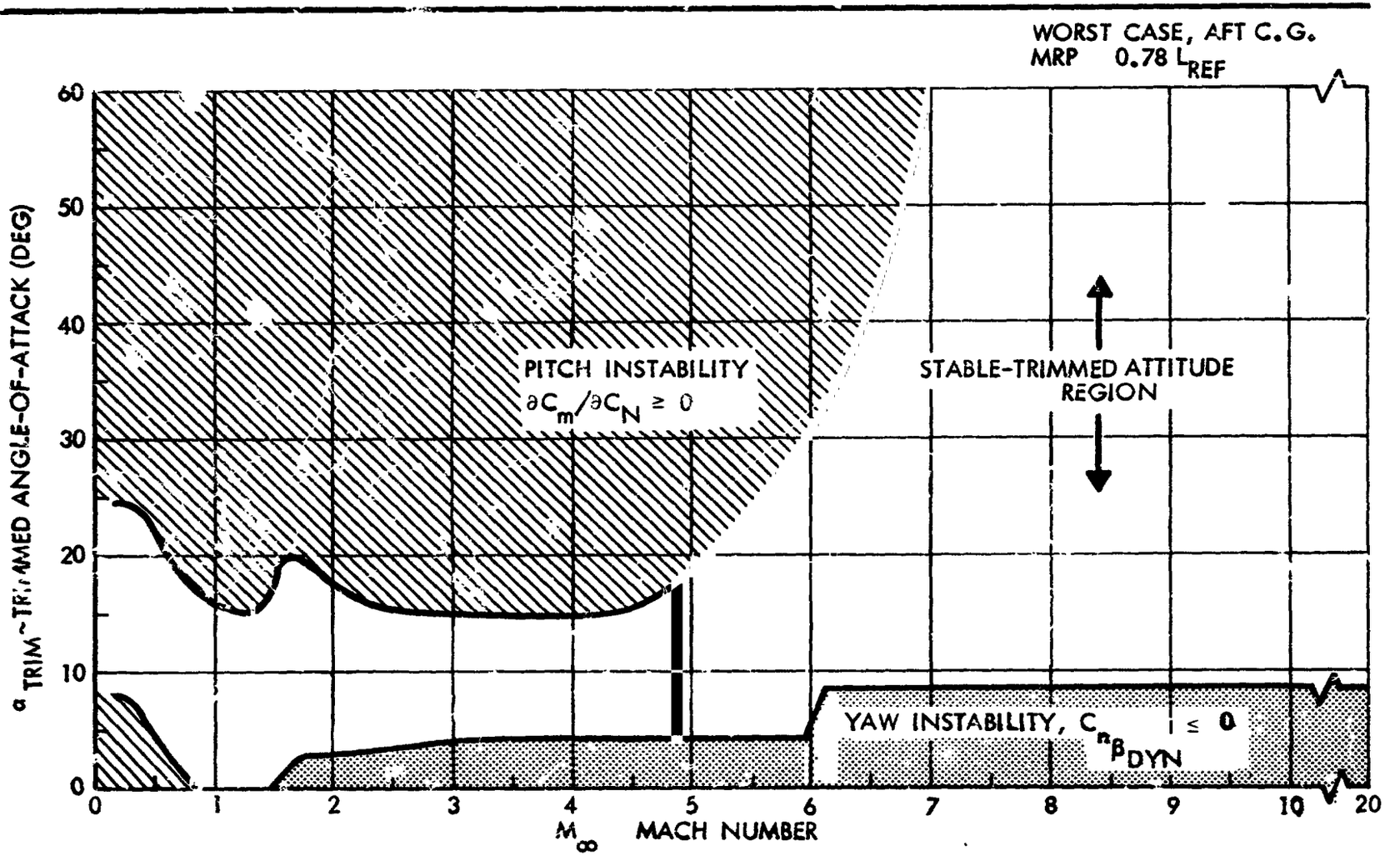

FIG. 66
6-67

D03015(1)

LOCKHEED

TRIM ANGLE-OF-ATTACK RANGE

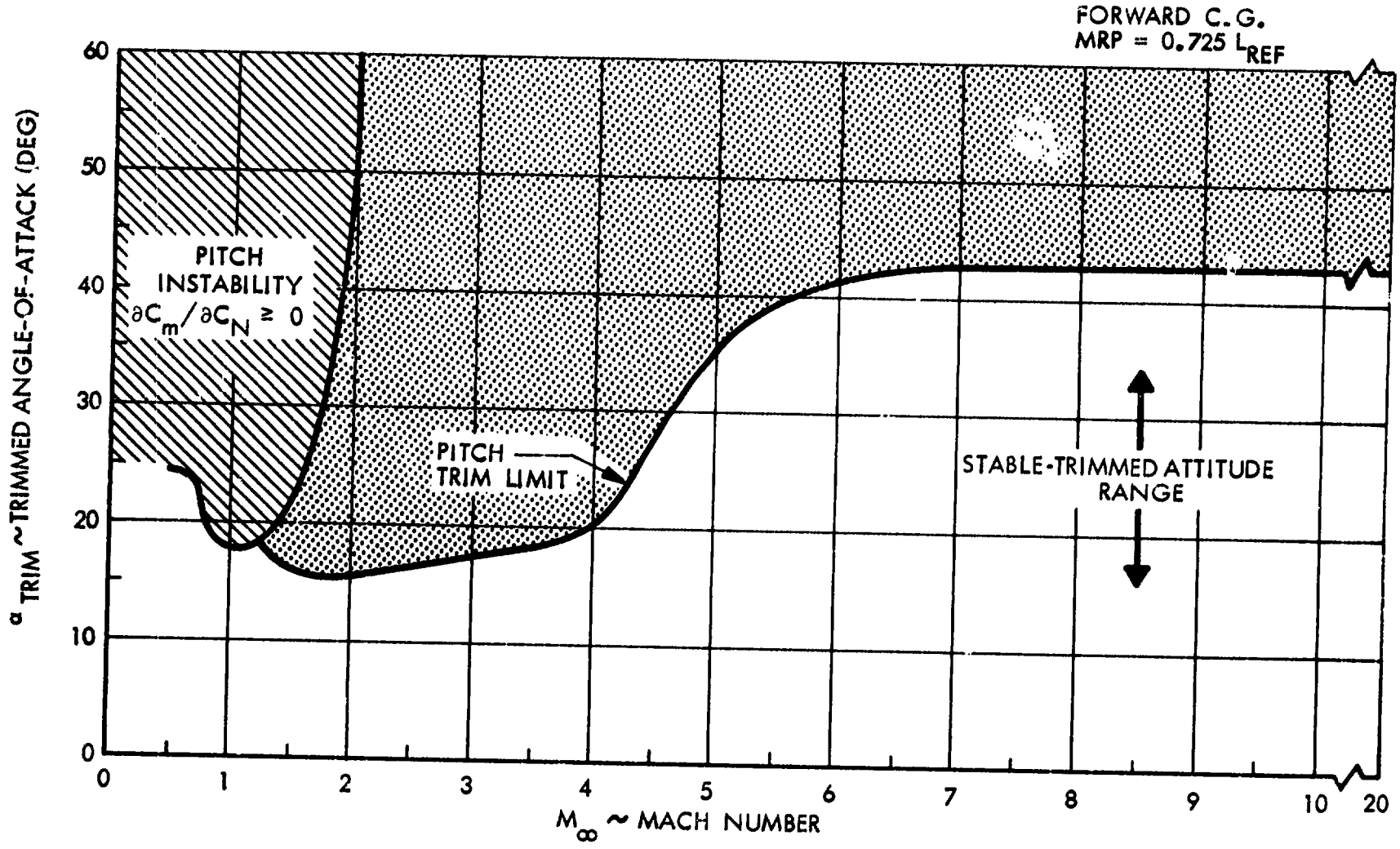

FIG. 67
6-68

D03013(1)

LOCKHEED

REFERENCE ENTRY TRAJECTORY

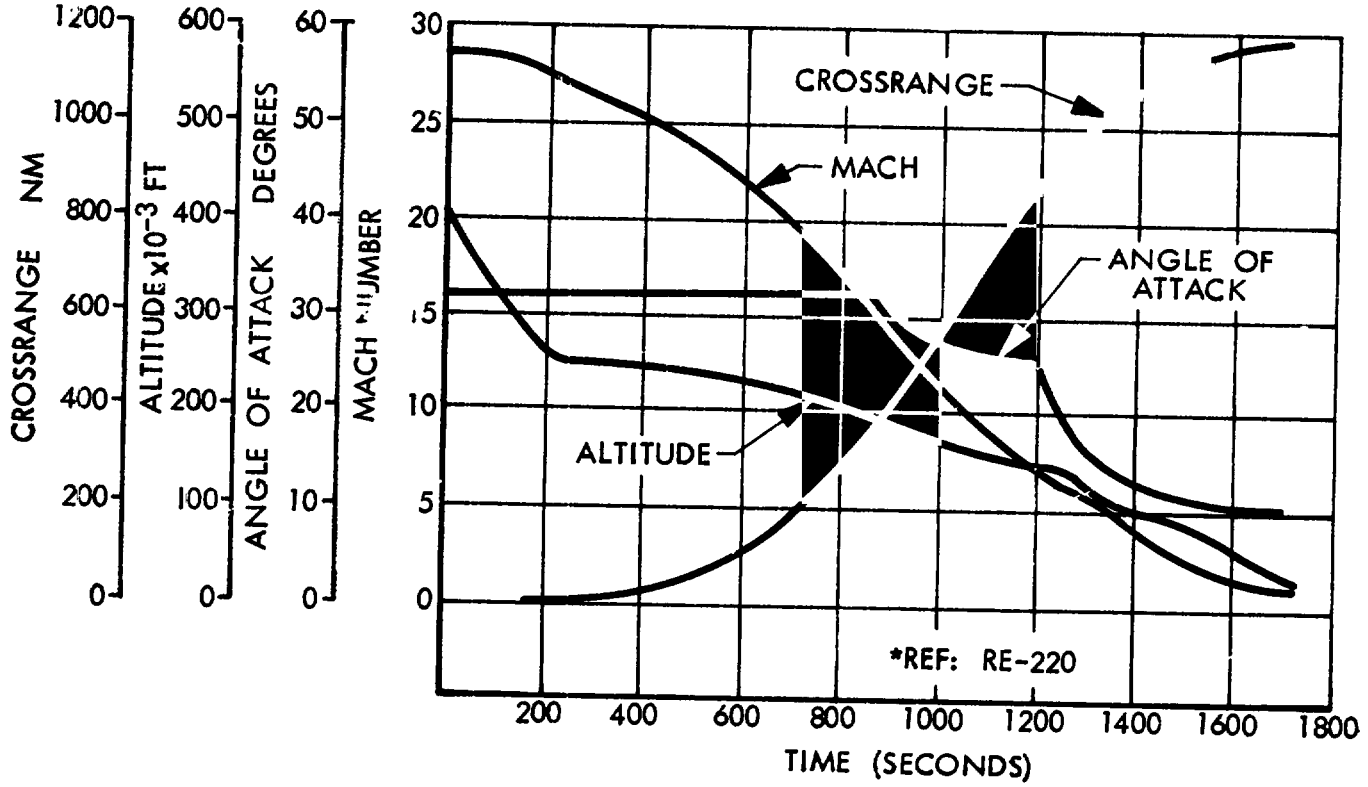

FIG. 68

69-9

D02851

fav

LONGITUDINAL STABILITY SUMMARY

(RE 220 TRAJECTORY)

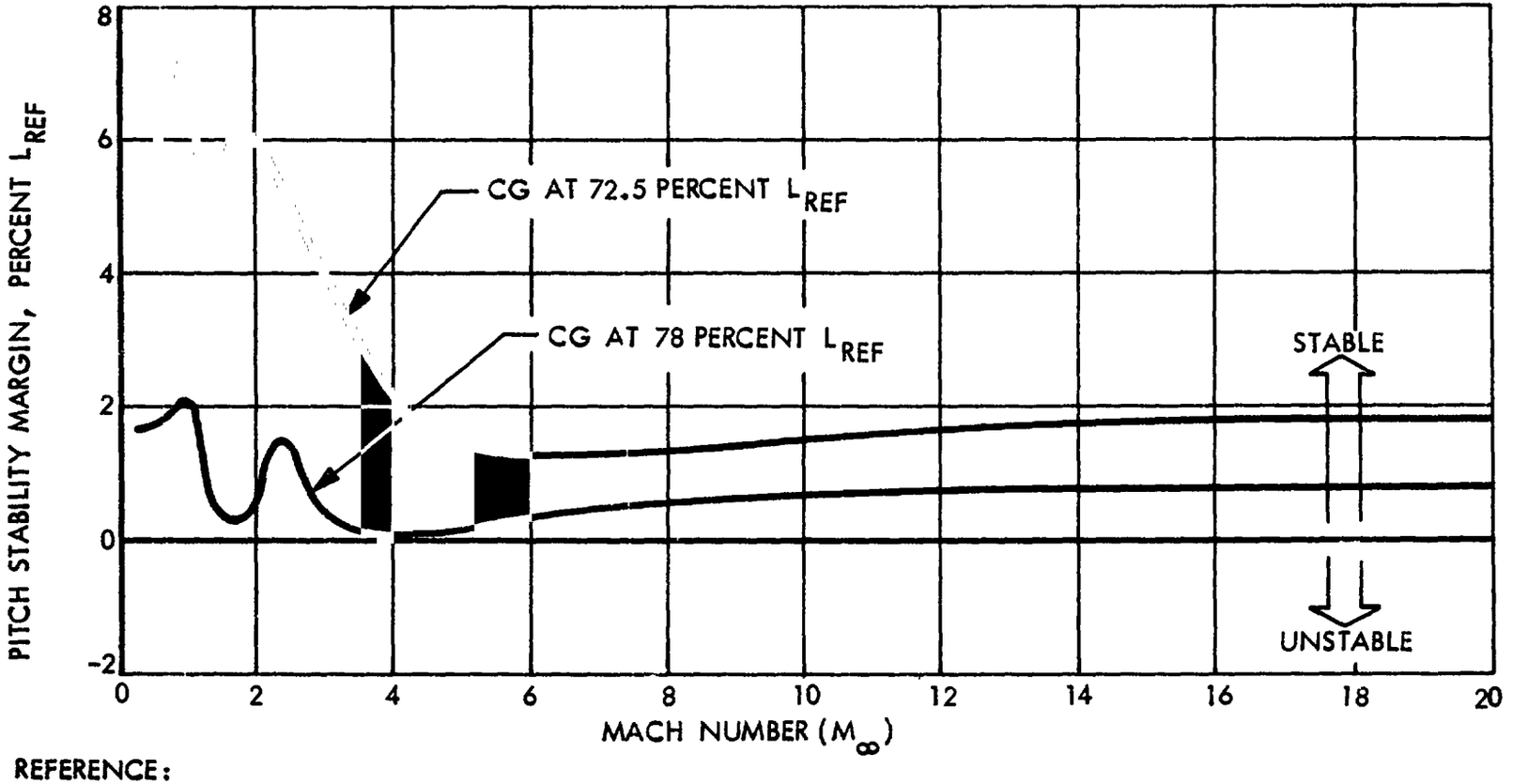

FIG. 69
6-70

REFERENCE:

- LOCKHEED 8 FT X 12 FT TEST L-324
- AMES 6 FT X 6 FT TEST 542
- LANGLEY UPWT TEST 955

D03282

DIRECTIONAL STABILITY SUMMARY

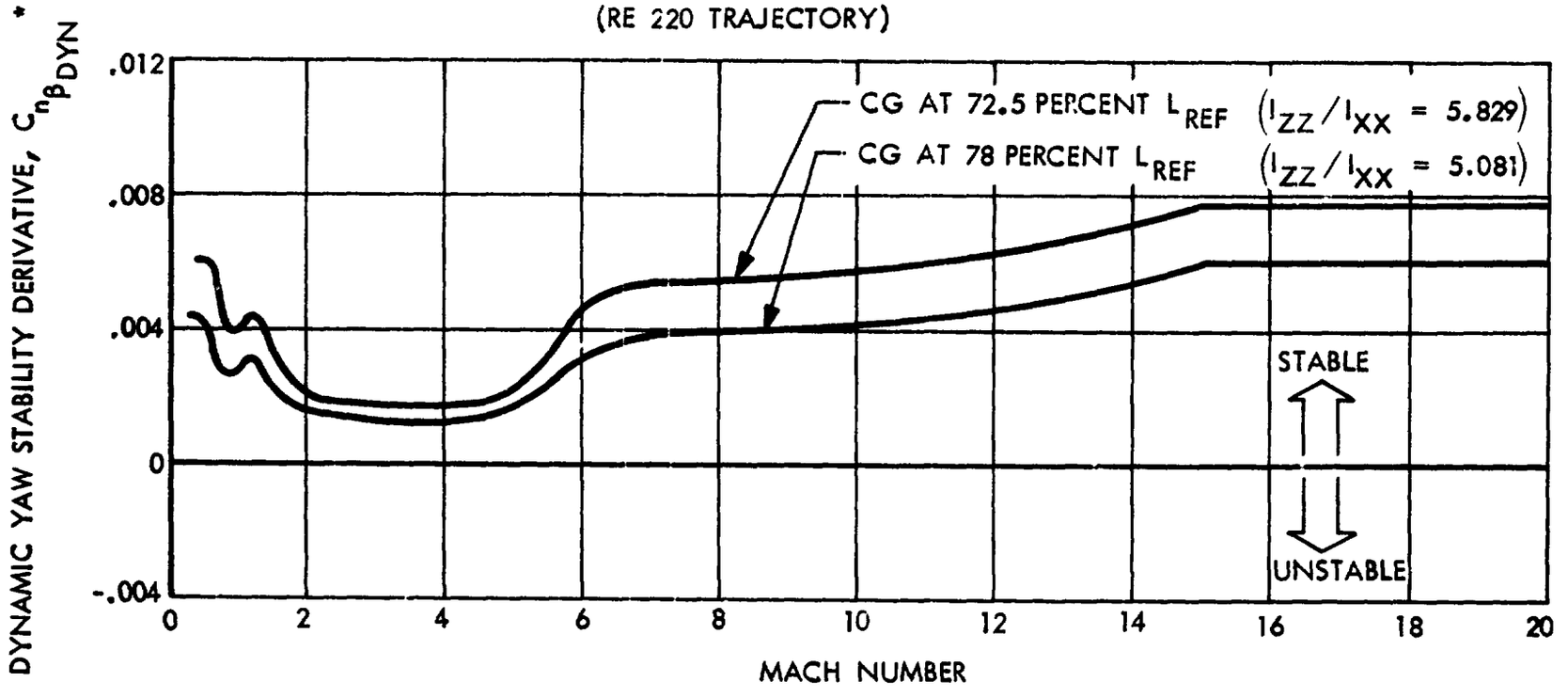

*BASED ON L_{REF}

FIG. 70

6-71

REFERENCE:

- LOCKHEED 8 FT X 12 FT TEST L-324
- AMES 6 FT X 6 FT TEST 542
- LANGLEY UPWT TEST 955

D03283

LAUNCH CONFIGURATION

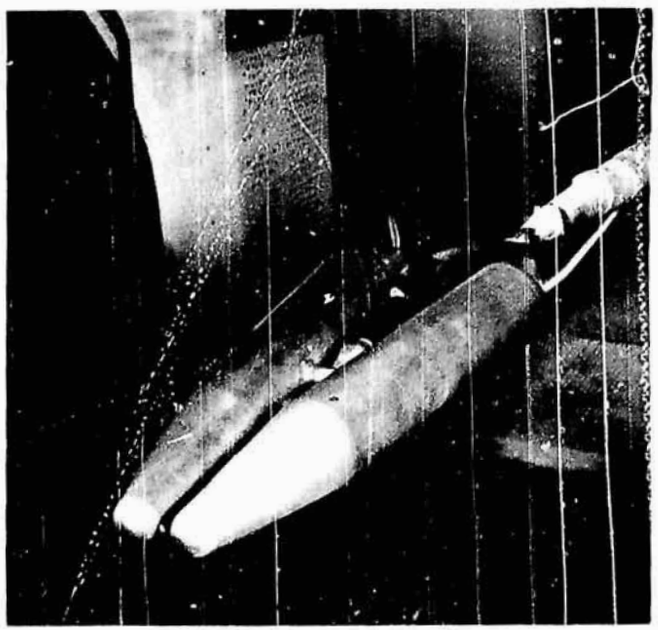

FIG. 71

	LAUNCH VEHICLE
TEST FACILITY	AMES 6 x 6 FT
RUNS	28
MACH NUMBER	0.60 TO 2.0
ANGLE-OF-ATTACK (DEG)	-10 TO 10
SIDESLIP ANGLE (DEG)	-4 TO 10
REYNOLDS NUMBER PER FOOT	2.5×10^6 TO 4.5×10^6

LOCKHEED

NORMAL FORCE CHARACTERISTICS

LAUNCH VEHICLE – 1-1/2 STAGE (LS 200-5)

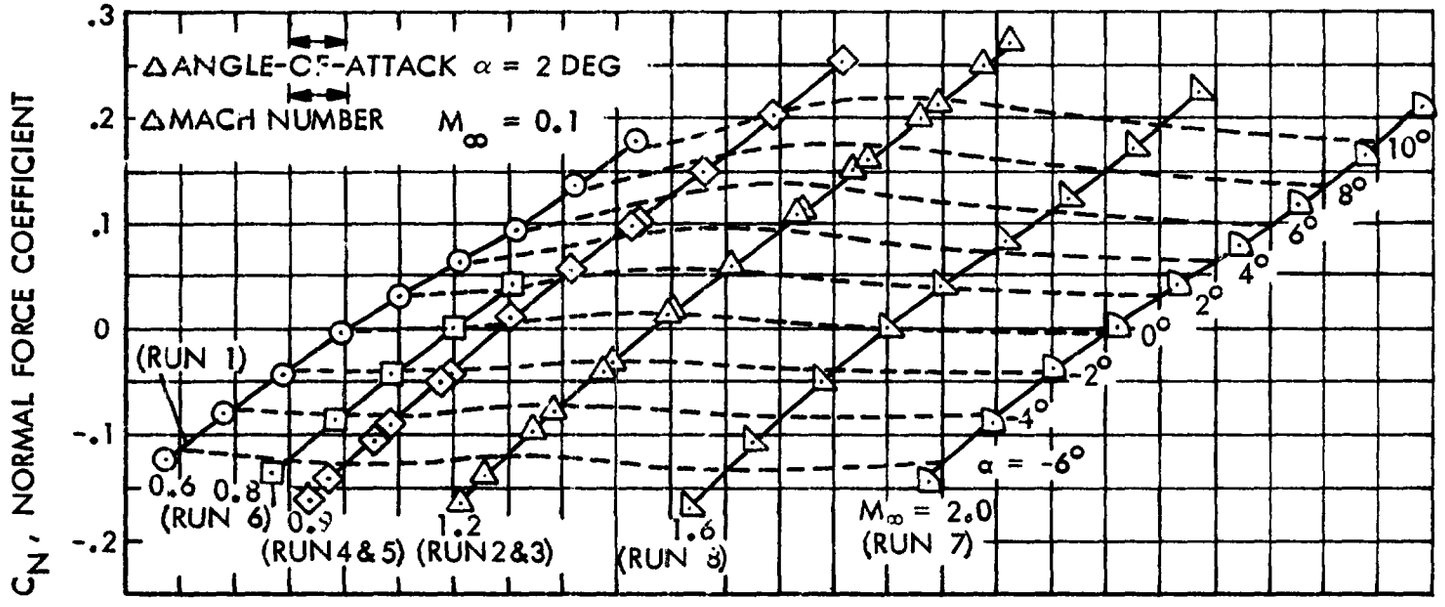

AMES 6 X 6 FT WIND TUNNEL TEST NO. 542

FIG. 72
6-73

D03261

LOCKHEED

AXIAL FORCE CHARACTERISTICS

LAUNCH VEHICLE – 1-1/2 STAGE (LS 200-5)

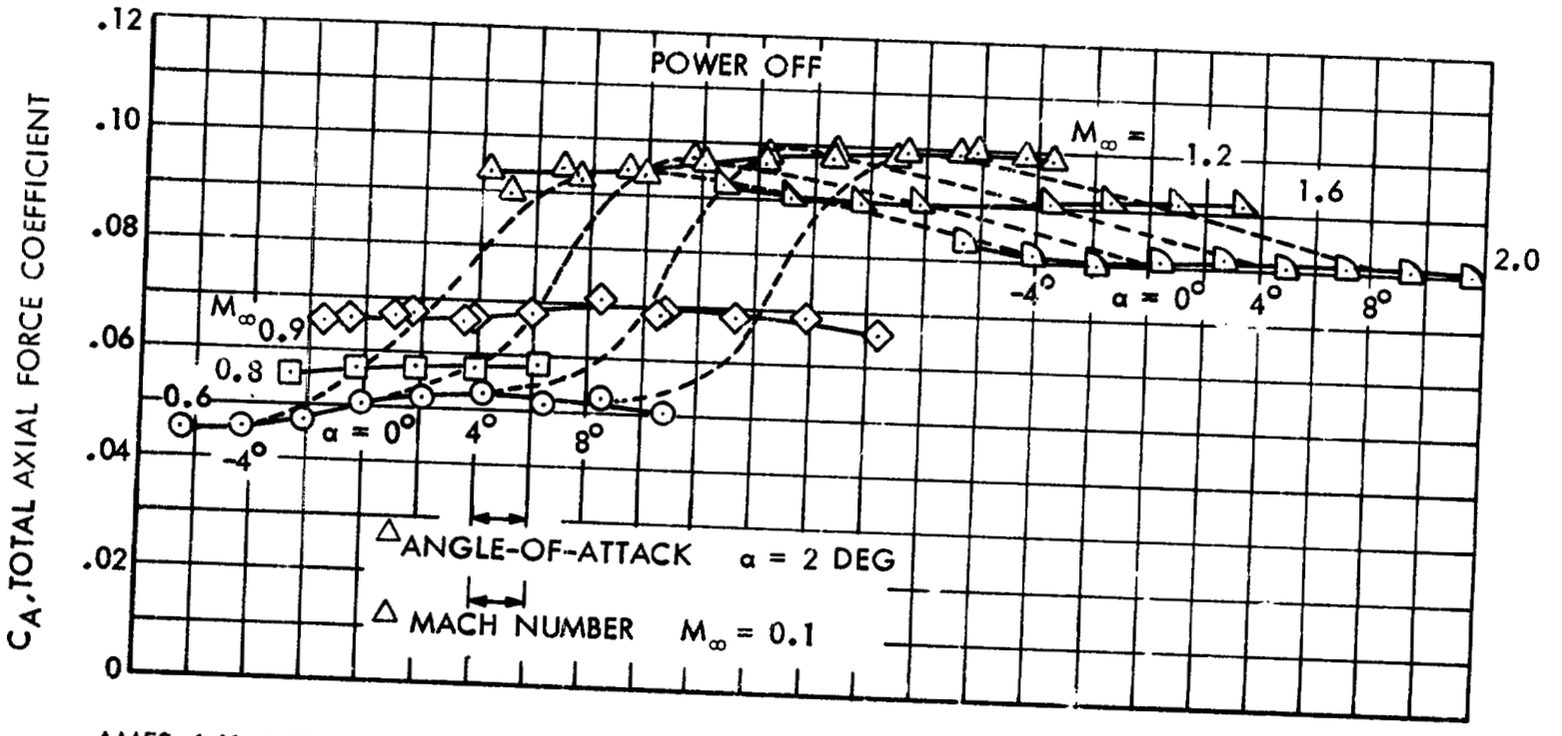

AMES 6 X 6 FT WIND TUNNEL TEST NO. 542

FIG. 73
6-71

D03262

LONGITUDINAL STABILITY CHARACTERISTICS

LAUNCH VEHICLE – 1-1/2 STAGE (LS 200-5)

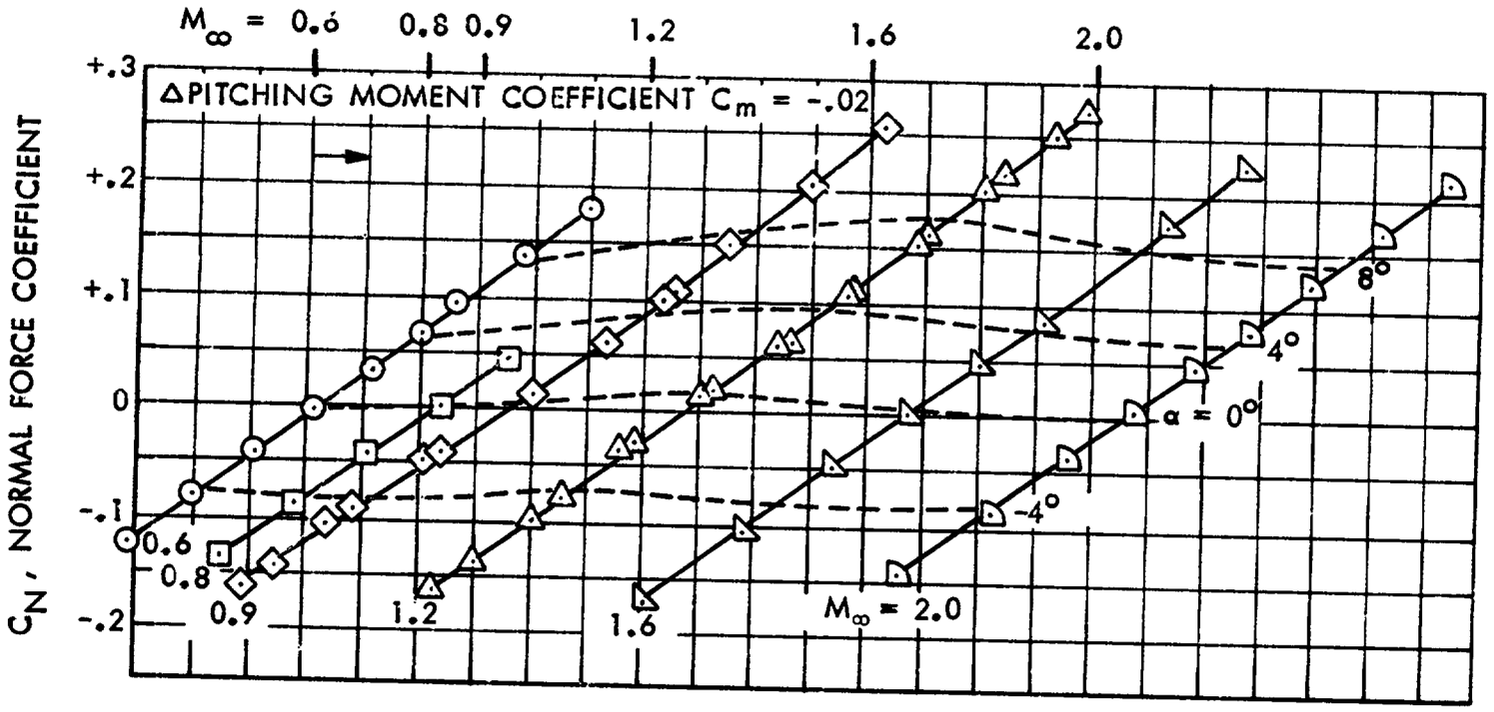

FIG. 74
6-75

AMES 6 X 6 FT WIND TUNNEL TEST NO. 542

LONGITUDINAL CHARACTERISTICS

LAUNCH VEHICLE – 1-1/2 STAGE (LS 200-5)

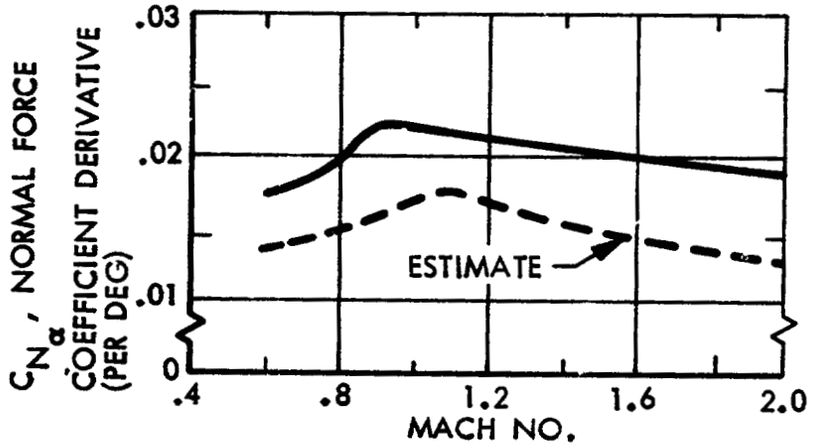

$S_{REF} = 12463\ FT^2$

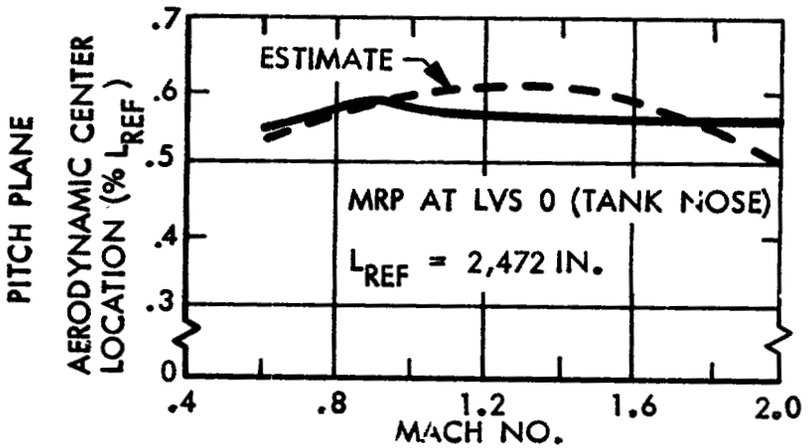

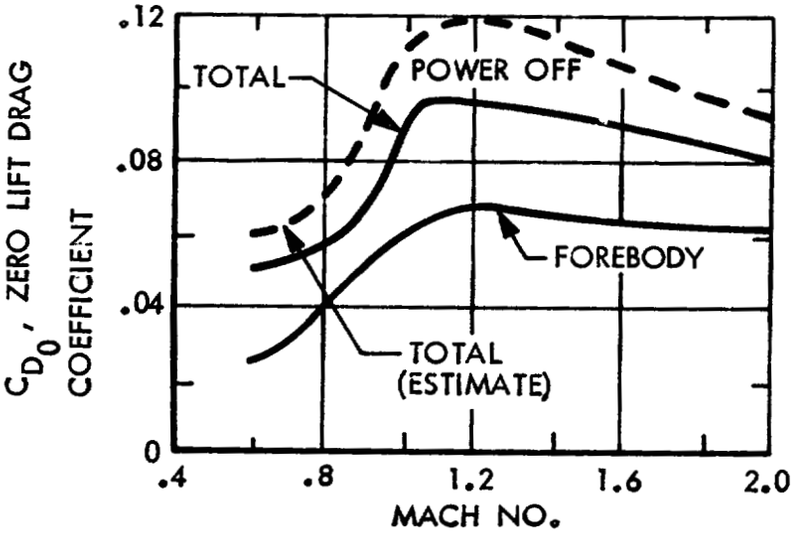

D03264

FIG. 75
6-76

LATERAL-DIRECTIONAL CHARACTERISTICS

LAUNCH VEHICLE – 1-1/2 STAGE (LS 200-5)

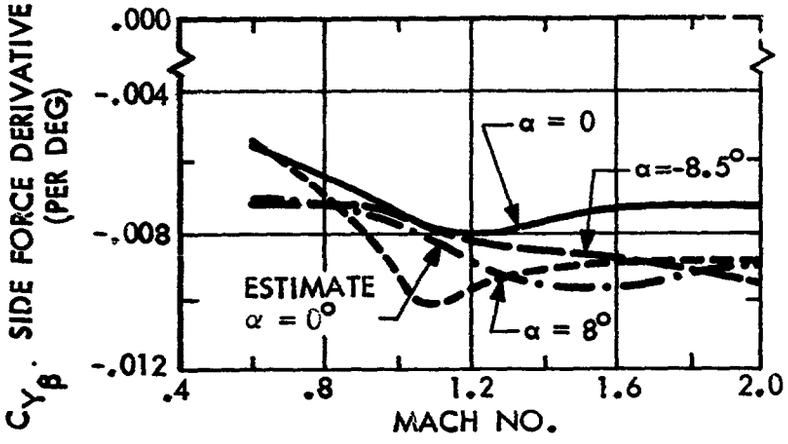

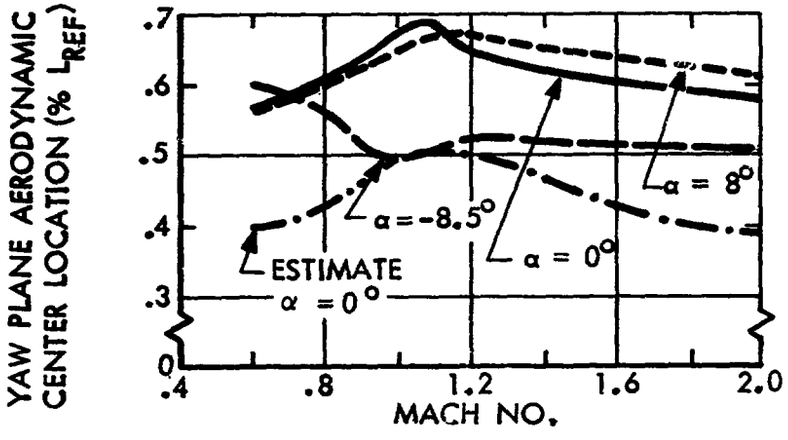

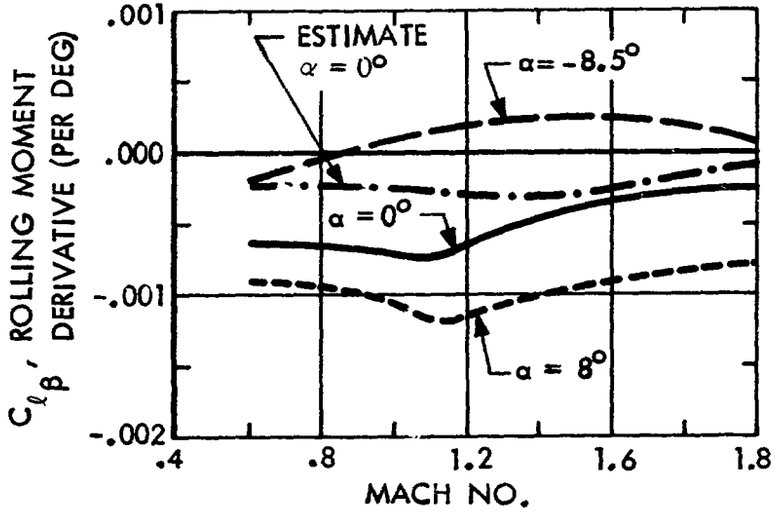

AMES 6 X 6 FT WIND TUNNEL TEST NO. 542

D03265

FIG. 76

REFINED 2-STAGE ORBITER

LS 400-7A

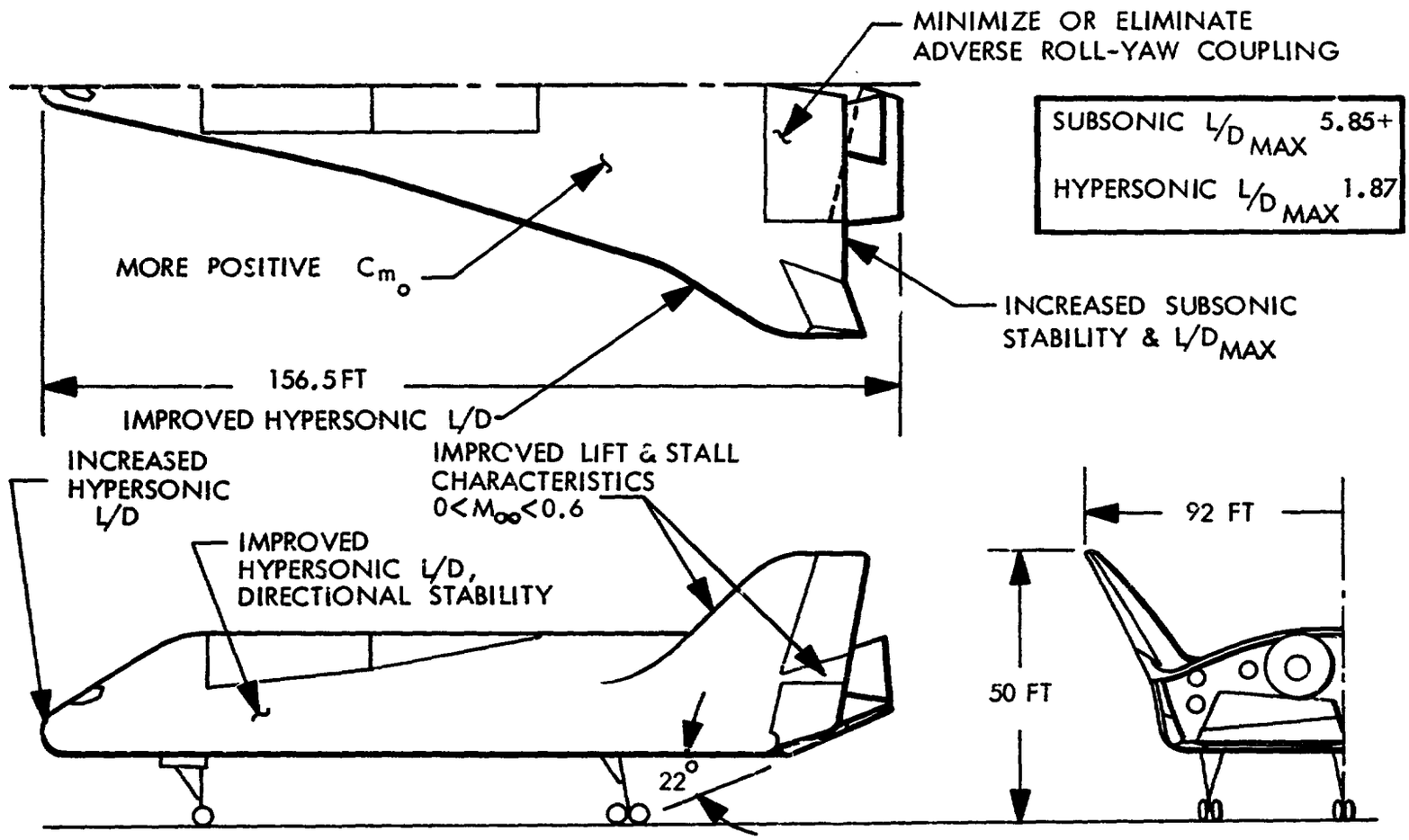

FIG. 77
6-78

D02875(1)

LOCKHEED

DELTA LIFTING BODY ORBITER

(HYPERSONIC ARBITRARY BODY COMPUTER PROGRAM)
(LS-400-7A)

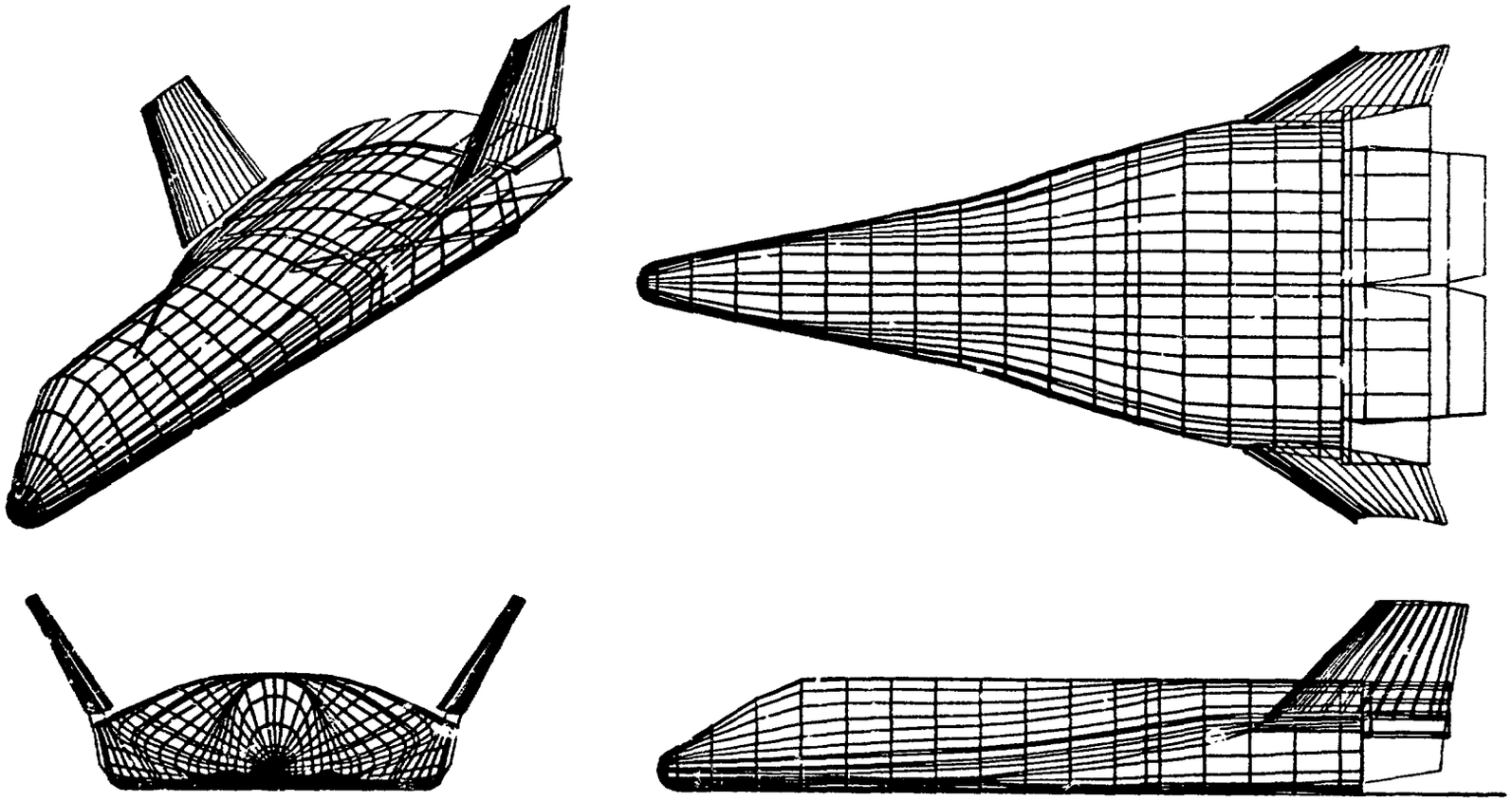

FIG. 78
6-79

D03235